

UNCLASSIFIED
LACP-85-0092

~~SECRET~~ ~~RD~~

SAC 200164750000

~~Nuclear Weapon Data
Sigma 1
Critical Nuclear Weapon
Design Information Per
DoD Directive 5210.2
Issued: May 1985~~

~~LIMITED ACCESS~~

~~Recipients should not disseminate this report further without the permission of David C. Cartwright, Principal Program Manager for Inertial Confinement Fusion, MS E527~~

This document consists of 111 pages
No. 53 of 80 copies, Series A.

Los Alamos National Laboratory is operated by the University of California for the United States Department of Energy under contract W-7405-ENG-36.

*minus page 4, 6, 8, 9
(88)*

Summary of Classified Research for the Inertial Confinement Fusion Program at Los Alamos National Laboratory (U)

~~Derivative Classifier
David C. Cartwright
Principal Program Manager
for Inertial Confinement Fusion~~

DEPARTMENT OF ENERGY DECLASSIFICATION REVIEW	
1st REVIEW DATE: <i>11/21/70</i>	4. DETERMINATION (CIRCLE NUMBER(S))
AUTHORITY: <i>FCR 1.2</i>	<input checked="" type="radio"/> 1. CLASSIFICATION RETAINED
NAME: <i>McFadden</i>	<input type="radio"/> 2. CLASSIFICATION CHANGED TO:
2nd REVIEW DATE: <i>8/14/92</i>	<input type="radio"/> 3. CONTAINS NO DOE CLASSIFIED INFO
AUTHORITY: <i>DD</i>	<input type="radio"/> 4. COORDINATE WITH:
NAME: <i>Phil Langston</i>	<input type="radio"/> 5. CLASSIFICATION CANCELED
	<input type="radio"/> 6. CLASSIFIED INFO BRACKETED
	7. OTHER (SPECIFY): <i>MISSING PAGES</i>

~~RESTRICTED DATA~~

~~This document contains Restricted Data as defined in the Atomic Energy Act of 1954. Unauthorized disclosure subject to Administrative and Criminal Sanctions.~~

4, 6, 8, and 88

Los Alamos Los Alamos National Laboratory
Los Alamos, New Mexico 87545

UNCLASSIFIED

~~SECRET~~ ~~RD~~

85/32
1
OISA20C000132

UNCLASSIFIED

~~SECRET~~ / RD
An Affirmative Action/Equal Opportunity Employer

Special thanks are due to Karyn Ames, Linda Bacher, Mary Louise Garcia, Vicki Hartford, and Susan Lewis for their assistance in assembling and publishing this review.

NOTICE: Reproduction of this document requires the written consent of the originator, his successor, or higher authority.

DISCLAIMER

This report was prepared as an account of work sponsored by an agency of the United States Government. Neither the United States Government nor any agency thereof, nor any of their employees, makes any warranty, express or implied, or assumes any legal liability or responsibility for the accuracy, completeness, or usefulness of any information, apparatus, product, or process disclosed, or represents that its use would not infringe privately owned rights. Reference herein to any specific commercial product, process, or service by trade name, trademark, manufacturer, or otherwise, does not necessarily constitute or imply its endorsement, recommendation, or favoring by the United States Government or any agency thereof. The views and opinions of authors expressed herein do not necessarily state or reflect those of the United States Government or any agency thereof.

UNCLASSIFIED

~~SECRET~~

RD

~~SECRET~~

~~LACP-95-0092
Nuclear Weapon Data
Signal
Critical Nuclear Weapon
Design Information Per
DoD Directive 5210.2
Issued: May 1985~~

*Summary of
Classified Research for
the Inertial Confinement
Fusion Program at
Los Alamos National Laboratory (U)*

Compiled by
David C. Cartwright
Principal ICF Program Manager

07000004

Los Alamos Los Alamos National Laboratory
Los Alamos, New Mexico 87545

~~SECRET~~

CONTENTS

ABSTRACT 7

Inertial Confinement Fusion Overview 9

Contributions by the ICF Program to the Nuclear
Weapons Program at Los Alamos 15

Capsule Implosion Physics 23

The Centurion Program 36

CO₂ Laser Plasma Interactions 74

Target Fabrication—Materials and Technologies to
Meet Unusual Demands 99

67070505

UNCLASSIFIED

~~SECRET~~ /RD

SUMMARY OF CLASSIFIED RESEARCH FOR THE INERTIAL
CONFINEMENT FUSION PROGRAM AT LOS ALAMOS
NATIONAL LABORATORY (U)

Compiled by David C. Cartwright
Principal ICF Program Manager

ABSTRACT (U)

The information presented in this report is a summary of the status of the classified research in the Inertial Confinement Fusion (ICF) program at the Los Alamos National Laboratory as of February 1985. This report contains sections on capsule physics, the Centurion underground test program, target fabrication, and the contributions of ICF to the Laboratory's weapons program. An unclassified companion report contains sections on the high-power, CO₂ laser driver (Antares), the KrF laser, heavy-ion accelerators, target fabrication, and laser-plasma interactions. The information contained in these two volumes is meant to serve as a status report on some of the technological components of the Los Alamos ICF program rather than as a detailed review of specific technical issues.

67070506

UNCLASSIFIED

~~SECRET~~ /RD

UNCLASSIFIED

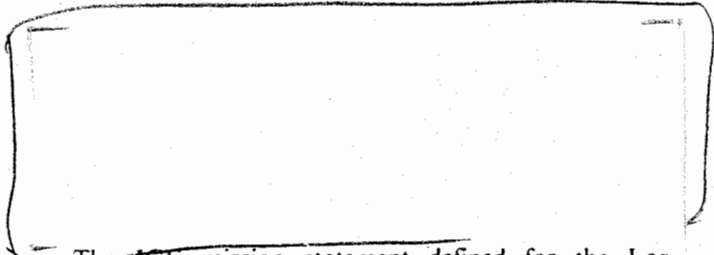
INERTIAL CONFINEMENT FUSION OVERVIEW

by David C. Cartwright

INTRODUCTION

The accomplishment of energy gain through nuclear fusion in laboratory experiments will require the solution of a number of interesting, although very complex, scientific and technological problems. Both the Inertial Confinement Fusion (ICF) and Magnetic Fusion Energy (MFE) programs have been somewhat overly optimistic in their initial evaluations of the difficulties involved in controlling nuclear fusion. In both programs, most of the major problems were identified only after the construction and operation of a new (usually more powerful) experimental facility. Researchers in both the ICF and the MFE programs are now trying to build solid technical foundations for their programs so that they can predict results under different experimental conditions. Los Alamos completed construction of the Antares CO₂ laser facility in December 1983 and placed it on operational status for experiments in ICF. Antares, the world's largest operational laser, is the first in a series of new, higher-intensity ICF drivers. The two others in the US are Nova at Lawrence Livermore National Laboratory (LLNL), to be operational in the spring of 1985, and PBFA-II at Sandia National Laboratories (SNL), to begin operation in the fall of 1987. These new facilities will permit experimentation with ICF targets under conditions of temperature and pressure that much more closely simulate those required for an energy gain target.

Because Antares has been in operation for more than a year and Helios was operational for 5 years before Antares, it is appropriate to review our present understanding of ICF physics based on CO₂ laser drivers.



b(3)

The ICF mission statement defined for the Los Alamos National Laboratory is as follows:

"The Los Alamos ICF program is one of the main efforts by the Department of Energy (DOE) to evaluate the scientific feasibility of inertially confined fusion, using intense lasers or particle beams to compress and heat small masses of deuterium-tritium fuel to thermonuclear burn conditions. The goals of the national program are:

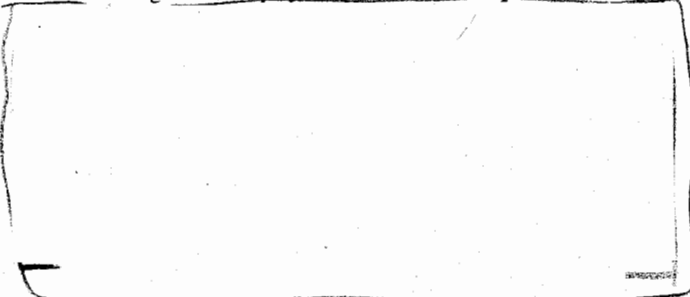
- to support nuclear weapons physics research, and
- to do research on the potential of inertial fusion for energy production.

Key technical elements within the ICF program are:

- the design and confirmation of performance of fuel-filled targets requiring minimum input energy, and
- the development of a laboratory driver suitable for driving such targets (at an acceptable cost).

Whether addressing weapons applications or possible long-term potential as an energy source, there is no significant difference in the short-term program. In the longer term, important scientific and engineering problems would have to be addressed before ICF could be considered for commercial electrical power generation. Since the primary source of the funding is the DOE defense programs, the weapon physics goals will continue to receive emphasis throughout this decade."

67070307



b(3)

UNCLASSIFIED

In an unclassified companion report to this report,¹ a summary of the progress that has been made in high-power CO₂ lasers, laser-plasma interactions, dense plasmas produced by CO₂, the KrF laser, heavy-ion fusion, and target fabrication is given. In subsequent sections of this report, the scientific and technological progress that has been made in the fields of caspule physics, Centurion, and the contributions from the ICF program to the weapons program's target fabrication will be reviewed. A review of the Los Alamos program to study the physics of laser fusion at short wavelength (that is, 1/4 μm) will be presented in a future publication.

small fuel masses to support thermonuclear burn, in which the energy produced by fusion reaction is used to sustain the burn, the fuel must be condensed to high density. Specifically, to trap the energy of the α-particles produced in the DT fusion reaction, the areal density (ρR) must be equal to or greater than a certain constant C. That is, a fundamental scaling parameter for all ICF is the product of fuel density ρ and the radius R of the volume containing the fuel. It can be shown that if the product ρR is equal to a constant, then the density to which the fuel must be compressed increases as the reciprocal of the square root of the fuel mass, $\rho \approx 1/\sqrt{M}$.

GENERAL REQUIREMENTS FOR ICF

ICF attempts to mimic, on a miniature scale, the success of thermonuclear weapons and the basic principles are the same. A fuel of deuterium and tritium (DT) is heated rapidly to temperatures high enough to promote fusion reactions in the fuel, and at the same time, the fuel is compressed to densities large enough to facilitate reaction of a large fraction of the fuel before cooling by hydrodynamic expansion. However, the efficient use of the DT fuel in ICF is much more difficult than in a nuclear weapon.

The difficulty arises from the requirement to confine (in the laboratory) the energy released by the fusion reaction. This can be accomplished only if the yield is sufficiently low, which implies a small mass of fuel. For

Achieving the required compression without expending excessive energy from the driver is the basic requirement of ICF.

Figure 1 shows schematically the various steps required to convert the incident laser energy into hydrodynamic work compression on the fuel.

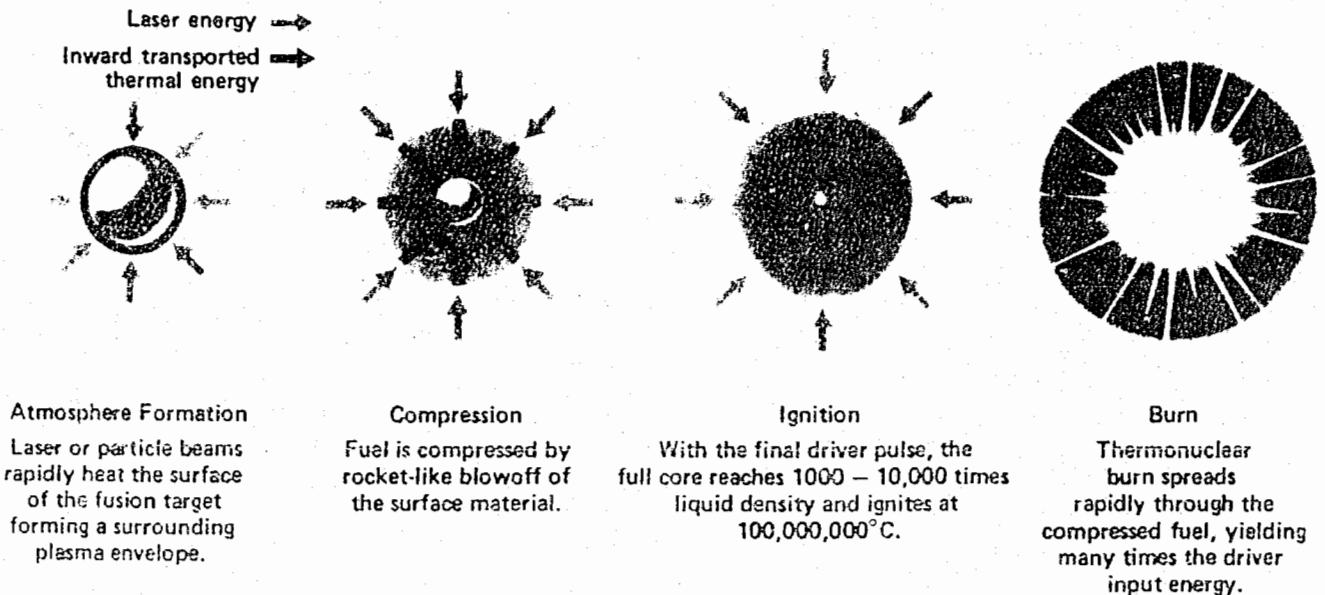
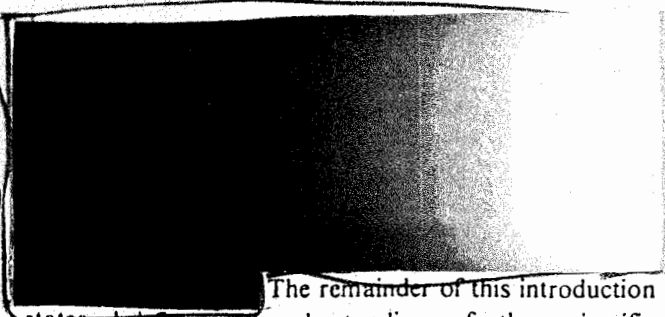


Fig. 1. Steps in the conversion of incident laser energy into hydrodynamic work compression on the fuel. Source is Ref. 2.

67070300



b(3)

The remainder of this introduction states briefly our understanding of the scientific processes governing each step known in the linkage of laser energy to fuel compression in Fig. 1. What is treated as an assertion at this level is explained, and qualified, in the sections that follow.

CHARACTERISTICS OF CO₂ IRRADIATED TARGETS

When high-intensity laser radiation ($>10^{15}$ W/cm²) strikes a surface, a plasma is formed. For open targets (for example, Fig. 1), the infrared radiation (10.6 μm) produced by the CO₂ laser is absorbed by the plasma through a collective process known as resonant absorption. This process, which we have come to understand primarily through theoretical work, converts all of the absorbed laser energy into energetic electrons. The measured absorption for flat surfaces is about 40%, whereas refraction of the incident light in the plasma reduces measured absorption to about 30% for curved surfaces. To achieve a greater absorption percentage, researchers have designed enclosed targets called "hohlraums" for which the absorption is increased to about 70%.

In open targets, the energetic electrons produced during the resonant absorption process approach temperatures of 80 keV. This distribution of so-called "hot electrons" can exist superimposed on a second "cold" distribution because there are very few collisions in the low-density corona formed around the target. Experiments show that hot-electron temperature increases with laser intensity as $I^{0.4}$. In hohlraum targets, the electron temperatures may exceed 200 keV. The combination of mechanisms responsible for this undesired increase in electron temperature is not yet fully understood, although one of the principal processes appears to be Raman scattering of incident light by oscillations in the low-density plasma filling the interior of the target.

Because all of the energy absorbed from the laser beam initially resides in the hot electrons, it is mandatory to understand the subsequent transport of the electrons

to predict how energy can be delivered to other portions of the target. For conditions characteristic of CO₂-laser-driven targets, we have found that very large electric and magnetic fields develop as a result of the large spatial gradients in temperature and density present in the plasma. The magnetic fields are confined to within a few hundred micrometers of the surface and may exceed a megagauss. Consequently, the magnetic forces dominate the motion of most electrons, and their transport is not described by mathematical solutions of the diffusion equations. The self-consistent, theoretical treatment of plasma motion under the influence of an intense laser radiation field has been a major accomplishment by the theorists in this program.

For CO₂ laser intensities exceeding 2×10^{15} W/cm², the self-generated magnetic fields become large enough to prevent hot electrons from returning to their origins on the surface defined by the critical plasma density (10^{19} cm⁻³ for 10.6-μm radiation). As a consequence of this magnetically enforced charge separation, ions are accelerated away from the target surface. This ion "blowoff" is not efficient in driving an implosion of the fuel because the momentum per unit energy of the ions is low and represents an energy loss for open targets. The more elaborate geometries discussed in the section on capsule physics attempt to efficiently recover the energy carried by the fast ions.

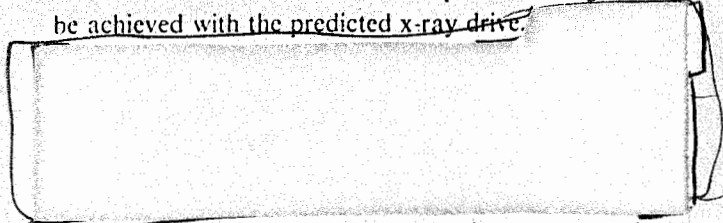
For good hydrodynamic coupling of momentum to the fuel, the ablation of a large mass at the (low) velocity set by the thermal energy content of the ablator material is required. To achieve energy deposition with a spatial profile shaped to achieve this type of ablation, researchers have turned to the technique used in thermal nuclear weapons; that is, the use of thermal x-ray radiation to drive the implosion. The basic concept in the hohlraum targets is to efficiently convert laser radiation into thermal x-rays. Unfortunately, because of the unexpectedly high electron temperatures discovered in hohlraum targets, the x-ray conversion efficiency is less than 30% when 10.6-μm laser radiation is used as the drive energy source. The reason is that the hot electrons deposit their energy much deeper in the "hohlraum wall" than can be reradiated by a radiation diffusion wave on the time scale of the target implosion. That is, the electrons heat too much mass; hence the temperature of the hohlraum is low, and the resulting conversion to x-ray radiation is inefficient. The efficiency of CO₂-laser-driven hohlraums has been improved by the utilization of the internally generated fields. That is, by reducing the hohlraum wall thickness to a few diffusion depths and

9
0
0
0
7
0

forcing the electrons to recycle through the wall many times (because of the space-charge potentials in the plasma), the energy per unit mass in the hohlraum wall and the radiation temperature are increased substantially. However, the preheat of the fuel by the recycling electrons remains a problem.

To minimize the energy needed to compress the fuel, it is necessary to minimize preheat to an energy level that places the fuel on an adiabat that does not greatly exceed $T \approx 5$ keV at the time of maximum compression. Further refinements are possible only if the central portion of the fuel is elevated to ignition temperatures by properly timed shock collisions. This central portion of the fuel can then serve as a "spark plug" to trigger heating of the remainder of the fuel by local deposition of the α -particles released in the DT reaction.

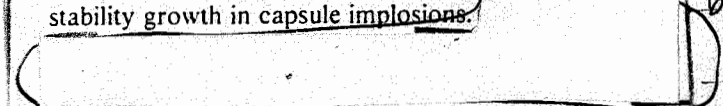
Centurion experiments along with actual capsule experiments at NTS will reveal what compression and gain can be achieved with the predicted x-ray drive.



In the Los Alamos program, we have attempted to capitalize on the great operational advantages of the CO₂ laser, the most efficient and inexpensive high-power laser yet discovered. To develop the next generation driver will require several hundred million dollars of investment. For this reason, all conceivable ways of using the absorbed energy in whatever form that might appear in the target (electrons, ions, x rays, and so forth) are being carefully and systematically explored.

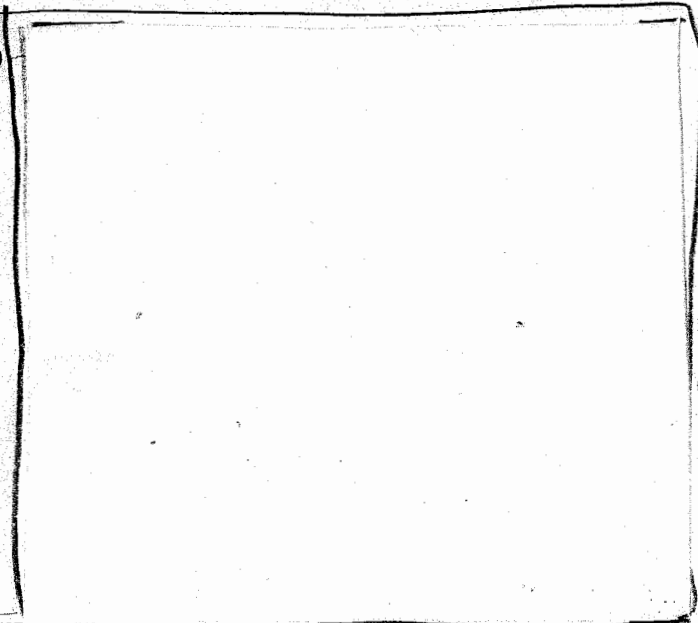
These efforts were reviewed by external panels of experts in 1982 and 1983. In the most recent review, the possible use of the large internal magnetic fields to provide insulation from preheat by hot electrons was suggested. Work in this regard has progressed to the development and computational testing of a novel target that combines advantages of both ICF and MFE by inclusion of magnetic fields for inhibition of electron thermal conduction. This target concept now is being tested using the Antares laser.

As noted above, the achievement of high density is fundamental to all ICF target performance. We have made considerable progress in developing computational techniques that are capable of predicting the extent of instability growth in capsule implosions.



The theory requires the experimental determination of coefficients that describe the drag of one fluid mixing into another. Although this is difficult experimentally, Antares may be able to determine information about these coefficients for a variety of material interfaces and thereby improve predictive capabilities for both ICF targets and weapons design.

THE CENTURION/HALITE PROGRAM



With this record of progress and the number of improvements in technology that have yet to be tried, Centurion/Halite experiments should continue as a mainstay of the ICF program for this decade. Correspondence to the NTS experiments is made by use of the coming generation of laboratory drivers. By measuring the conversion efficiencies described in steps (a) and (b) of Fig. 1, experiments with these machines will define the input required to achieve a certain energy and power of x rays. At the same time, predictive capabilities developed for

CONTRIBUTIONS BY ICF TO THE WEAPONS PROGRAM

Almost since its inception, the ICF program has been viewed as a potentially significant contributor to the understanding of the physics of nuclear weapons design. Numerous studies over the years have attempted to

b(3)

b(3)

67070510

b(3)

b(3)

define a role for ICF in weapons physics, identifying the potential for equation-of-state measurements, opacity measurements, thermonuclear burn studies once ignition was achievable, and large-scale x-ray vulnerability facilities once yields approaching 200 MJ were obtained. In recent years, the ICF program has indeed made substantial contributions to the weapons design program. In the last section of this review, an appraisal of the contributions that have been made, and are potentially to be made, is provided. These contributions are summarized below.

b(3) [Redacted]

The importance of Centurion/Halite for providing experimental information will continue until laboratory drivers capable of achieving significant thermonuclear burn are developed.

b(3) [Redacted]

- The national ICF programs would be critical to the US defense program in event of a comprehensive test ban treaty (CTBT) or a limited test ban treaty (LTBT) on nuclear testing.

b(3) [Redacted]

These drivers, in turn, can provide a means of exercising and maintaining design capability under a CTBT as well as a means of addressing the feasibility of fusion itself.

b(3) [Redacted]

- Improvements in material fabrication developed by ICF have been important ingredients in testing cer-

tain x-ray concepts for the Strategic Defense Initiatives (SDI) program.

- The Antares laser facility is a unique source of x-ray and microwave radiation and can be of direct use in studying certain SDI concepts. A future laboratory fusion facility could indeed serve an important function for nuclear vulnerability, lethality, and effects, particularly in the event of a CTBT. The Antares facility has potential for studies on laser radiation cone weapons lethality, and short-pulse, broadband microwave lethality and propagation.
- Measurements of equations of state (EOS) and opacity are now possible in both laboratory laser-driven and underground experiments. Useful confirmation of calculated high-Z opacity in the range of 100-450 eV has been obtained in recent underground tests.
- The physics of rare-gas halide lasers studied in the ICF program is highly beneficial to SDI considerations of laser weapons.

In addition to the early-identified results cited above, both the weapons and ICF programs have benefited from sharing and exchanging personnel. During its 12 years at Los Alamos, the ICF program has attracted many outstanding technical people to the Laboratory, who might not otherwise have come, and helped them develop in technical areas of direct interest to the weapons program. Specifically, more than 50 highly skilled staff members have come to work on ICF (or ICF "spin-off" programs) and are now elsewhere in the Laboratory, including at least one Laboratory Fellow and two Associate Directors.

THE FUTURE

Should our attempts to invent a CO₂ laser target that will achieve high-energy gain fail, technology development programs for both a new laser system (KrF) as well as an alternative to all lasers, a heavy ion-beam accelerator, are in progress at Los Alamos. These programs are not so much intended to provide target-shooting capabilities as to establish the cost scaling of these particular systems for potential megajoule-level systems. The research activities in these areas are

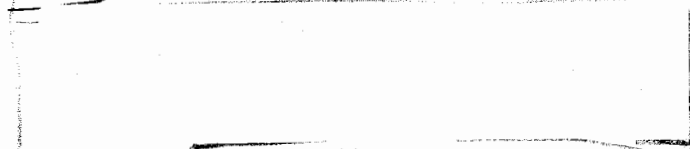
described in the unclassified portion of this two-part review.¹

Over 10 years of research have taught us a great deal about ICF on a laboratory scale, and it is certainly more difficult than originally envisioned. The inevitable inefficiencies in all the steps between providing incident energy and igniting a fuel have plagued the program.

warrants a sustained national effort. For at least the remainder of this decade, we should fully utilize the potential of the research facilities and the technology base we have already established.

REFERENCES

1. D. C. Cartwright, Comp., "Summary of Research for the Inertial Confinement Fusion Program at Los Alamos National Laboratory," Los Alamos National Laboratory report LA-10380 (March 1985).
2. H. G. Ahlstrom, *Physics of Laser Fusion, Vol. II*, "Diagnostics of Experiments on Laser Fusion Targets at LLNL," Lawrence Livermore National Laboratory (January 1982) p. 5.



b(3)

Success would give the ICF program the unique capability of proof of principle before the country is asked to commit to the construction of another driver. In our quest to provide unlimited energy by control of fusion, the workability of ICF should not be overlooked. We are still far from any practical use, but the promise

07000012

CONTRIBUTIONS BY THE ICF PROGRAM
TO THE NUCLEAR WEAPONS PROGRAM AT LOS ALAMOS

by George R. Spillman, William J. Krauser, Thomas A. Sandford, and David C. Cartwright

INTRODUCTION

Almost since its inception, the Inertial Confinement Fusion (ICF) program has been viewed as a potentially significant contributor to the understanding of the physics of nuclear weapons design. Numerous studies over the years have attempted to define a role for ICF in weapons physics, identifying the potential for equation-of-state (EOS) measurements, opacity measurements, thermonuclear burn studies once ignition was achievable, and large-scale x-ray vulnerability facilities once yields approaching 200 MJ were obtained. Recent studies by Los Alamos and Lawrence Livermore National Laboratory (LLNL)^{1,2} have reviewed the potential for significant contributions to the weapons program by the ICF laser facilities, and a recent study³ summarized specific experiments that could be conducted at the Antares facility in support of Strategic Defense Initiatives (SDI). In recent years, the ICF program has made substantial contributions to the weapons design program. In this report a realistic appraisal of the contributions that have been made, and that are potentially to be made, is provided. These contributions are summarized below.

- The national ICF programs would be critical to the US defense program in the event of a comprehensive test ban treaty (CTBT) or a limited test ban treaty (LTBT) on nuclear testing.

[Redacted]

b13

These drivers, in turn, can provide a means of exercising and maintaining design capability under a CTBT as well as a means of addressing the feasibility of fusion itself.

[Redacted]

b(3)

- Improvements in material fabrication developed by ICF have been important ingredients in testing certain x-ray concepts for the SDI program.
- The Antares laser facility is a unique source of x-ray and microwave radiation and can be of direct use in studying certain SDI concepts. A future laboratory fusion facility could indeed serve an important function for nuclear vulnerability, lethality, and effects, particularly in the event of a CTBT. The Antares facility has potential for studies on laser radiation cone weapons lethality and on short-pulse, broadband microwave lethality and propagation.
- Measurements of EOS and opacity are possible underground and have been done. Useful confirmations of calculated high-Z opacity in the range 100-450 eV have been obtained.

0 0 1 3
0 7 0

[Redacted]

b(3)

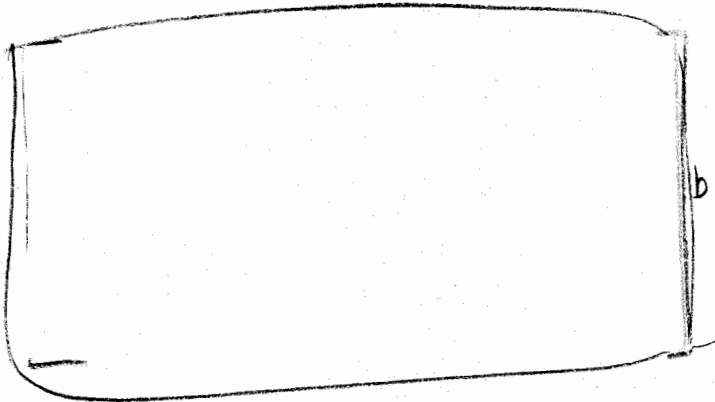
The importance of Centurion for providing experimental information will continue until laboratory drivers capable of achieving significant thermonuclear burn are developed.

[Redacted]

b(3)

- The physics of rare-gas halide lasers studied in the ICF program is highly beneficial to SDI considerations of laser weapons.

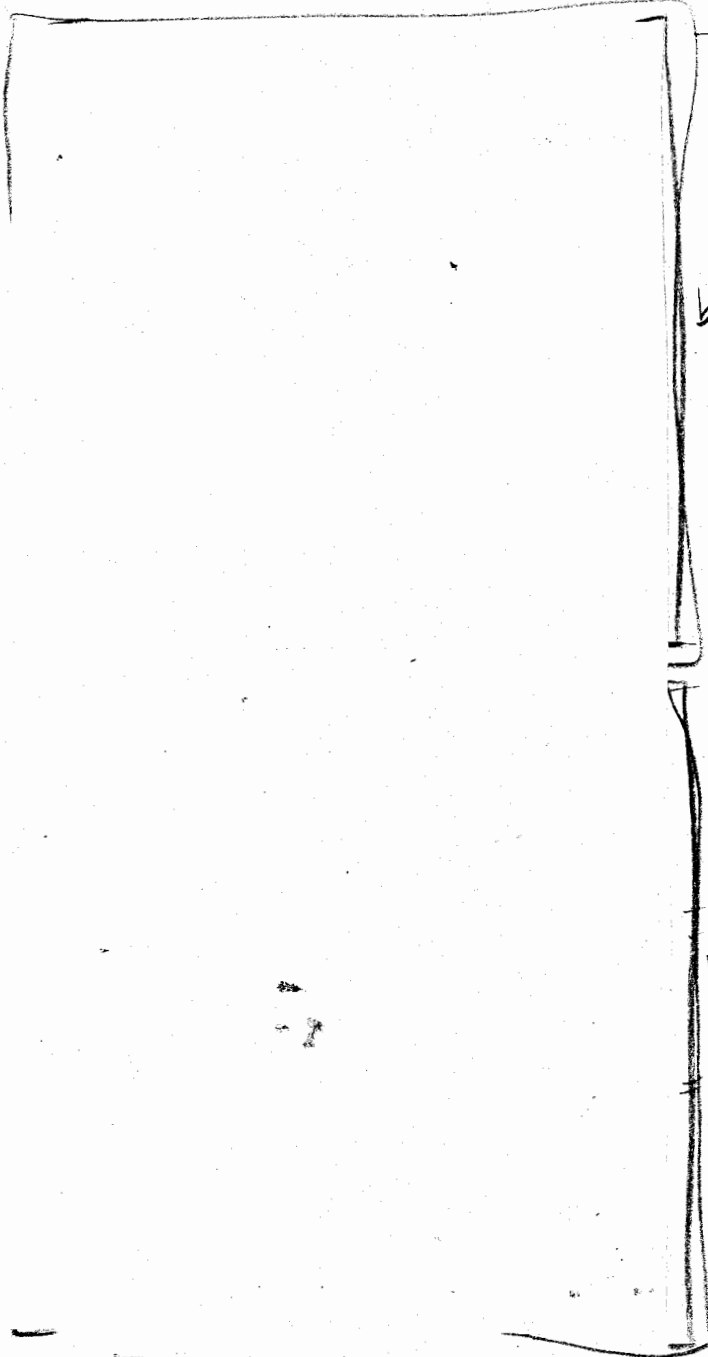
In addition to the specific examples cited above, both the weapons and ICF programs have benefited from sharing and exchanging personnel. The ICF program has attracted many outstanding technical people to the Laboratory who might not otherwise have come and helped them develop in technical areas of *direct* interest to the weapons program. The Laboratory now benefits from their contributions to other Laboratory activities.



Special Computer Code Capabilities

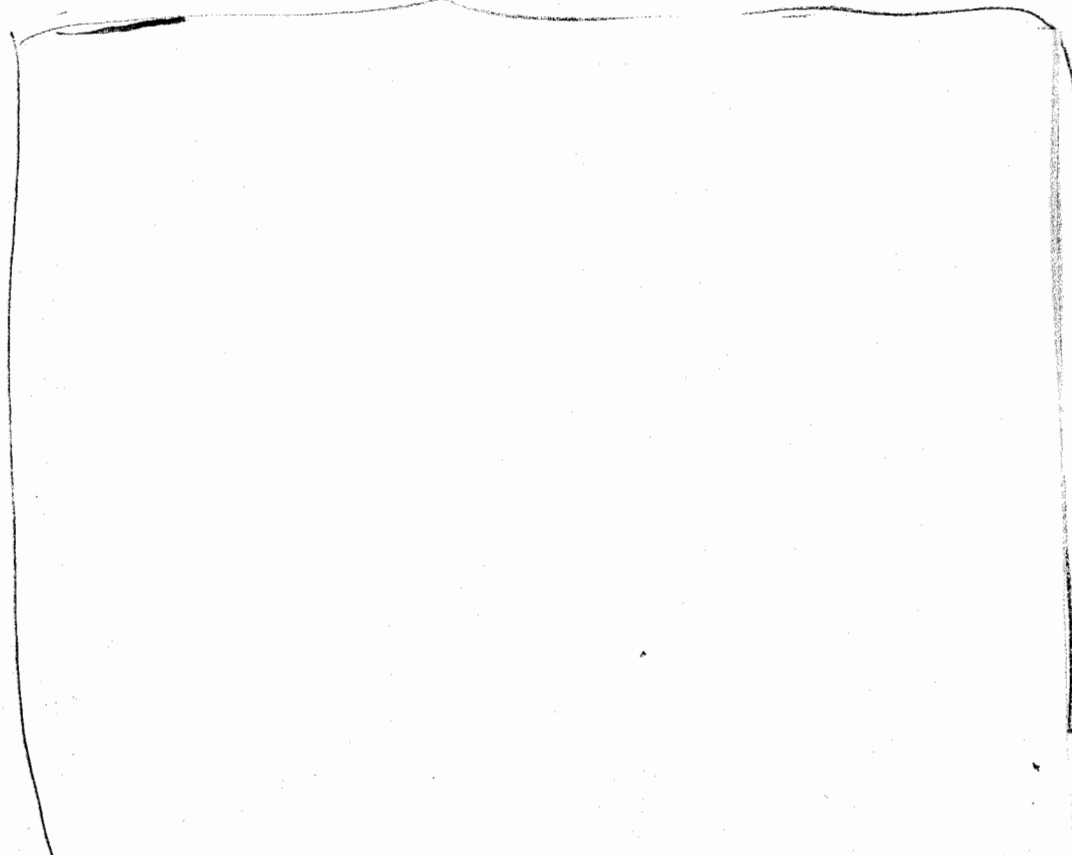
SPECIFIC CONTRIBUTIONS FROM ICF TO THE WEAPONS PROGRAM

Centurion



b(3)

67090614



b(3)

07070615
b(3)

It is significant that postshot results are in nearly perfect agreement with the preshot predictions. It is expected that increasing use of these techniques will be made in future design efforts.

b(3)

b(3)

~~SECRET/RO~~

EOS and Opacity

EOS. It has been stated² that high-pressure EOS studies could be useful to the weapons program. A properly configured, short-wavelength laser is capable of achieving pressures in excess of 100 Mbar at laser intensities of less than 10^{15} W/cm², and a significant fraction of the NOVA laser shots will be devoted to this class of experiments. The Los Alamos KrF laser facility, because of the favorable λ^{-2} scaling of the achievable pressure, could be similarly useful for EOS studies. In addition to laser-driven shocks, HE-driven devices may provide pressures up to 100 Mbar.

Opacities. The Los Alamos ICF program has produced useful data on opacity of high-Z materials at sub-keV temperatures. Experiments on Helios established that the calculated gold opacity at 100 eV was correct to within at least a factor of 2

This combination of data now confirms the calculation of high-Z opacities at near-normal densities over a wide temperature range.

(s)

670 0516

~~SECRET/RO~~

b(3)



Pure Fusion Technology and Applications

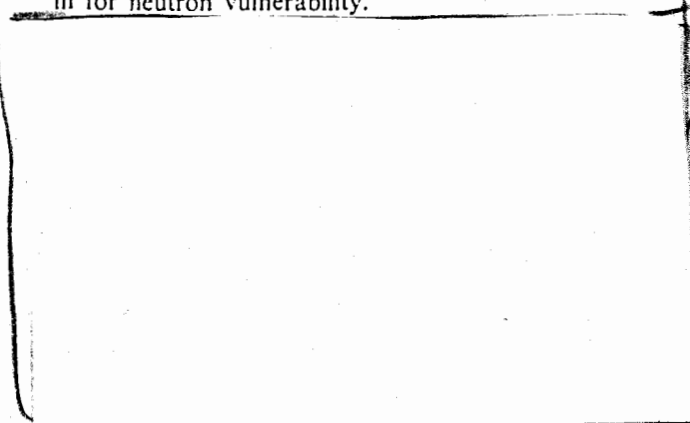
ICF studies should be expected to provide insight into the potential of pure fusion weapons, assist the development of weapons program capability to study fissionless fusion, provide a place to keep weapons design skills active in the event of a CTBT/LTBT, and eventually lead to laboratory nuclear vulnerability facilities for supplement to the Nevada Test Site (NTS) testing or replacement of NTS testing in the event of a CTBT. For example, with a capsule yield of 400 MJ and an assumed 30% x-ray yield, 230 cal/cm² could be provided at 1 m for reentry vehicle (RV) material vulnerability testing, 1 cal/cm² at 15 m for SGEMP testing, or 10¹⁵ n/cm² at 1 m for neutron vulnerability.

As discussed above, the Los Alamos weapons program is pursuing options for fusion drivers in addition to those pursued by ICF. Any ICF driver reaching fusion could provide all of the same benefits except perhaps for a possibility of weaponization.

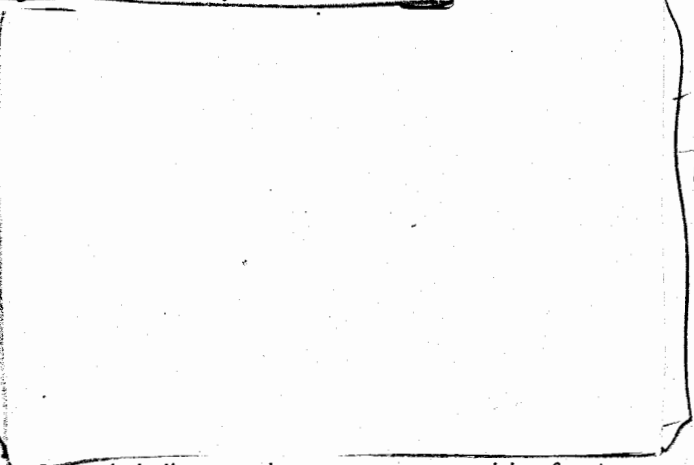
X-ray Lasers and Other SDI Applications

Use of the Los Alamos CO₂ lasers for various SDI applications has been considered including x-ray laser studies, microwave generation, microwave lethality, gamma ray lethality, and laser lethality.

b(3)



Trailmaster uses an HE-driven magnetocumulative generator to produce a large pulse of electrical energy that is rapidly switched into an inductive load (a very thin metallic cylinder) that implodes upon an axisymmetric DT capsule.

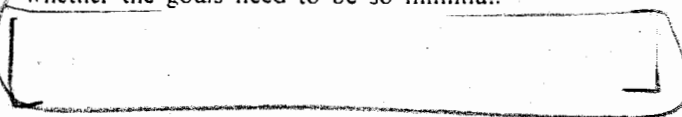


Laser lethality experiments appear promising for Antares. Theoretical studies indicate no significant effects caused by interaction differences in CO₂ and shorter wavelengths that might be applied in weapons concepts. By converting Antares to a long (2- to 5-μs) pulse, we can obtain about 200 kJ to deliver to a target, which will provide a capability for lethality experiments in a parameter regime not currently explored. Most existing

b(3)

The current Trailmaster goals for capsule drive are very similar to those of ICF, but it is not known whether the goals need to be so minimal.

b(3)



Diagnostics

b(7) This resolution represents a factor of 4 improvement over the resolution of the conventional PINEX used for weapons physics diagnostics. Central to this improvement is a new uniform taper design, 50-um-diam pinhole, which requires an innovative combination of metalworking technologies (precision vapor deposition, electroforming, electric discharge machining, and conventional precision machining) to fabricate.

are also sensitive to the models used to calculate burn performance (and instabilities).

- *PINEX Imaging Fluor Improvements.* Rarex, an imaging fluor, has been used in some PINEX applications to weapons tests because of its high light emission.

b(7) Although a small innovation, this will almost certainly be useful for certain weapons PINEX applications.

- *Advanced Diagnostics.* Although we rely primarily on the advanced technologies being developed for weapons diagnostics to improve Centurion ICF diagnostics, it is anticipated that some advances made to meet special ICF requirements will be available for the weapons program, sooner than if there were no Centurion program.

b(3) • Precision Alignment of PINEX Rack Geometry.

b(3) Distortion of the rack following alignment and downhole placement can adversely affect the actual geometry at shot time.

b(3) This alignment performance will no doubt be useful for planning diagnostics for future weapons tests.

b(3) • Tri-head Detectors.

b(3) Some of these improvements have been incorporated in PINEX systems for weapons diagnostics. Neutron data from these detectors can be used to derive the average temperature of the thermonuclear burn and

CTBT/LTBT Considerations

In the event of an LTBT or a (zero-fission) CTBT, a major concern for the national defense would be how to maintain some weapons design expertise and to be able to determine if significant advances in weapons are being made by other parties during the ban.

Under a comprehensive test ban, maintenance of expertise in secondary design would be particularly difficult. An ICF (or other pure fusion) program provides

almost the only substantial method of exercising secondary design talent and comparing calculations with experimental results.

b(3) [redacted] Even a minimal level of testing would help preserve design expertise. Some experimental input may be crucial to retaining a core staff able to resume conventional design and testing, if deemed necessary. Another crucial contribution of ICF in a CTBT could be the vulnerability/lethality testing capability that could be provided by a laboratory fusion facility as discussed earlier.

REFERENCES

1. G. Spillman, J. Brownell, G. Fraley, and D. Giovanielli, "Report of the Weapons Physics Experiments Group," Los Alamos National Laboratory memorandum P-DO/82-GRS-3 (March 1982).
2. C. T. Alonso et al., "Proposals for Laboratory Weapons Physics Experiments," Vol. 1, Executive Summary, Lawrence Livermore National Laboratory report UCRL-53293, Vol. 1, M-3679 (May 30, 1983).
3. D. C. Cartwright, D. Forslund, D. Gill, G. McCall, and F. Morse, "Applications of the Antares Laser Facility," Los Alamos National Laboratory memorandum DRP/FRA:DCC:004 (January 1985).

6707040

CAPSULE IMPLOSION PHYSICS

by George R. Spillman

THE BASIC CONCEPT OF ICF

The basic concept of Inertial Confinement Fusion (ICF), illustrated by the diagram of Fig. 1, is one in which a small mass of deuterium and tritium (DT) is contained in a shell that is heated and ablated by the driving energy. This process results in rapid outward expansion, a "rocket exhaust," of the heated regions of the outer shell (ablator/pusher), and the remaining shell moves inward, providing compression and heating of the DT fuel to conditions required to obtain thermonuclear ignition and burn. Target design variations may include a two-component (low-Z/high-Z) ablator/pusher, multiple shells, and multiple fuel regions.

Raising all the mass of the DT fuel to ignition condition by the energy of the driver (laser or ion beams) requires excessive driver energy. An alternative is to raise a small fraction of the fuel (hot spot or sparkplug) to the temperature and mass density required for ignition and depend upon the resulting explosion to ignite the rest of the fuel. For greatest efficiency, the rest of the fuel should be compressed at the lowest possible temperature (the most nearly degenerate condition). The optimum condition that can then be obtained is to compress the fuel so that stagnation is achieved (zero velocity everywhere in the fuel so that all energy is expended in compression and heating of the fuel) with uniform fuel pressure but nonuniform density and temperature.¹

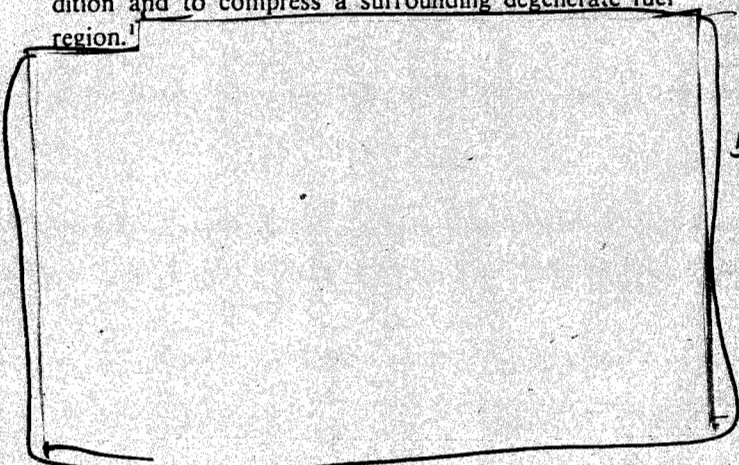
With these assumptions, we can calculate the energy required to compress a spherical hot spot to ignition condition and to compress a surrounding degenerate fuel region.¹

IDEALIZED IMPLOSION HYDRODYNAMICS

Energy/Requirements of the Fuel

The conditions for thermonuclear burn of DT fuel are that

- the fuel must be raised to a few kiloelectron-volt temperature to initiate adequate thermonuclear reactions to heat the fuel faster than it loses energy by radiation,
- the heated fuel must be thick enough (a few tenths of a gram per square centimeter) to trap the α -particle from the thermonuclear reaction to provide self-heating, and
- the thickness of the fuel region must be large enough that the fuel does not disassemble before significant burn occurs (satisfied if the time for a sound wave at the burning fuel to traverse the fuel is comparable to the time required for the fuel to burn up if stationary).



We may obtain a curve of capsule gain vs fuel energy, as shown in Fig. 2 (here x is the ratio of cold fuel pressure and energy to that for a completely degenerate gas).

Getting the Energy From Ablator to Fuel

To transfer energy into the fuel, we use the rocket-like propulsion that results from the heating of an ablating

07010021

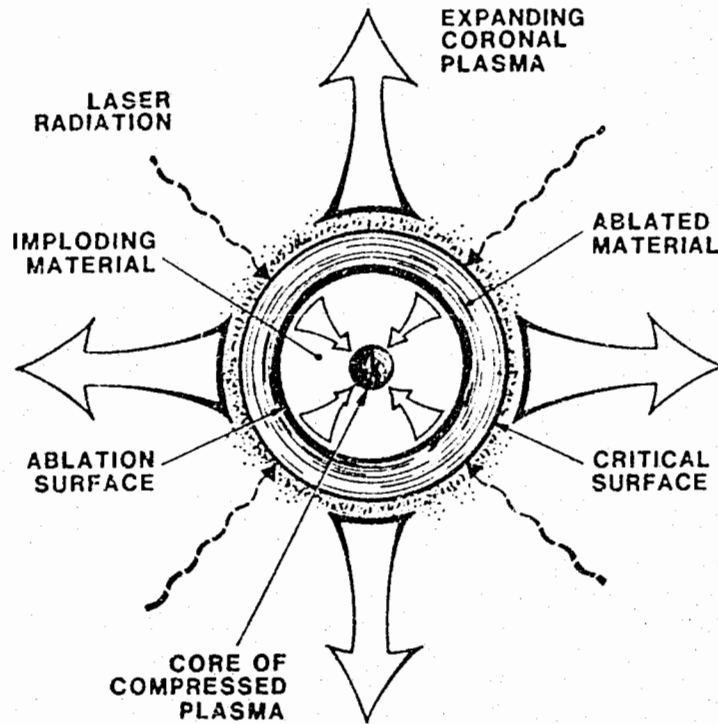


Fig. 1. Schematic for basic concept of DT capsule implosion.

ENERGY GAIN vs DRIVER ENERGY

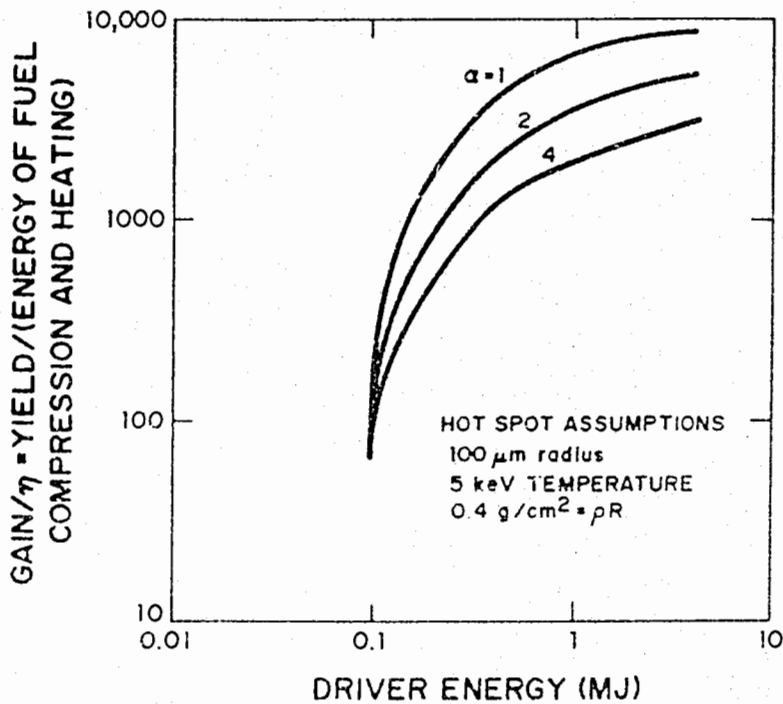


Fig. 2. Energy of fuel compression and heating.

outer layer of the capsule by the energy from the driver. The rocket exhaust is that outside part of the ablator that is heated to high temperature and pressure and expands outward at high velocity.

Simple rocket model equations show a maximum efficiency of imparting kinetic energy to a payload of about 64% for a cold, essentially uniform-velocity exhaust.³ In our case, the exhaust is not cold and does not have uniform velocity, resulting in less efficient energy transfer. We can illustrate with the following simplified example.

We consider the isothermal expansion of an ideal gas, initially at rest and bounded by vacuum at time $(t) = 0$ and $X = 0$, which is the space coordinate normal to the surface (positive toward vacuum). The speed of sound in the gas is

$$c = \sqrt{(\gamma - 1)I}$$

where I is the specific internal energy and γ is the ideal gas constant. At time t , the gas at $X \leq -ct$ is unchanged, but the gas at $X > -ct$ has expanded to a density ρ , given by

$$\rho/\rho_0 = e^{-(1 + X/ct)}$$

where ρ_0 = initial gas density and has a velocity u given by

$$u/c = (-X/ct)$$

The mass (m), momentum ($m\langle u \rangle$), and kinetic energy ($1/2 m\langle u^2 \rangle$) in the rarefaction may be obtained by integrating these two equations to obtain

$$m = \rho_0 ct \text{ and}$$

$$1/2 m\langle u^2 \rangle = \rho c_0 t^3 = mc^2 = \frac{(m\langle u \rangle)^2}{m} = m(\gamma - 1)I$$

The kinetic energy in the expansion is $(\gamma - 1)$ times the internal energy, or for $\gamma = 5/3$, 40% of the energy in the expanding gas is in kinetic energy. The momentum is only one-half that of a uniformly moving exhaust of the same kinetic energy. This suggests that for an exhaust heated externally, as by fusion driver, the efficiency of imparting kinetic energy to the fuel and pusher might drop as low as 13%. Because the expansion is not strictly isothermal and some additional internal energy may be converted to kinetic after the driver pulse is turned off

(but in time to impart added momentum to the fuel), the efficiency of conversion of ablator energy to fuel kinetic energy can be somewhat higher than 13%.

Keeping the cold fuel degenerate requires shockless (adiabatic) compression and no external (preheat) sources of heat for the cold fuel. Possible sources of unwanted preheat are energetic charged particles, particularly electrons for lasers, bremsstrahlung from hot electrons, and nuclear fragments for heavy-ion drivers. It is also appropriate to consider the heating due to an initial shock as preheat.

Achievement of ignition temperature requires high velocity, of the order of 20 cm/ μ s. Achieving such large implosion velocities without strong shocks in the fuel requires gradual buildup of velocity over much of the capsule implosion time. If we consider the fuel to be at solid density, a given mass establishes the radius and the velocity establishes a minimum implosion time. From the above discussion, it is then suggested that the main energy delivery from the driver should take place over a time. Thus,

$$t \sim 5 [M_{DT}(mg)]^{1/3} ns$$

and that the total energy delivery time should be several times that.

We have discussed capsule implosion principally in terms of energy requirements, although we have alluded to minimum requirements on implosion velocity and ignition temperature, and we have suggested some requirements on drive-pulse shape and length as well as a need for preheat minimization. These requirements are not independent for the driver or for capsule design. The requirement for minimum implosion velocity establishes a minimum acceptable ablation pressure if one is to operate at maximum rocket efficiency, optimum transfer of energy from exhaust to payload. This, in turn, establishes a requirement of minimum driving temperature. Achieving a high-drive temperature in a hohlraum may conflict with achieving low preheat and good drive uniformity.

The requirement of minimum temperature may be relieved in various ways, at least in idealized calculations. Examples include

- cryogenic targets in which the principal fuel mass is in a solid DT shell next to the pusher,
- use of multiple concentric shells in a target to obtain velocity multiplication,

- use of a large-diameter, thin pusher, and
- perhaps use of high-density pusher for more efficient transfer of energy to the fuel.

Cryogenic targets are attractive from a physics viewpoint, although difficult target fabrication and handling problems are introduced.

High-density pushers may present the possibility of an increased and more deleterious mix of pusher material into fuel, thus quenching burn. Additionally, high-density pushers imply either massive or thin shells. Massive pusher shells require additional energy, hence, reduce capsule gain. Thin shells raise the potential problem of loss of pusher integrity due to instability growth. The use of higher-density pushers may simplify fabrication problems.

Concentric shells may be used as separate pushers for the hot spot and cold fuel, providing some separation between ignition and compression functions, and not only allowing smaller driving temperature but above a threshold providing higher-calculated gain than single-shell targets. The use of additional shells results in loss of hydrodynamic efficiency. In an elastic collinear collision of a shell of mass M and initial velocity V with a stationary mass m , the initially stationary mass reaches velocity

$$v = 2V(1 + m/M),$$

and the fraction of kinetic energy transferred to the initially stationary mass is

$$\left(\frac{v}{V}\right)^2 \left(\frac{2V}{v} - 1\right)$$

Additionally, shell collisions are not purely elastic so that in typical calculations of capsule design, energy transfer efficiencies between shells are about 50%.

In principle, we could use a large-diameter ablator mass/pusher with a large ratio of ablator/pusher mass. This would allow lower drive temperature because it could be applied for a longer time, and the ratio of pusher velocity/exhaust velocity would be increased because of the mass ratio. This results in less efficient transfer of energy and lower rocket efficiency, and also introduces the same problems of thin-shell stability and integrity discussed for high-density pushers.

Problems Affecting Capsule Performance

In the preceding discussions, we have identified a number of design issues that can affect target gain or drive requirements; these issues include

- the fraction of fuel mass in hot spot or ignitor,
- excess energy in cold fuel,
- high-density vs low-density pushers,
- multiple shells, and
- pusher aspect ratio (ratio of radius to thickness).

Most of these issues are influenced by nonideal aspects of the implosion—the growth of hydrodynamic instabilities and intermixing of materials across interfaces. Instability growth is expected to limit the minimum radius of a hot spot and the useful minimum thickness of shells, and in general is expected to degrade fuel burn by mixing pusher into fuel. We believe this, the most poorly understood aspect of implosion hydrodynamics, is a fruitful and necessary area for extensive study.

From many detailed capsule calculations that have been performed at the design laboratories, best-judgment curves of capsule gain vs x-ray energy in the ablator have been derived (Fig. 3). These curves contain inherent assumptions for design constraints principally resulting from instability growth. *Ab initio* idealized calculations show much better capsule performance than these best-judgment curves. The goal of implosion physics is to develop the basis for more confident curves corresponding to that of Fig. 3 and to demonstrate the approximate drive requirements for ICF capsules. This objective necessitates extensive studies of the development and control of hydrodynamics instabilities in capsule design.

NONIDEAL HYDRODYNAMICS—THE PHENOMENOLOGY OF UNSTABLE HYDRODYNAMICS OF CAPSULE INFORMATION

In the preceding section, we mentioned several aspects of potentially deleterious effects of fluid instabilities on capsule performance. These effects included limitations on achievable minimum ignition (hot spot) radius, mixing

6700 U 24

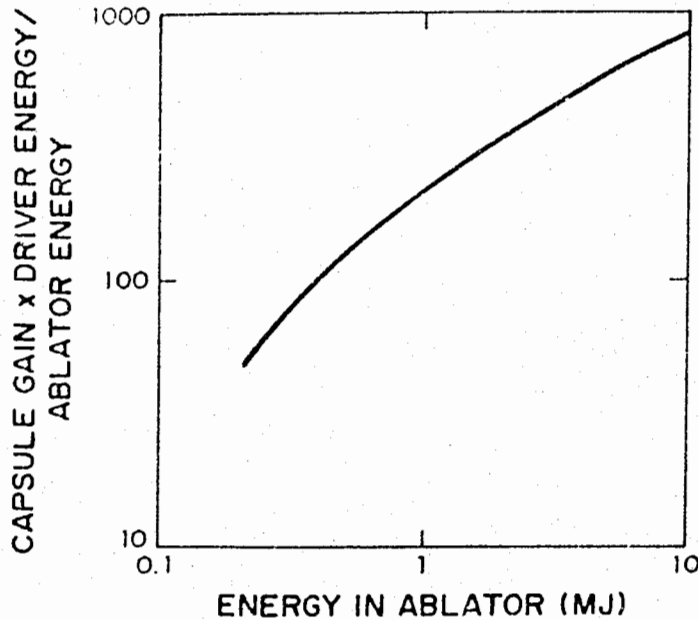


Fig. 3. Best estimate of capsule gain as a function of driver energy.

of pusher material into fuel, and limitations on minimum shell thicknesses. Hydrodynamics of unstable fluids is the least predictable aspect of the implosion and ignition physics and is expected to continue to be a major research concern of ICF for the foreseeable future.

Small Amplitude Theory

In this section, we begin by discussing the instability at a planar interface between two incompressible fluids of infinite extent and then discuss the effects of spherical geometry, finite extent, and compressibility.

The basic concept of hydrodynamic instability is illustrated by the instability inherent in a dense fluid in a gravitational field supported by a light fluid, or equivalently, a dense fluid accelerated by a light fluid.⁴ If a dense, incompressible fluid of infinite extent is bounded along a surface that is planar except for a sinusoidal perturbation of wavelength λ and amplitude $a \ll \lambda$, the amplitude will change (as long as it remains small) under the gravitational acceleration (g) according to the equation

$$\frac{d^2a}{dt^2} = \sigma^2 a$$

where σ is defined from

$$\sigma^2 \cong \frac{2\pi g\alpha}{\lambda}$$

and α is the Atwood number defined by the densities (ρ^1, ρ^2) on either side of the interface,

$$\alpha \cong \frac{\rho_1 - \rho_2}{\rho_1 + \rho_2}$$

and the product $g\alpha$ is taken as positive when the acceleration is in the direction from light fluid to dense fluid. Two cases of particular interest are those of a sudden, impulsive acceleration [$g = \pm v\delta(t)$] and a constant acceleration. If we start from an initial amplitude, a_0 , rate of change, \dot{a}_0 , integration of the growth equation gives

$$\begin{aligned} \dot{a}(t) &= a_0 2\pi\alpha v/\lambda + \dot{a}_0, \text{ and} \\ a(t) &= (a_0 2\pi\alpha v/\lambda + \dot{a}_0)t + a_0 \end{aligned}$$

for impulsive acceleration, or

$$a(t) = a_0 \cosh \sigma t + \frac{\dot{a}_0}{\sigma} \sinh \sigma t \quad (\sigma^2 > 0)$$

$$= a_0 \cos |\sigma| t + \frac{\dot{a}_0}{|\sigma|} \sin |\sigma| t \quad (\sigma^2 < 0)$$

for constant acceleration.

From these equations, note the following.

- The effect of an impulsive acceleration on an initially stationary perturbation is growth (Richtmyer-Meshkov instability). If the acceleration is from light to dense fluid, an amplitude reversal occurs.
- A constant acceleration from heavy to light is stabilizing. In the case of an impulsive acceleration followed by a constant acceleration from heavy to light fluid, the linear growth is limited to an envelope

$$|a| < a_0 \left(1 + \sqrt{\frac{2\pi a}{\lambda g}} v \right)$$

where, as before, v is the impulsively delivered interface velocity.

- An acceleration from light to heavy fluid leads to exponential growth (Rayleigh-Taylor instability). This growth generally is much faster than that due to impulsive acceleration in a capsule, but at the pusher/fuel interface the time available for the impulsively driven growth may be much longer than that for decelerative growth.

The instability problem as we have discussed it so far has been limited to the perturbed planar interface between two infinite incompressible fluids. ICF capsules are not planar, incompressible, or infinite.

Finite shell thickness may allow interface perturbations to propagate all the way through a shell; that is, the shell may break up. Also, the perturbation in fluid motion is not limited to the interface.

For an incompressible planar fluid layer of thickness d , which has an initial perturbation on side 1 that grows because of an acceleration to amplitude a_1 and a side 2 that is initially smooth, an amplitude a_2 will develop on side 2 given by³

$$\frac{a_2(t)}{a_1(t)} \approx e^{-2\pi d/\lambda}$$

Therefore, a perturbation may grow at an interface that would be described as stable from infinite medium calculations; that is, the perturbation can feed through from one interface to another.

Perturbations at a converging interface in the absence of accelerations will grow (to maintain the volume of the perturbation for incompressible flow).⁴ For impulsively accelerated interfaces, the result of convergence of a spherical interface from radius R_0 to $R = R_0/C_R$ is a multiplication of the growth by a factor

$$C_R(C_R + 1)/2$$

Compressibility is sometimes estimated in terms of uniform compression in which the perturbations are simply compressed, or decompressed, with the material. The finite sound speed in compressible fluids also results in transient oscillations for a few sound transit times over a wavelength. This may be of particular importance for feedthrough of perturbations in thin shells.

Large-Amplitude Instability Growth and Mix

As the perturbation wavelength becomes large (comparable to a wavelength), the growth becomes more complex and difficult to predict from *ab initio* theory. The growth slows, the shape becomes distorted by shear instabilities (Kelvin-Helmholz) because of relative motion of the two fluids, and perturbations of different wavelengths interact with one another. First, we discuss the asymptotic behavior of single-wavelength perturbations and then discuss the effects of the presence of more noisy initial perturbations that give rise to multiple modes (wavelengths) and mode interaction.

As the perturbation grows in the Rayleigh-Taylor instability, it develops into a buoyantly rising bubble of light material penetrating dense material and spikes of dense material penetrating light. The bubbles rise with a velocity that is constant for constant acceleration given by

$$v_B \sim \sqrt{g\lambda}$$

where the proportionality constant is a weakly varying function of the density ratio across the interface. For an infinite density ratio, the spike penetrates to the free-fall

line, the position the interface would have reached if the acceleration had been zero. For finite density ratio, shear instability along the spike deforms the spike, blunting it into a "mushroom" shape, which, from 2D hydrodynamics simulations, in the far asymptotic region penetrates at a rate proportional to but larger than the bubble velocity. The ratio of bubble to spike growth is also a function of density.⁵

The theory of asymptotic multimode growth is based upon dimensional and heuristic arguments, 2D hydrodynamics simulations, and a few experiments.

Dimensional and heuristic arguments suggest that, at an interface, two fluids subjected to a constant acceleration will mix turbulently so that the dominant perturbation wavelength (λ_D) in the mix region and the thickness of the mixed region (l_m) both grow in time:

$$\lambda_D \sim f(\rho_1/\rho_2)gt^2 \text{ and}$$
$$l_m \sim h(\rho_1/\rho_2)gt^2 .$$

Note the consistency with the bubble growth formula for single modes for which

$$v_B \sim \sqrt{g\lambda} .$$

The mechanism for λ_D to increase with time is thought to be vortex combination. The increase of λ_D with time is expected from 2D turbulence theory, but is not so clearly expected from 3D turbulence theory.

For slowly varying acceleration, one might argue from the linear equations that to preserve the correct growth parameter the factor gt^2 should be replaced by

$$[\int \sqrt{g} dt]^2 .$$

For impulsive acceleration, we note that the preceding equation for l_m is derivable from

$$\frac{d^2 l_m}{dt^2} \sim gh(\rho_1/\rho_2) ,$$

and for $g = v\delta(t)$ we could integrate to obtain

$$l_m \sim h(\rho_1/\rho_2)gt .$$

Not only are the forms of these equations *ad hoc*, but coefficients are required to use them in a quantitative way. The 2D hydrodynamics simulations and a few experiments with incompressible fluids indicate that a reasonable choice is

$$l_m = a_B + a_s .$$
$$a_B \approx 0.07 \text{ } \mu g t^2 , \text{ and}$$
$$a_s \approx (1.5 \text{ to } 2.5) \times a_B ,$$

where a_B is the distance of penetration of light fluid into heavy and a_s is the distance of penetration of heavy fluid into light.

Bubble penetration, as calculated from the above formula, typically exceeds that calculated for a single mode by the time the single-mode growth is a wavelength.

The form of equations to be integrated within hydrodynamic codes is different from that above and will be discussed very briefly in a subsequent section.

THE RESEARCH PROGRAM IN IMPLOSION PHYSICS

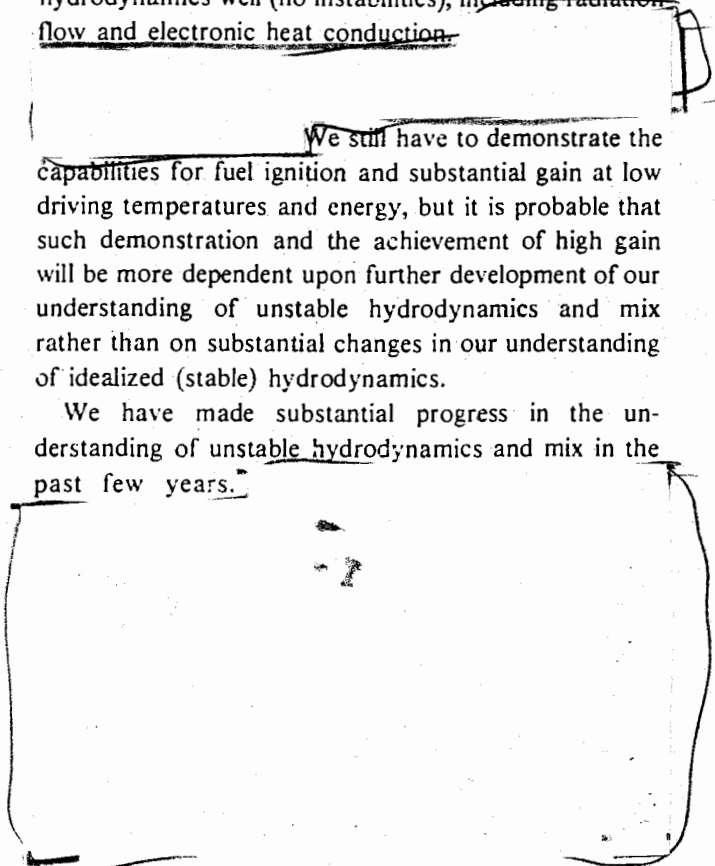
Summary and Introductory Comments

In the preceding sections, we presented a discussion of simplified phenomenology of implosion physics. In this section, we concentrate on discussion of research that addresses the phenomenology in quantitative detail.

We generally believe that we can calculate idealized hydrodynamics well (no instabilities), including radiation flow and electronic heat conduction.

~~We still have to demonstrate the capabilities for fuel ignition and substantial gain at low driving temperatures and energy, but it is probable that such demonstration and the achievement of high gain will be more dependent upon further development of our understanding of unstable hydrodynamics and mix rather than on substantial changes in our understanding of idealized (stable) hydrodynamics.~~

We have made substantial progress in the understanding of unstable hydrodynamics and mix in the past few years.



670, 0-27

[Redacted]

[Redacted] The more sophisticated, and less well understood, physics aspects associated with coupling to the driver are more *ad hoc* and parameterized.

b(3)

An unstable hydrodynamics experimental program is planned at the Antares laser to provide the necessary input and represents a new approach to mixing, which promises the potential of a breakthrough in predictive capability.

[Redacted]

b(3)

The achievement of this goal requires improvements in ideal hydrodynamics efficiency by pulse shaping and more and more quantitative, detailed understanding of unstable hydrodynamics as we proceed to the lower driving temperatures and energies corresponding to ICF. Fortunately, the two aspects of the problem, improved ideal hydrodynamic efficiency and control of instabilities, appear to be compatible. As we noted in the previous section, continued acceleration at the pusher-fuel interface as required for efficient compression is also stabilizing.

[Redacted]

b(3)

However, as we have also discussed, problems may arise due to instabilities at other interfaces. Ultimate capsule design may involve very careful tradeoffs among various aspects of the instability problem, idealized efficiency, and aspects of the capsule drive.

Much fusion design work incorporated instability considerations through lore, such as

The theoretical gain curve of Fig. 3 includes judgment of the constraints imposed by instability growth and mix. As judgment is replaced by understanding, the replacement for this curve may be more optimistic or more pessimistic.

- mix follows the "free-fall line" (extends into fuel from zero-order interface to $\int \int g dt' dt$)
- do not allow free-fall line to penetrate more than ϵ of fuel,
- require that fuel calculate to ignite with inner ϵ deduced,
- turn off yield calculation when the second reflected shock reaches the pusher,
- perturbations grow only during the "unstable" phase (when acceleration is from light to dense material),

6700

The Calculation Techniques

Idealized (Stable) Hydrodynamics—The LASNEX Code. LASNEX is the workhorse code of ICF.

[Redacted]

b(3)

- perturbations of wavelength λ grow up from initial perturbations of wavelength λ ,
- the most dangerous wavelength is one comparable to a shell thickness,
- the shell aspect ratio ($r/\Delta r$) should be limited to some maximum, and
- the convergence ratio (r_0/r) should be limited to some maximum.

existing perturbation codes may not be reproducing the Richtmeyer-Meshkov instability.

The SACI code is being written to provide a new and careful look at first-order perturbation theory. It is demonstrating reproduction of the Richtmeyer-damped oscillation about the incompressible-like interface solution for shocks. Additionally, it is showing transient behavior (oscillations) propagating away from the interface, which may present worse interface coupling problems than predicted from incompressible theory.

SACI is also predicting greater pusher/fuel interface instability growth with increasing implosion velocity.

A drop in performance at lower velocities is believed to be due to preburn temperature, which is too low. It is tantalizing to associate the performance drop at higher velocities with the SACI-predicted instability growth, but this cannot yet be confidently done.

At present, SACI does not include the equations of radiation diffusion, and this will be part of the continued development.

Global Perturbation Theory (Small Amplitude Growth)—The DOC and SACI Codes. A more nearly complete way to treat instability growth in the small amplitude regime is via first-order perturbation theory. In the DOC code,⁷ the radiation diffusion or conduction and hydrodynamics equations are solved as a zero-order solution (idealized, stable hydrodynamics) obtained from a standard radiation hydrodynamics code plus a first-order spherical harmonic perturbation. The solution of perturbation variables is on the whole mesh rather than just at interfaces, which gives the propagation and transient behavior of disturbances throughout the mesh due to perturbations introduced anywhere in the problem. As noted above, the perturbation technique allows consistent solution of the hydrodynamics equations with equations of energy transfer as well.

The basic limitation of perturbation theory codes is limitation to small amplitude. Even with a first-order perturbation, there is currently some controversy over possible neglect of terms, and there is some suggestion that

As a result, experiments are required to provide coefficients for the phenomenological equations and also to check upon assumptions of functional dependence.

Post-processing codes have been developed by Youngs and Roberts,⁸ AWRE, and Burke and Rupert, LLNL.

SECRET

b(3)

6707 UN 29

b(3)

b(3)

b(3)

KCl SHOULD BE SEEN IN EMISSION,
ONLY IF MIXED INTO CORE

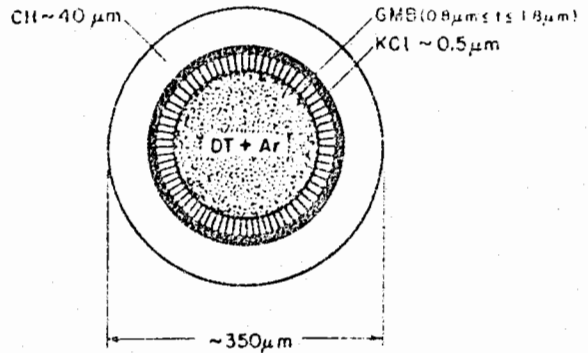


Fig. 4. Capsule for shell breakup experiment.

A major effort is planned on unstable hydrodynamics with the Antares laser facility

Preliminary work was done on the Helios laser to prepare for an unstable hydrodynamics program on Antares. The potential of using both x-ray backlighting (shadowgraphy) and self-emission for diagnostics was explored. The capability of the laser to provide pulsed uniform backlighting line sources of photon energy up to 25 keV was demonstrated. The capability of achieving uniform cylindrical implosions and the degrading effects of planned initial perturbations were demonstrated; cylindrical implosions are potentially interesting for instability studies because of diagnostic accessibility while retaining convergence effects on instability growth. A technique of detecting mix from thermally excited x-ray spectra, used earlier in diagnostic interpretation of high-fuel-density implosion experiments, was also demonstrated.

Planar experiments will use the x-ray backlighting technique to obtain photographs of the distribution of two materials in a mixed region. Characteristic x radiation (K_{α}) from the backlighter driven by the hot electrons in a laser-driven cylindrical hohlraum will be photographed by pinhole cameras with x-ray filters. Time resolution is provided by the short pulse length of the laser.

A schematic of a target for a spherical mix experiment is shown in Fig. 4. Pusher and gas are differentiated by the much higher temperature in the gas at final compression. The width of the argon x-ray lines is used to obtain the compressed gas density and the slope of the continuum gives the gas temperature. If the potassium

chloride shell is mixed into the gas, emission characteristic of potassium and chlorine will also be observed.

A characteristic spectrum for this experiment (Fig. 5) shows argon in emission but potassium and chlorine in absorption only. This demonstrates that the pusher shell in this experiment did not break up as a result of instabilities. Similar and much earlier experiments had indicated shell breakup for severely asymmetric drive conditions, which has not been repeated in recent experiments.

REFERENCES

1. J. Meyer-ter-vehn. "On Energy Gain of Fusion Targets: the Model of Kidder and Bodner Improved." *Nuclear Fusion* 22, 4 (1982).
- 2.
3. G. I. Taylor. "The Instability of Liquid Surfaces When Accelerated in a Direction Perpendicular to Their Planes I." *Proc. Roy. Soc. A* 201, 192 (1950).

4. M. S. Plesset, "On the Stability of Fluid Flows with Spherical Symmetry," *Jour. Appl. Phys.* 25, 96 (1954).

the Inertial Confinement Stability Code DOC," Los Alamos Scientific Laboratory report LA-7214-MS (November 1978).

5.
6.

b(3)

8. P. David Youngs and Peter Roberts, JOWOG-37, Aldermaston England, December 3-7, 1983.

9.

b(3)

7. Anthony J. Scannapieco and Charles W. Cranfill. "A Derivation of the Physical Equations Solved in

67070502

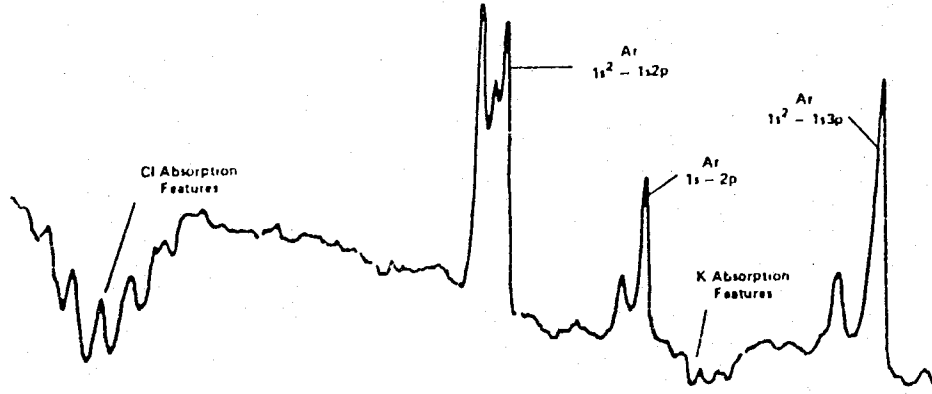


Fig. 5. A typical observed spectrum that shows K, Cl in absorption only.

67090533

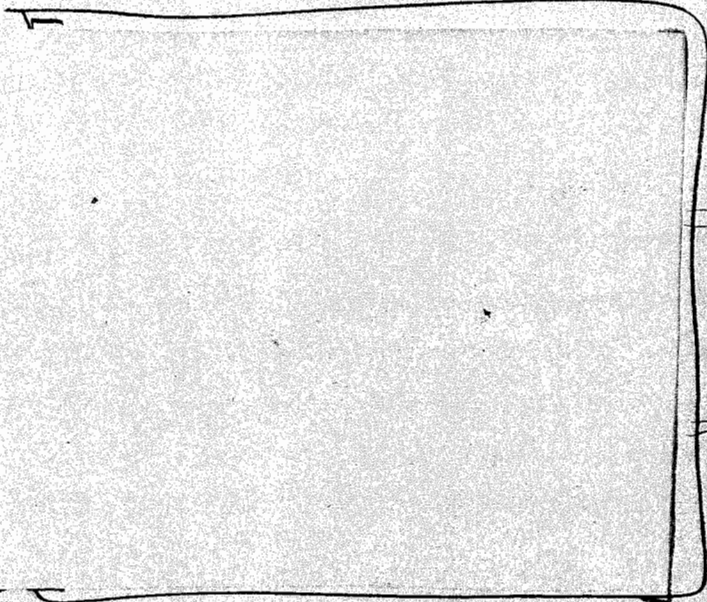
UNCLASSIFIED

THE CENTURION PROGRAM

by Thomas A. Sandford, Douglas C. Wilson, Robert H. Day, Frederick A. Morse, Elbert W. Bennett,
Roddy B. Walton, Charles A. Wingate, and Warren R. Doty

INTRODUCTION

In the late 1970s the Inertial Confinement Fusion (ICF) program determined that the feasibility of reactor capsule ignition and burn should be pursued in parallel with laser and ion driver development using underground nuclear tests.



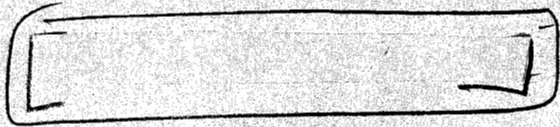
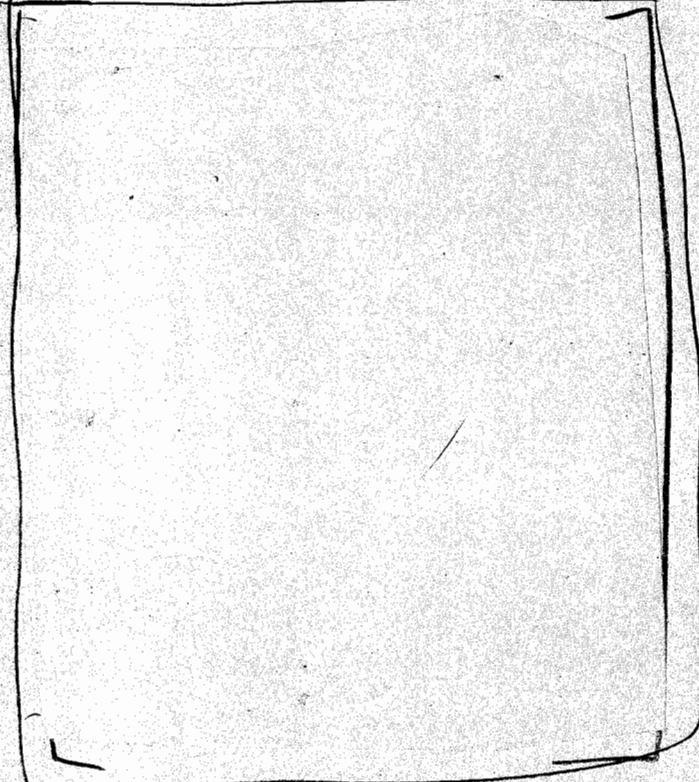
b(3)

b(3)



67070534

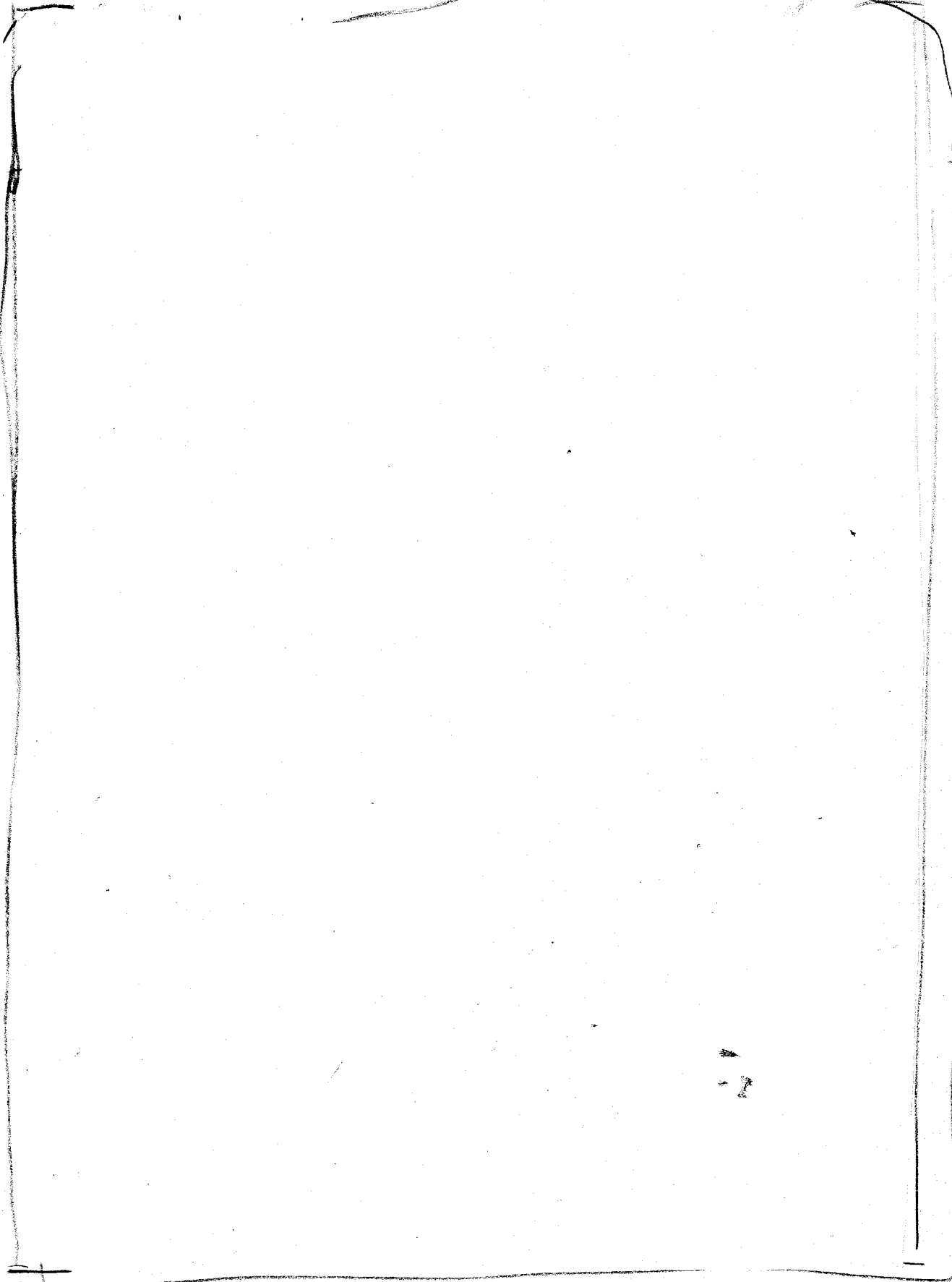
b(3)



b(3)

UNCLASSIFIED

~~SECRET/BD~~



b(2)

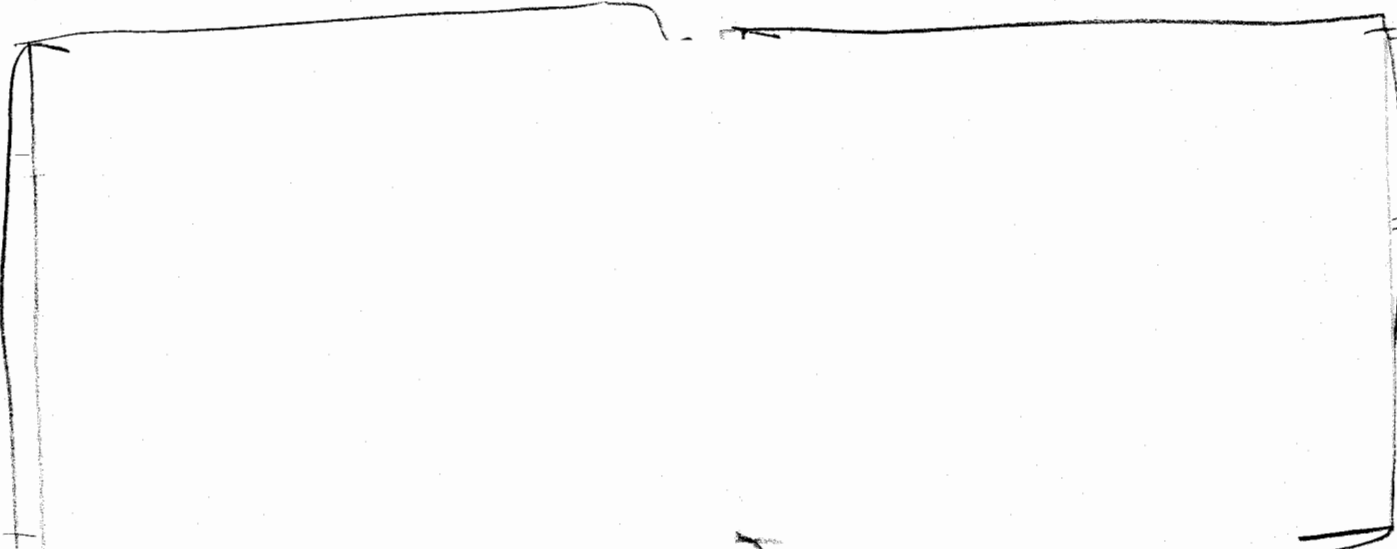
6707 UJ35

UNCLASSIFIED

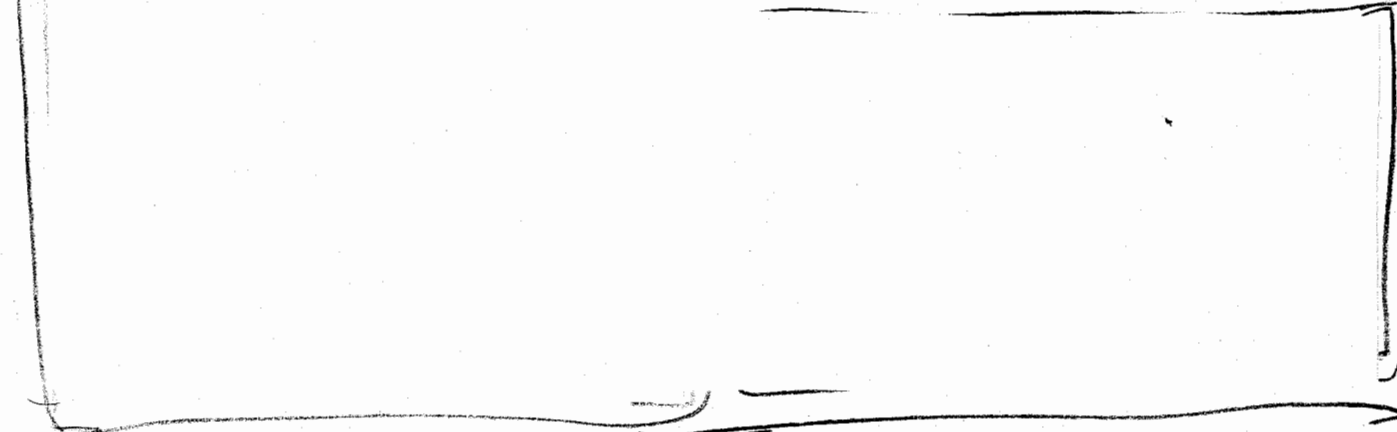
~~SECRET/BD~~

UNCLASSIFIED

~~SECRET / RD~~

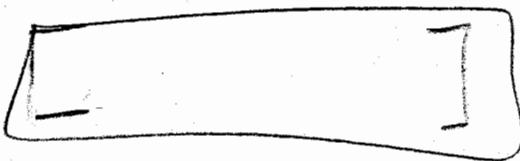


Introduction

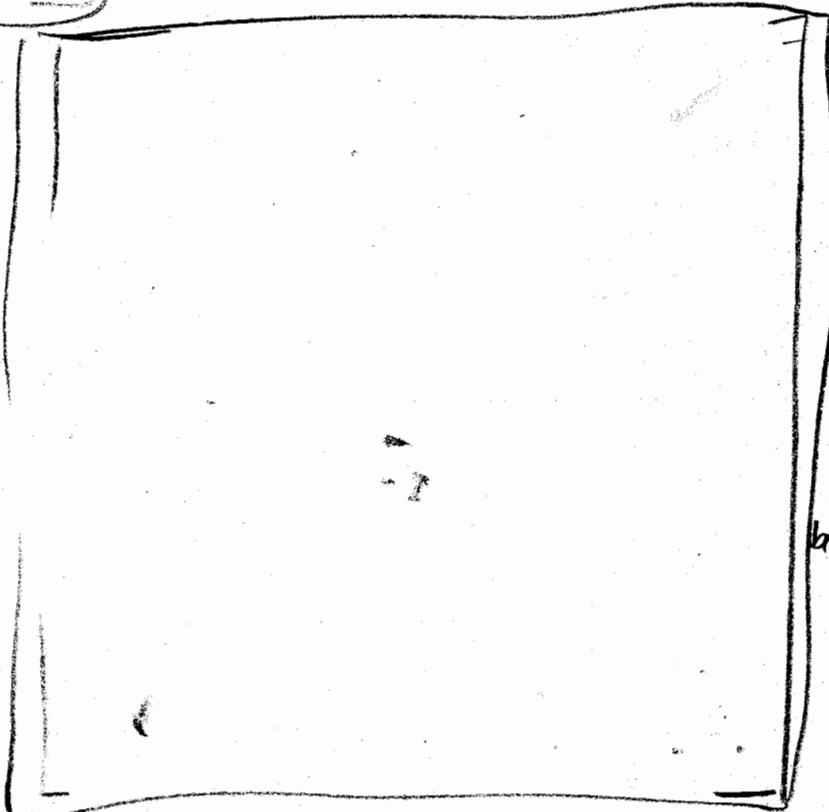


b(3)

67070536



b(3)

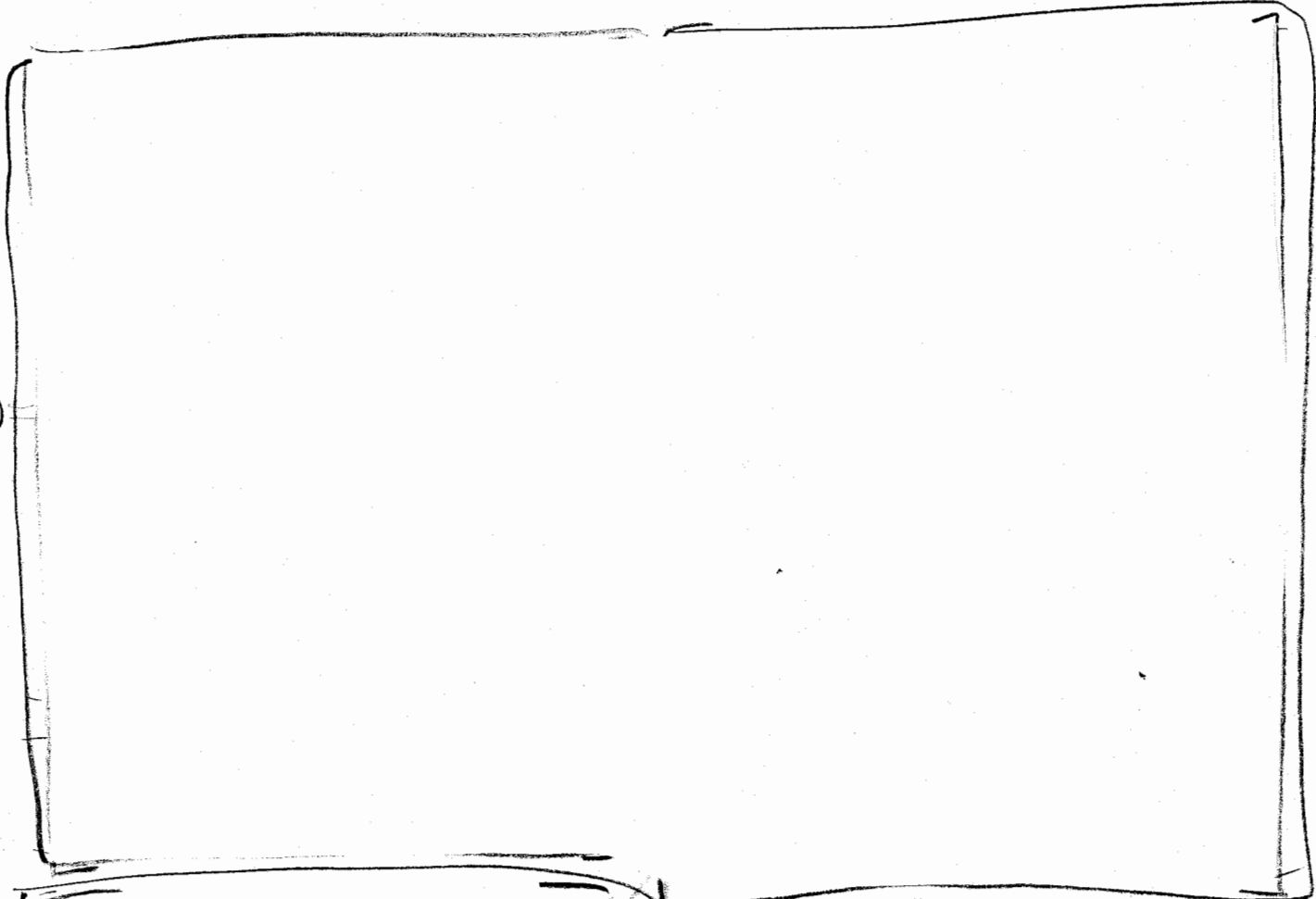


UNCLASSIFIED

~~SECRET / RD~~

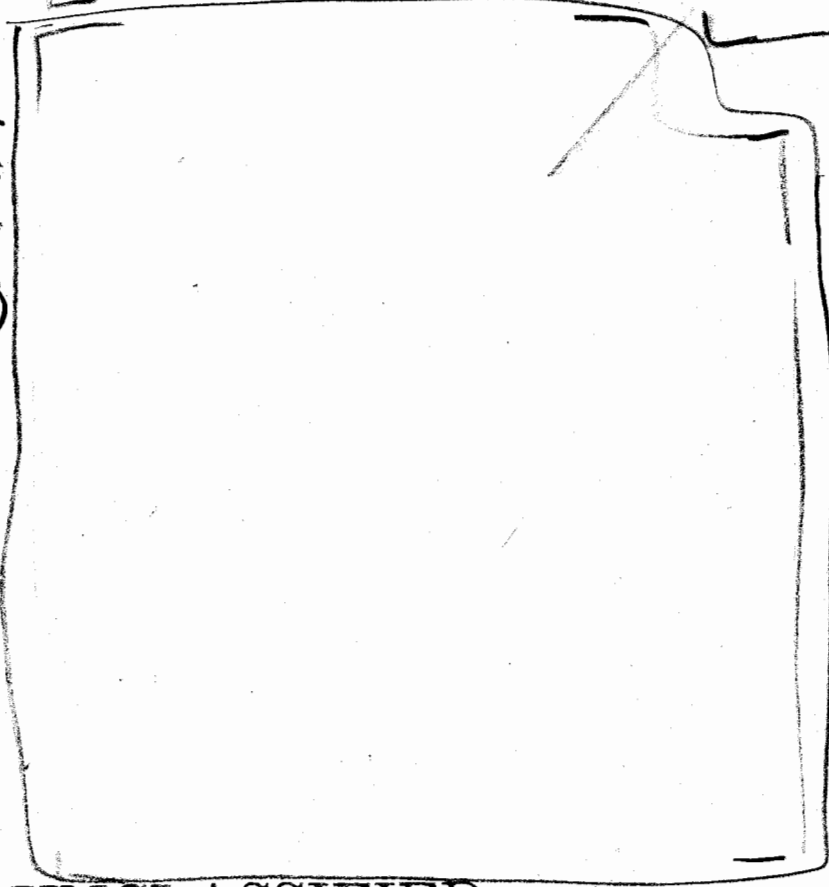
UNCLASSIFIED

~~SECRET/RD~~



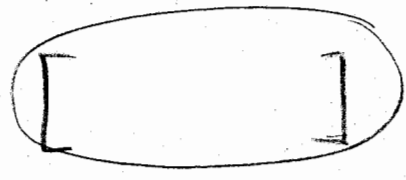
b(3)

b(3)



b(3)
b(7)(D)

b(3)



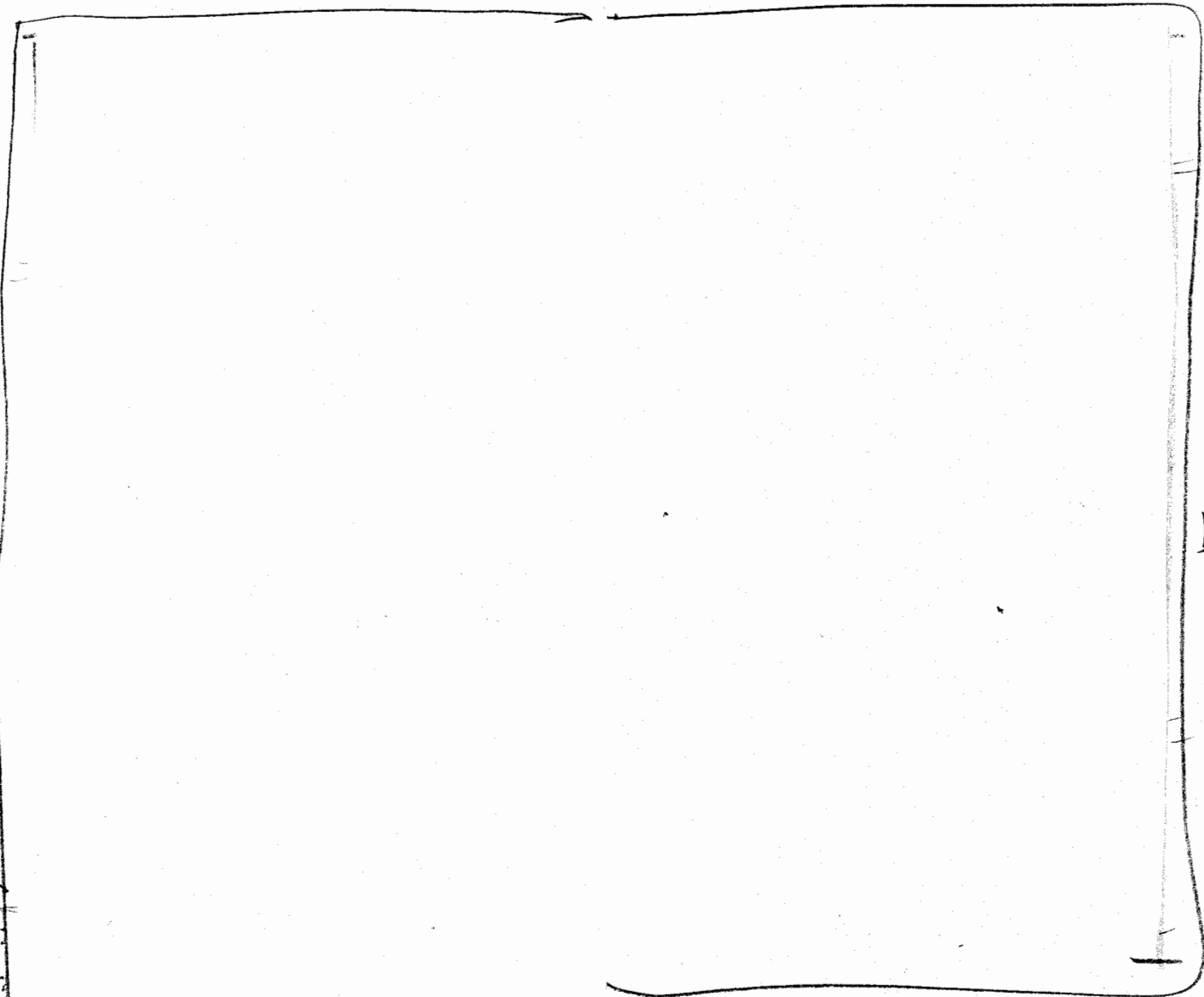
b(3)

UNCLASSIFIED

~~SECRET/RD~~

UNCLASSIFIED

~~SECRET~~ / RD



Capsule Experiments



b(3)

6700000000

b(3)

b(3)

UNCLASSIFIED

~~SECRET~~ / RD

UNCLASSIFIED

~~SECRET~~ /RD

b(3)

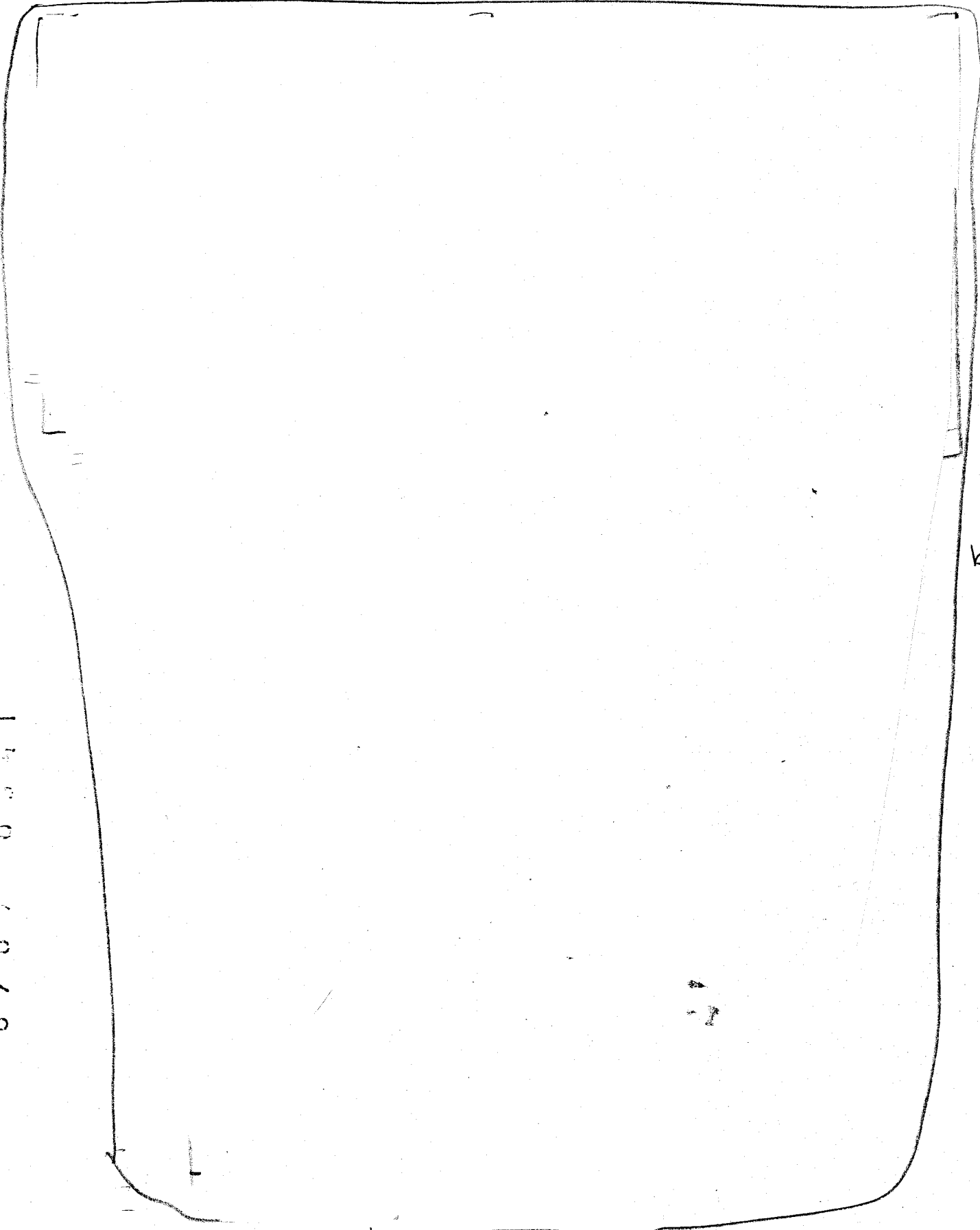
670 / 0 10

UNCLASSIFIED

~~SECRET~~ /RD

UNCLASSIFIED

~~SECRET/AD~~



67070341

b1

UNCLASSIFIED

~~SECRET/AD~~

UNCLASSIFIED

~~SECRET~~ / RD

6707 0002

UNCLASSIFIED

~~SECRET~~ / RD

UNCLASSIFIED

~~SECRET~~ / RD

b(3)

6707 0343

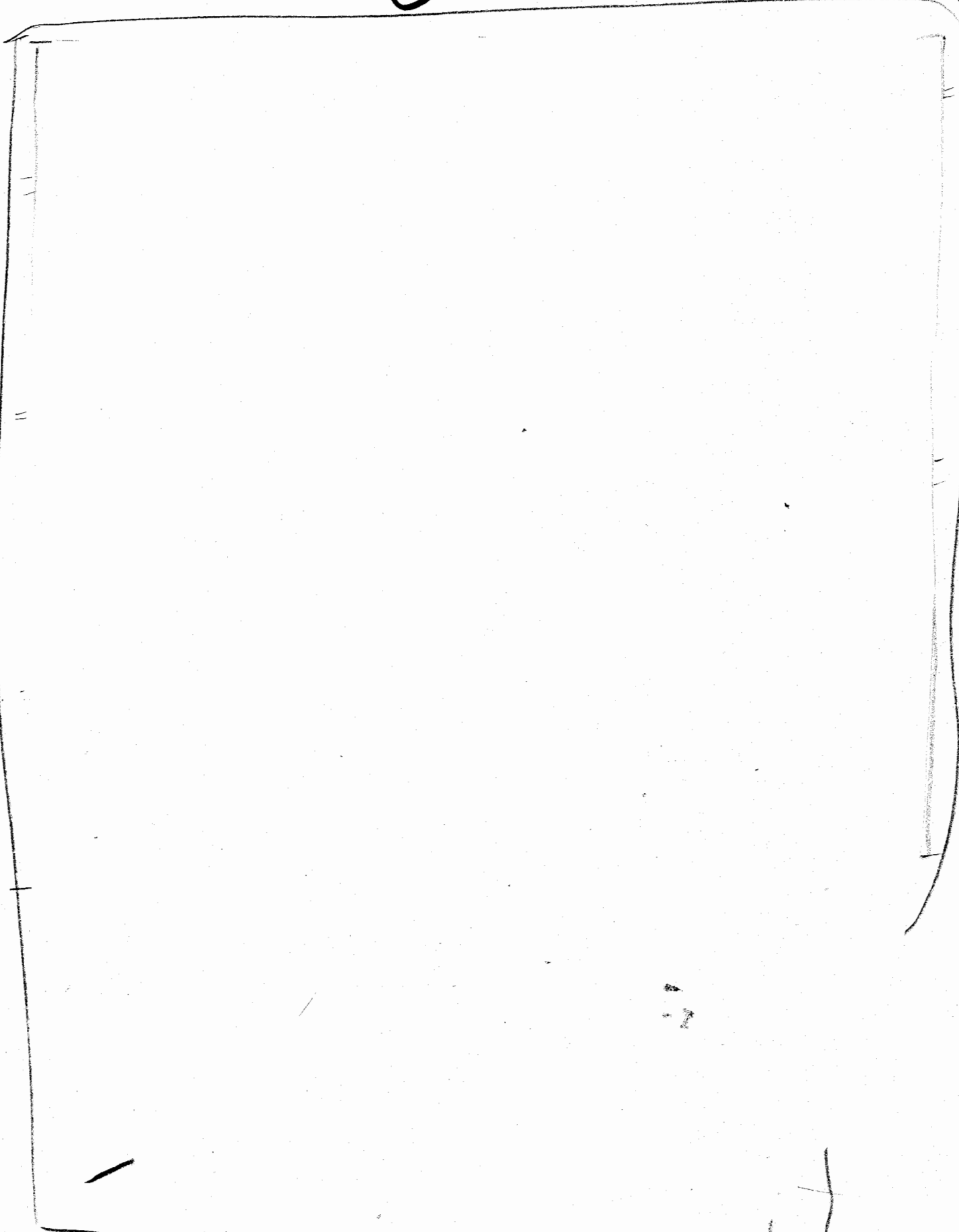
UNCLASSIFIED

~~SECRET~~ / RD

UNCLASSIFIED

~~SECRET/RD~~

b2



67080544

UNCLASSIFIED

~~SECRET/RD~~

UNCLASSIFIED

~~SECRET~~ /AD

b(3)

6700 U.S. 15

UNCLASSIFIED

~~SECRET~~ /BD

b(3)

Diagnostics

b(3)

Success of the experiment depended upon being able to characterize these quantities.

b(3)

0

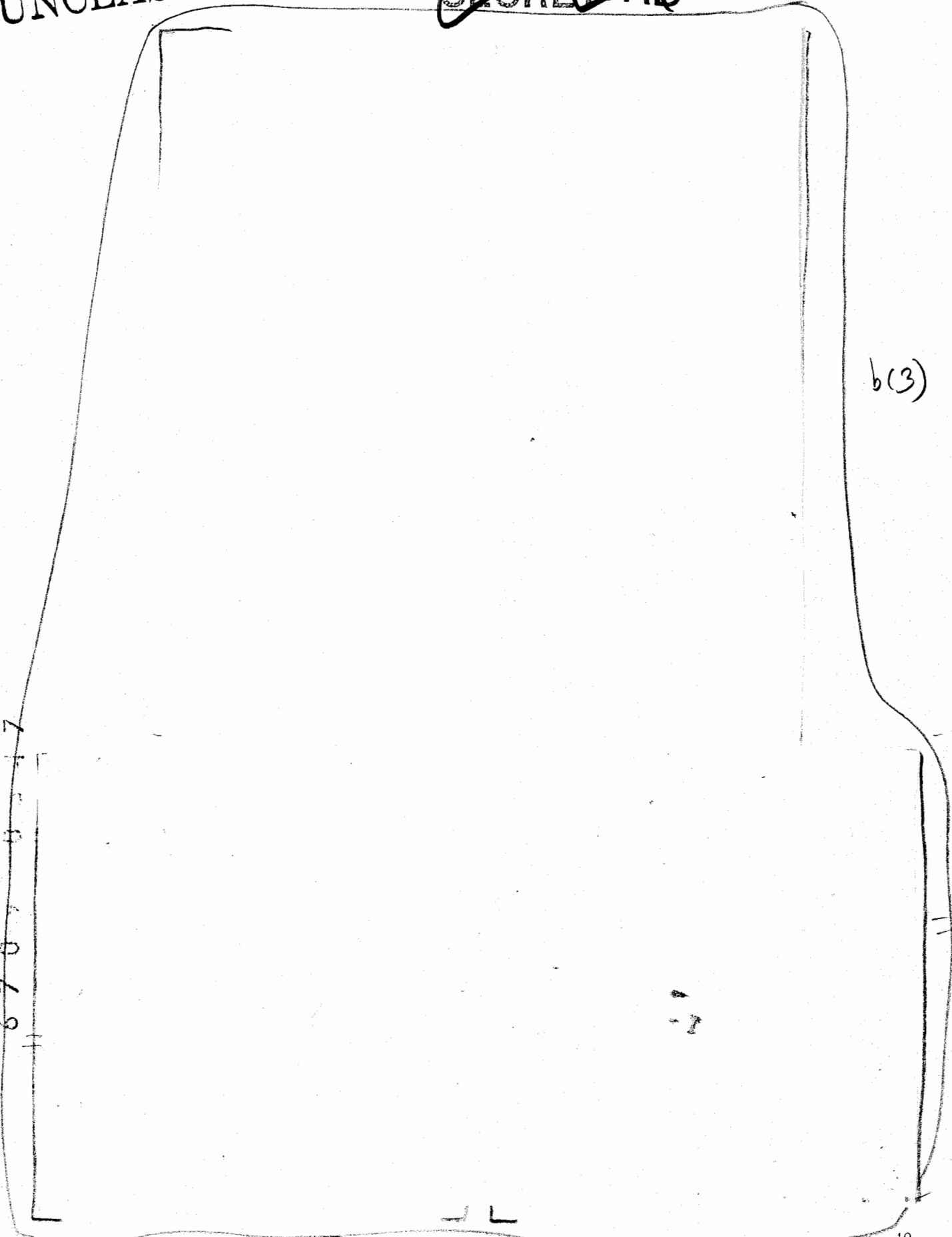
0

0

b(3)

UNCLASSIFIED

~~SECRET/RO~~

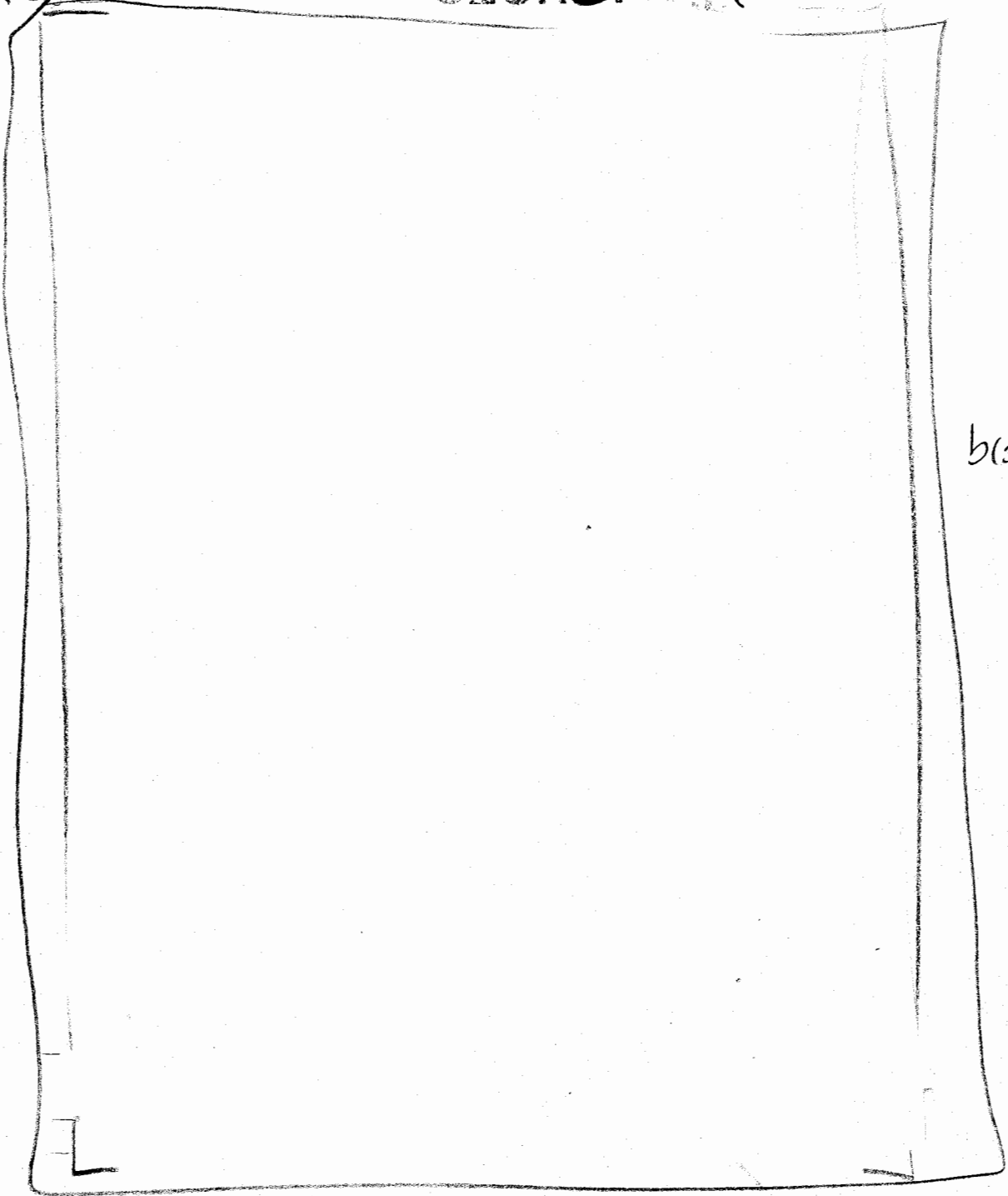


b(3)

670747

UNCLASSIFIED

~~SECRET/RO~~



b(3)

6707 U S 49

IV, were selected as the optimum: for the balance of factors comprising resolution, magnification, flux at the detector, and field of view. Also listed for comparison are parameters for a conventional pinhole.

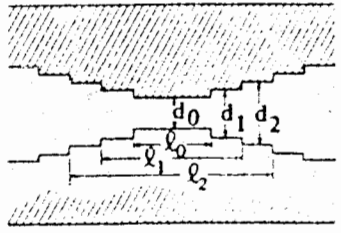
Clearly, the tapered design gave the smallest effective pinhole diameter and, hence, the best pinhole resolution. The pinhole resolution in the object plane for the smaller diameter tapered pinhole should be better than approximately 0.14 mm, and the corresponding resolution for

gamma rays should be better than 0.21 mm. By comparison, the neutron and gamma-ray source diameters at 10% maximum intensity would be approximately 1.2 and 3.6 mm, respectively. These higher resolution pinhole designs will, however, suffer larger image distortions and higher risks associated with alignment precision required for their relatively smaller fields of view.

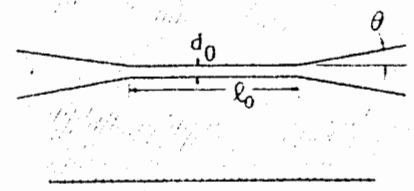
b(3)

UNCLASSIFIED

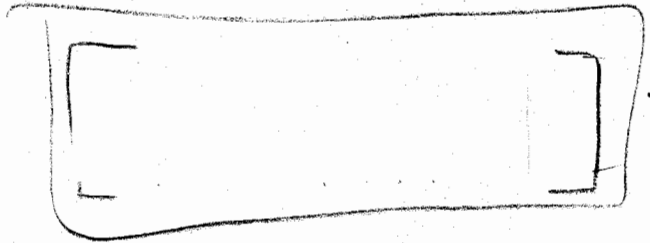
~~SECRET~~ / RD



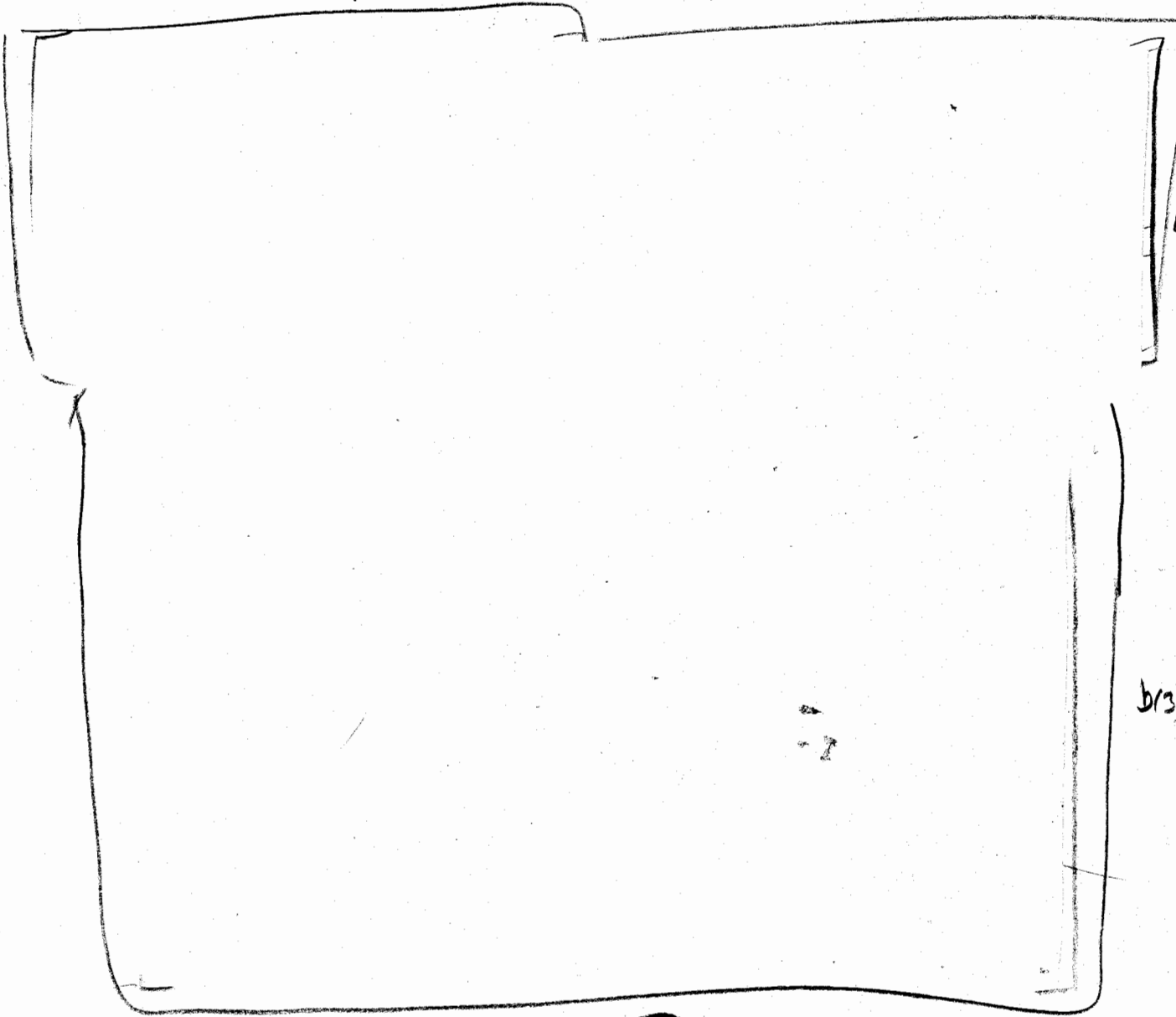
Conventional stair step



Uniform taper



b(3)



b(3)

67070550

b

b(3)

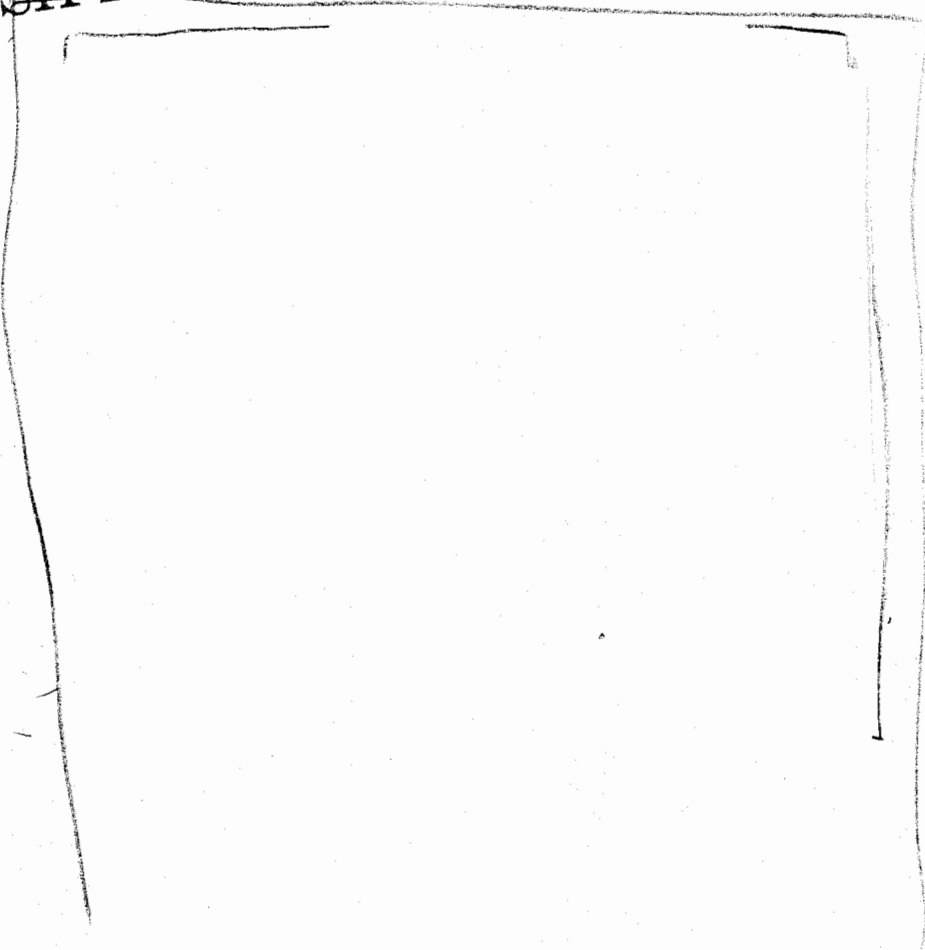
-1

UNCLASSIFIED

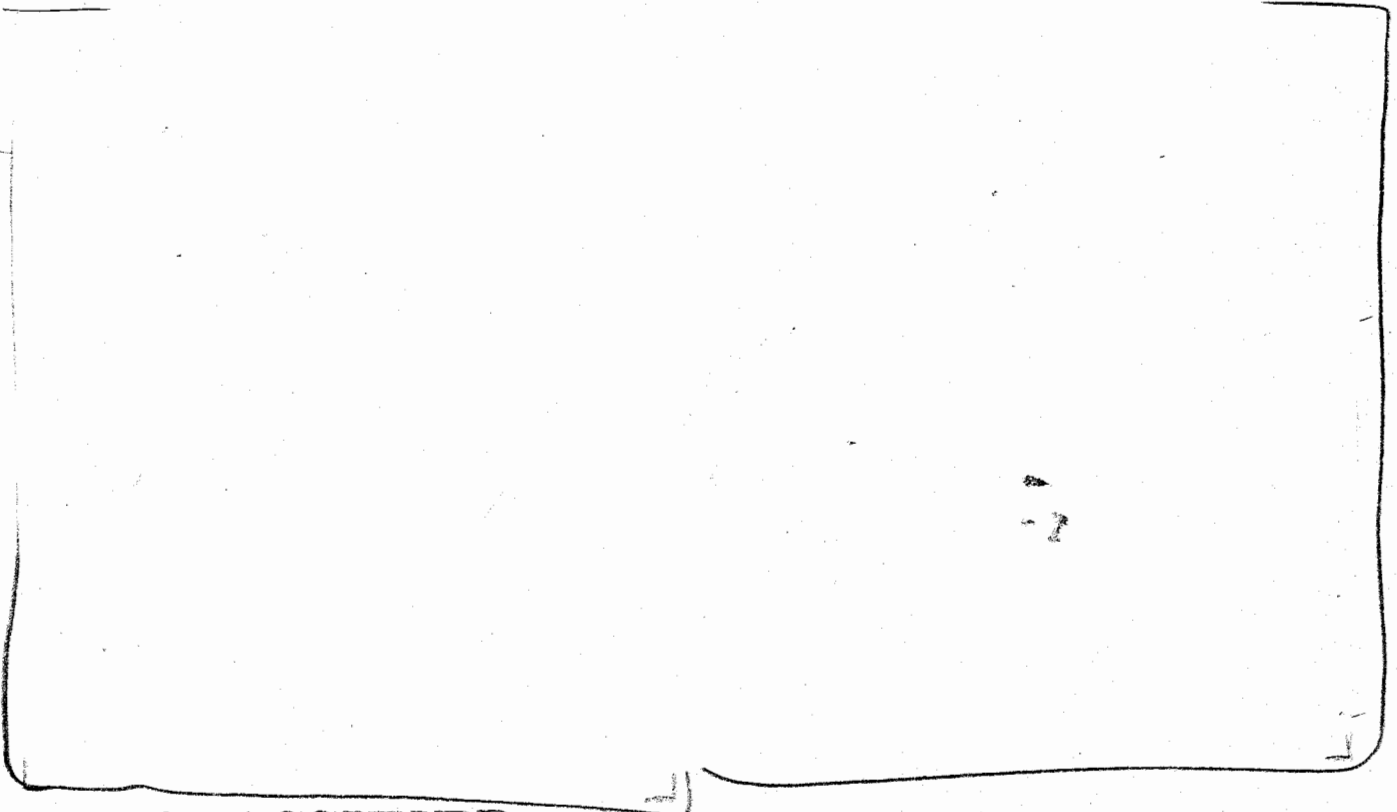
~~SECRET~~ / RD

UNCLASSIFIED

~~SECRET/RO~~



b(3)



67000001
b(3)

b(3)

UNCLASSIFIED

~~SECRET/RO~~

UNCLASSIFIED

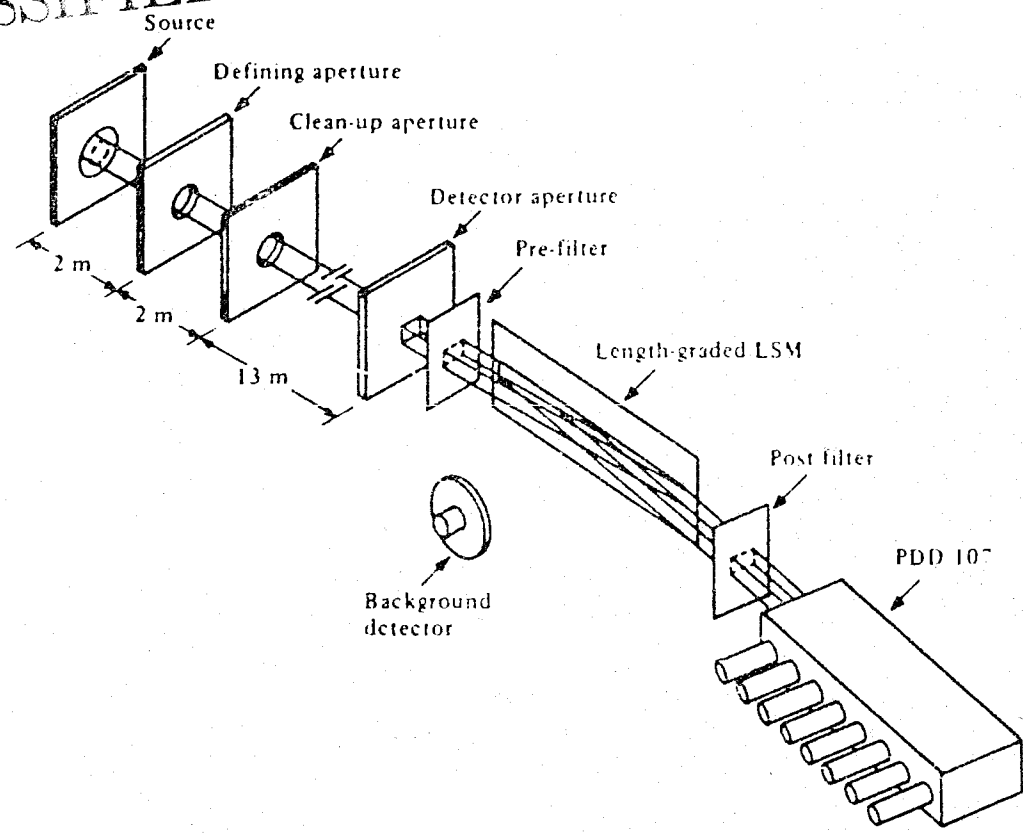
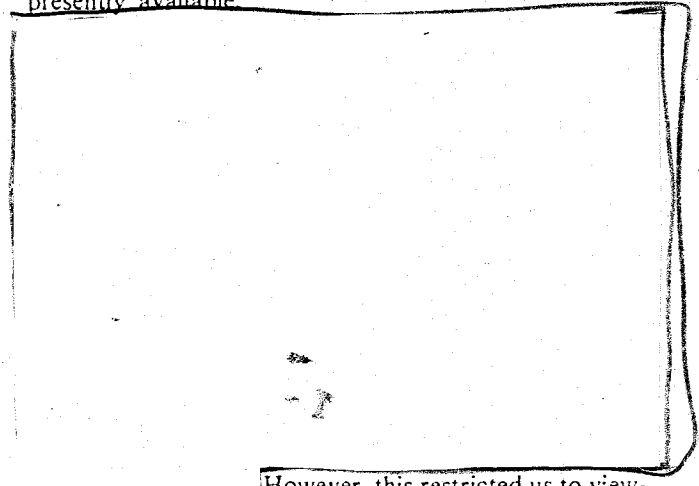


Fig. 17. SPEX LOS geometry.

The spectrometer was of novel design incorporating a synthetic x-ray diffraction crystal composed of alternating layers of carbon and palladium. The thickness of these layers was varied from one end of the crystal to the other so that 1.5-keV x rays were diffracted from one end while 2.5-keV x rays were diffracted from the other end of the flat crystal. The manufacture of these synthetic crystals was being worked on collaboratively by Los Alamos and Stanford University and represents a new class of x-ray optical elements that can be used in the design of x-ray diagnostics.

The detector used in this spectrometer was also of unique design and consisted of eight individual channels that intercepted different portions of the diffracted beam. The bandpass of each channel was determined by the fraction of the beam intercepted by each detector and the total energy spread across the beam. This design allowed us to build a moderate bandpass system with high throughput, relatively simple alignment, a very small single LOS, and a compact detector. Further extensions

of this concept will allow us to perform routine measurements of x-ray spectra with moderate to high sensitivity and simpler and less expensive detector systems than are presently available.



However, this restricted us to viewing only higher energy x rays.

67070002

UNCLASSIFIED

b(3)

b(3)

Table VI summarizes the capsule performances.

b(3)

b(3)

b(3)

b(3)

b(3)

UNCLASIFIED

[Handwritten signature]

b(3)

6700000004

b(3)

UNCLASIFIED

[Handwritten signature]

UNCLASSIFIED

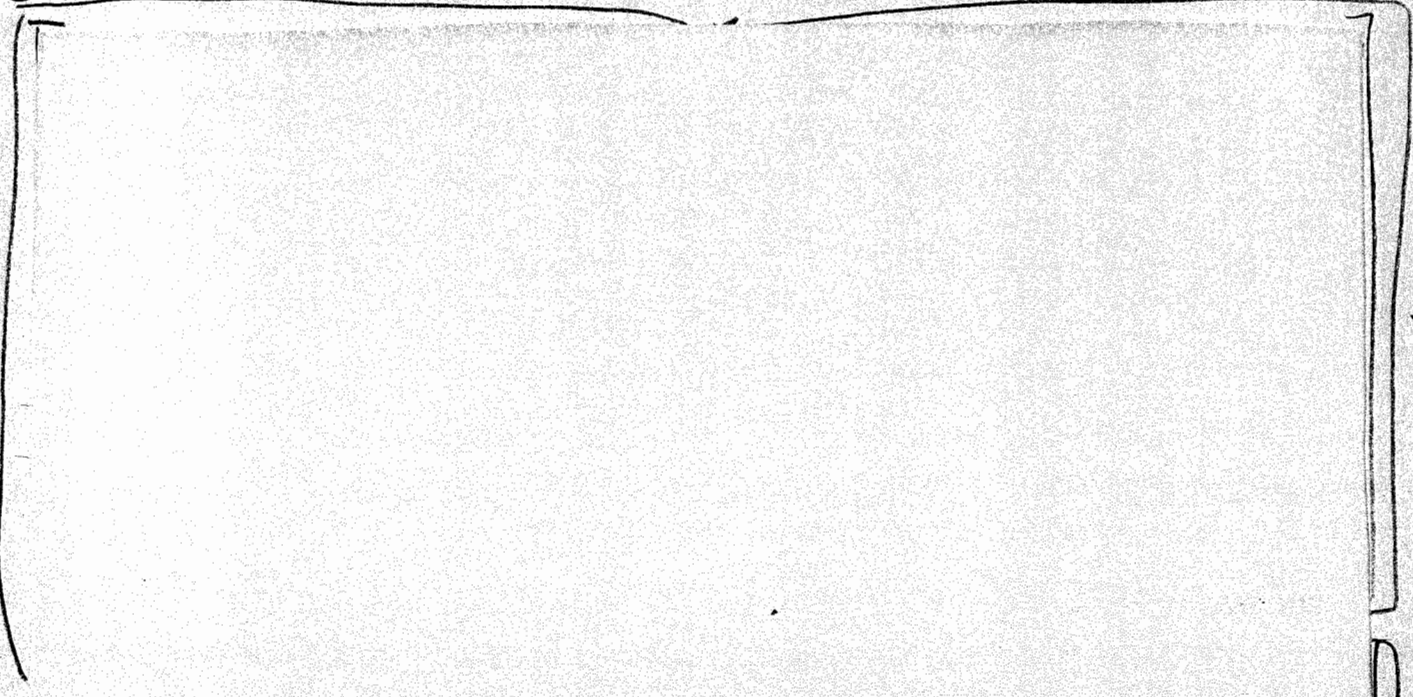
~~SECRET / RD~~

67070355

UNCLASSIFIED

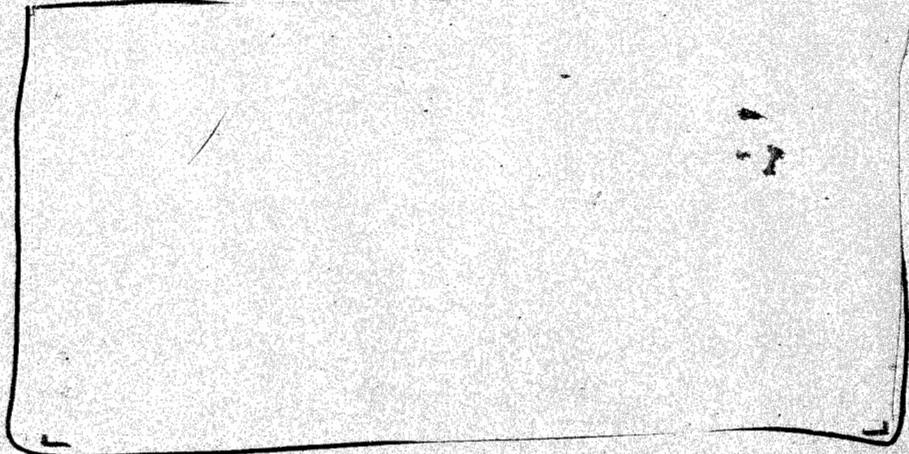
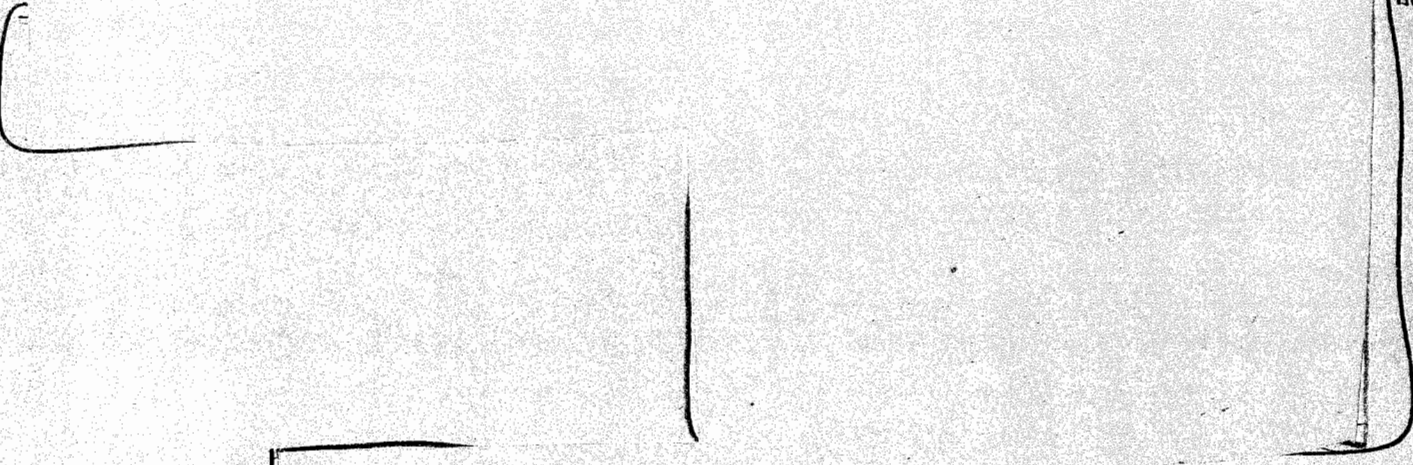
~~SECRET / RD~~

b(3)

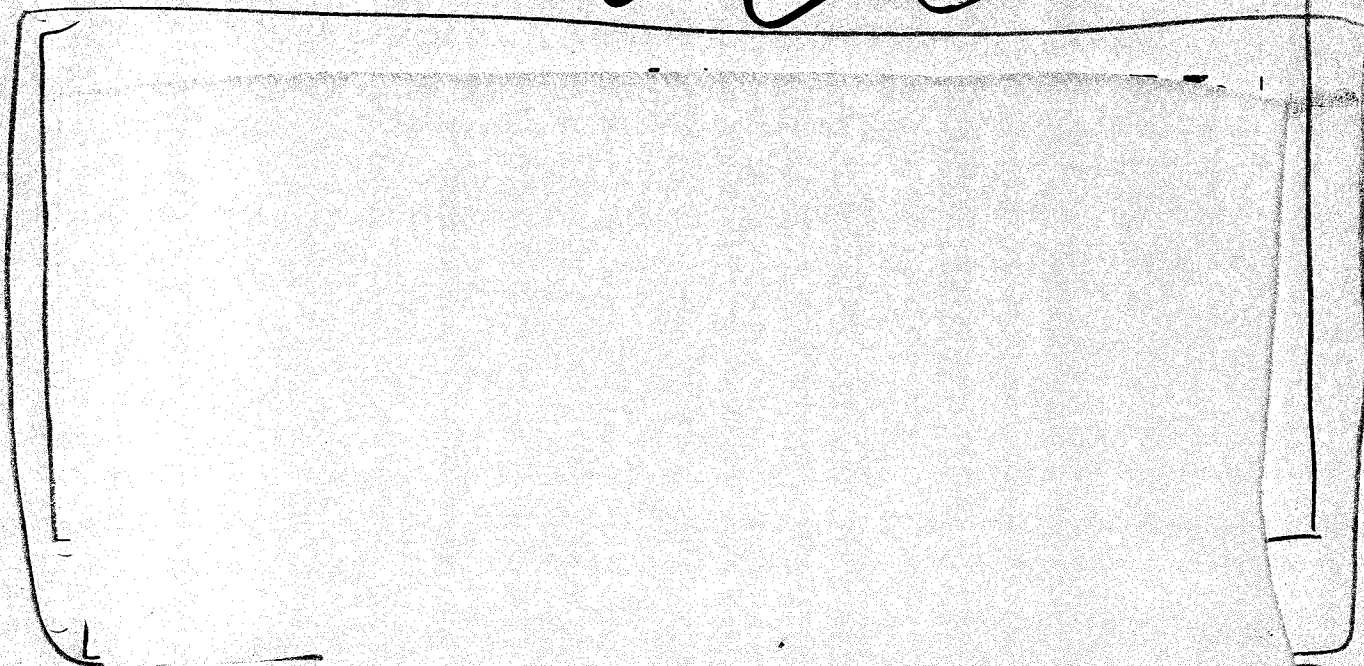


b(3)

67020256



b(3)



b(3)

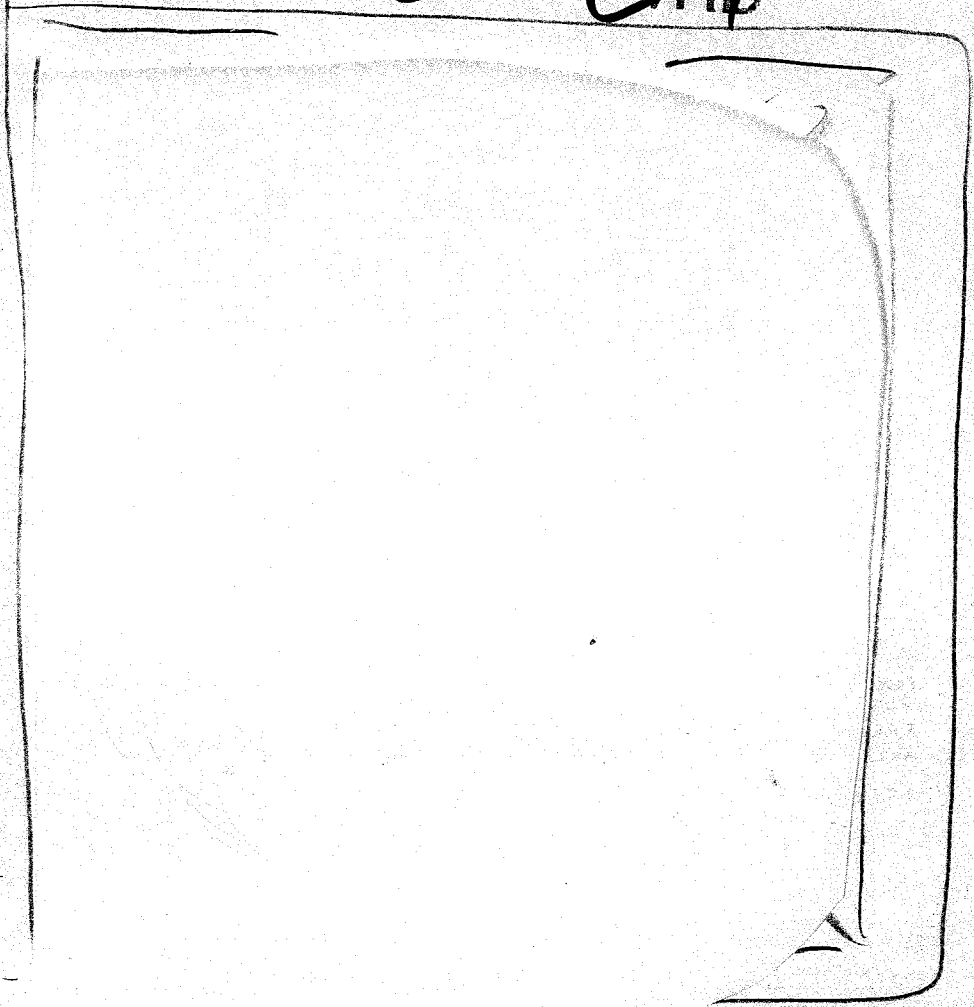
Livermore Experiments

b(3)

b(3)

67000557

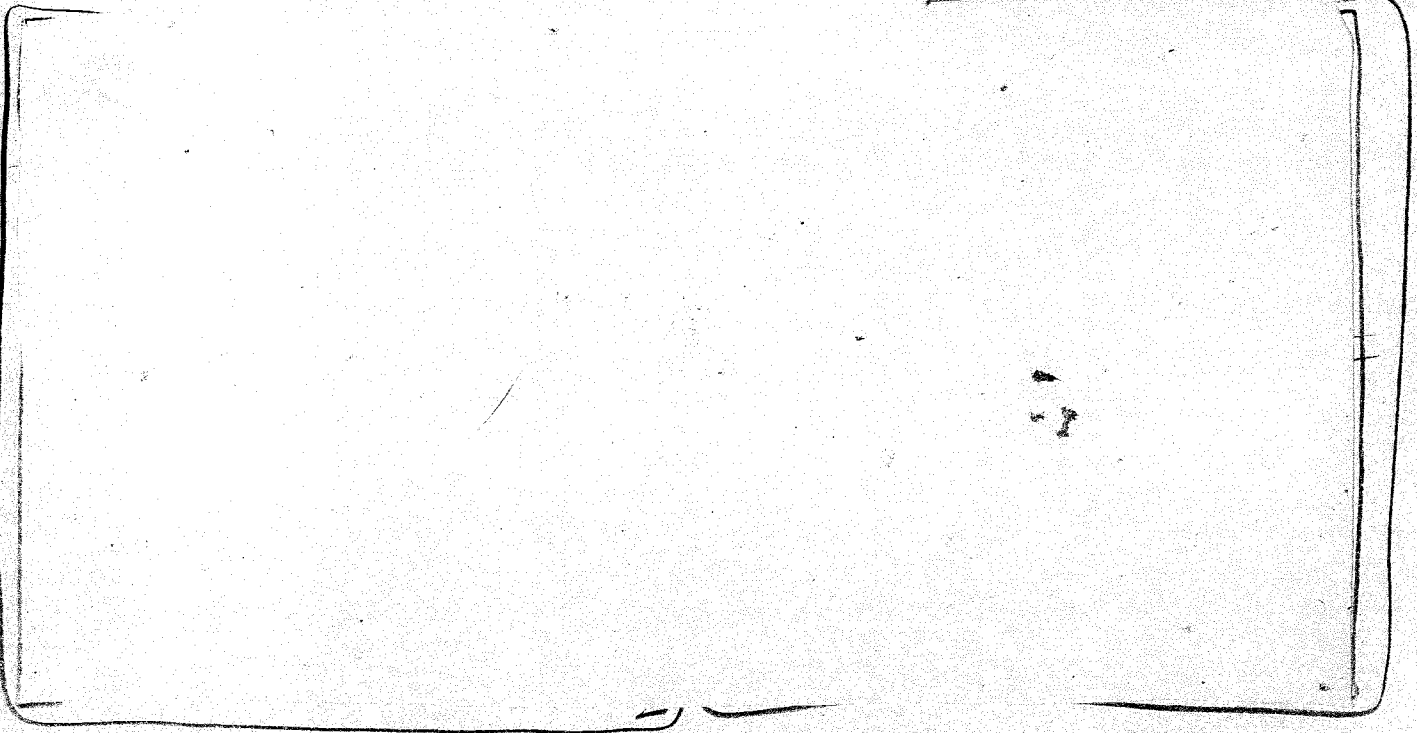
b(3)



b(3)

b(3)

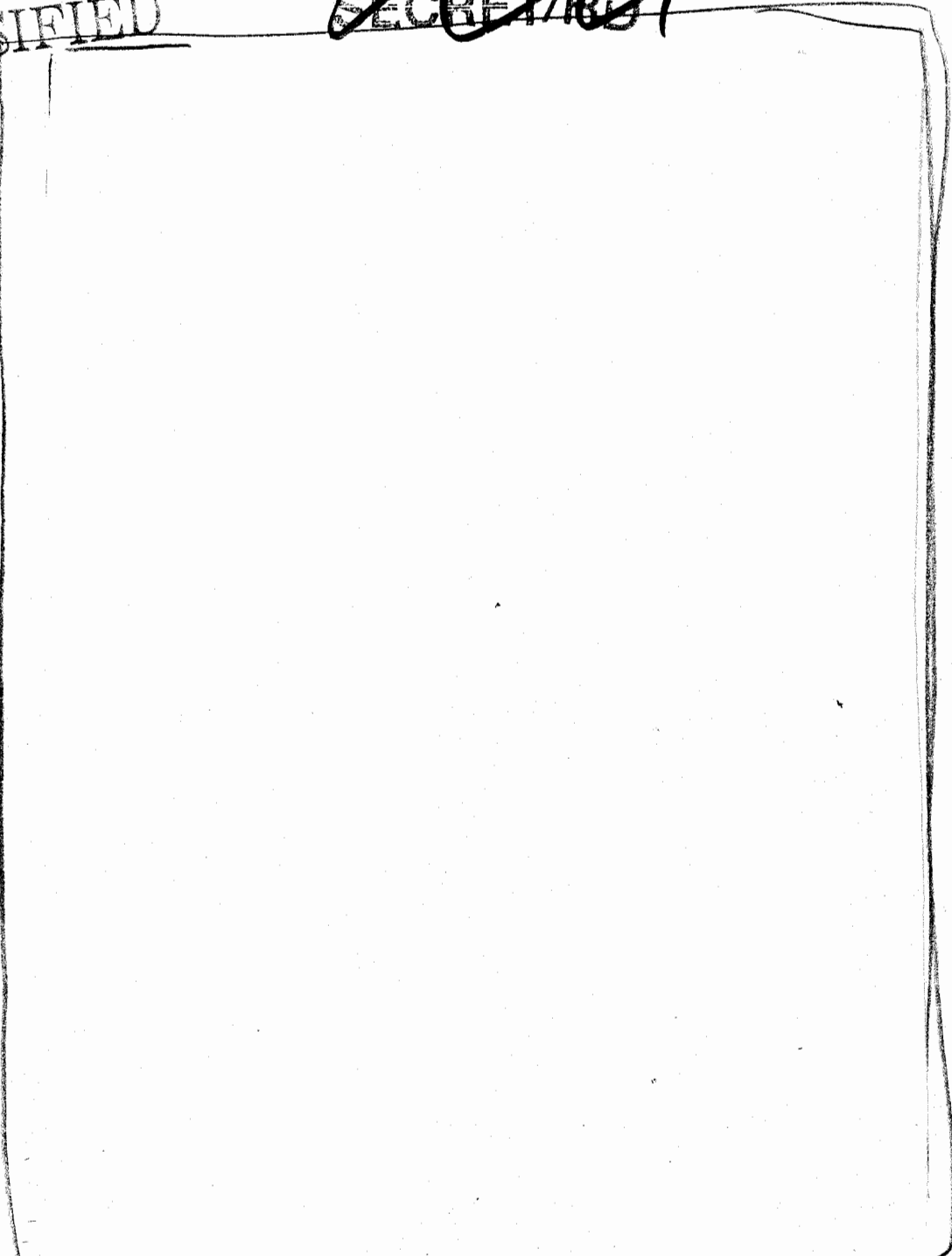
6709
b(3)
0559



b(3)

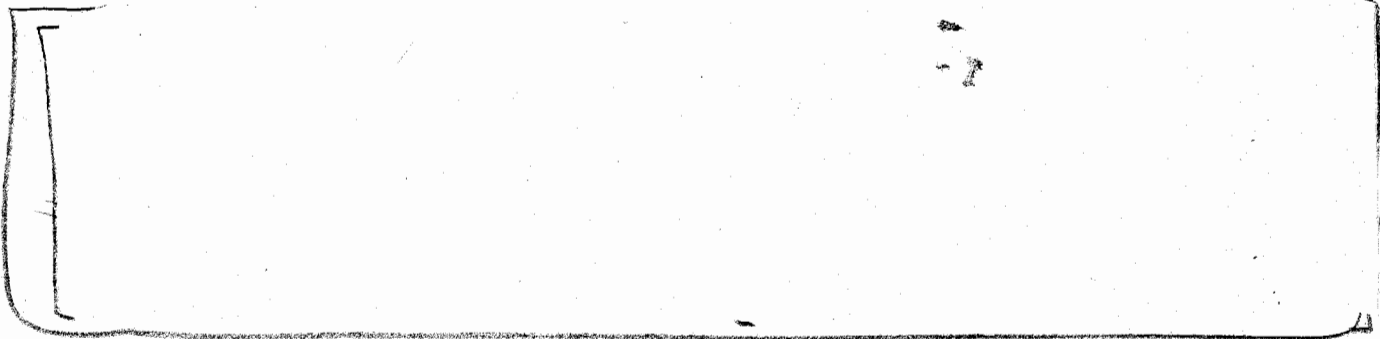
UNCLASSIFIED

~~SECRET/RO~~



b(3)

67070560



⁶² UNCLASSIFIED

~~SECRET/RO~~

UNCLASSIFIED

~~SECRET/RO~~

b(3)

b(3)

6
7
0
3
6
1

b(3)

b(3)

6
7

UNCLASSIFIED

~~SECRET/RO~~

UNCLASSIFIED

~~SECRET~~ RD

67040562

b(3)

~~SECRET~~ RD

UNCLASSIFIED

and the detector, and by varying the source-detector distance.

Another type of detector is indicated in Fig. 29—an NPD-76Q. This is a conventional detector in which Cherenkov light generated in a quartz cylinder is detected by a biplanar photodiode (FW114). This detector is a factor of 1000 more sensitive than a Compton detector but has a smaller electrical bandpass (about 600 MHz).

The useful range of electrical currents for the Compton detectors is from ~0.1A to ~100A and for the photodiode from ~0.1A to ~50A.

Two types of Compton detectors are currently the most commonly used—the Vacuum Compton Diode (VCD) developed by Livermore and the High-Frequency Kenertium (HFK) developed by Los Alamos.

The sensitivities to gamma rays and 14-MeV neutrons for either type of detectors are a few times 10^{-22} coulombs per MeV (gamma ray) and a few times 10^{-23} coulombs per 14-MeV neutron. The coverage of a detector for a given source is adjusted by choice of inner diameter of a collimator placed in front of the detector, by selection of attenuator thickness between the source

b(3)

b(3)

b(3)

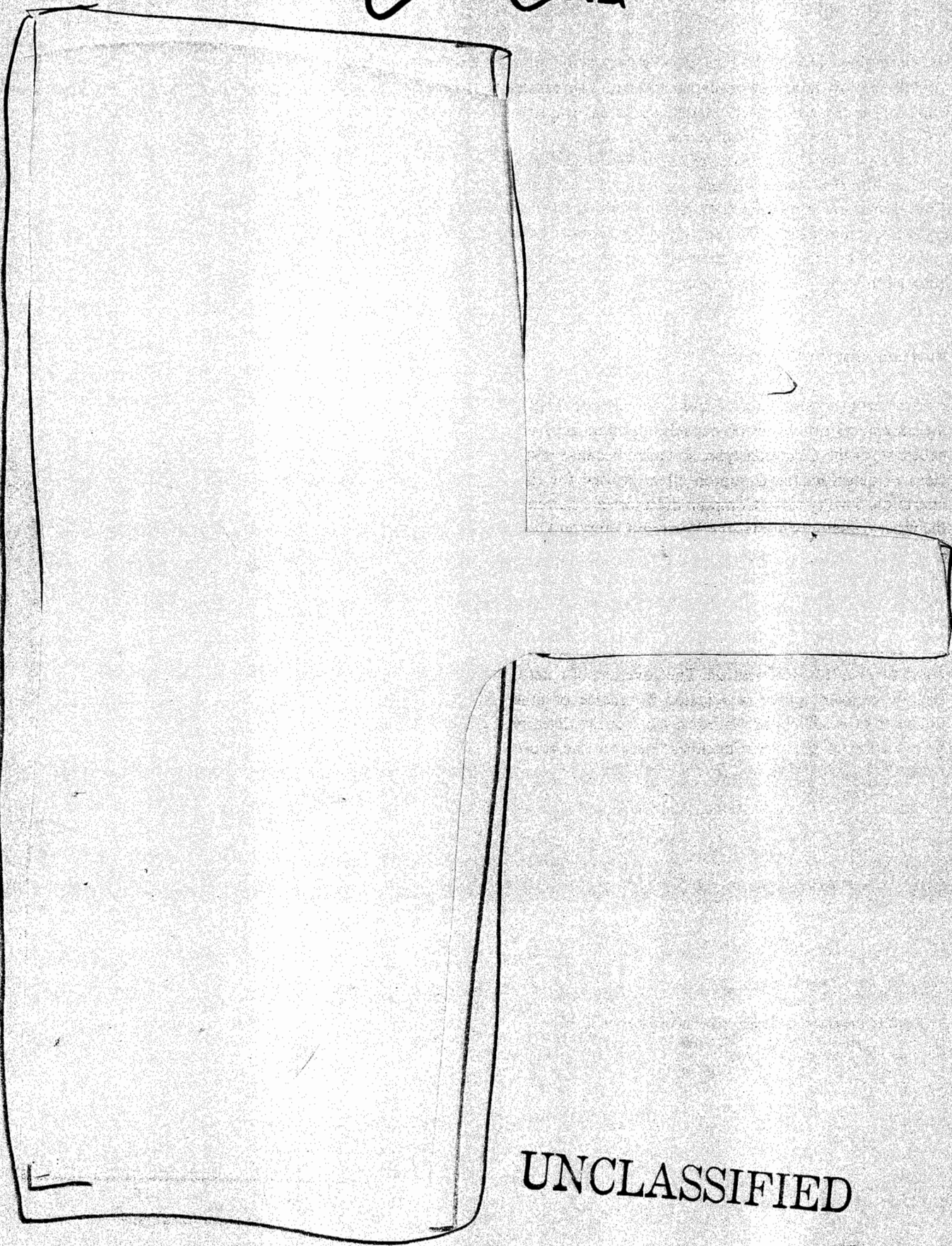
b(3)

6709 0563

b(3)

UNCLASSIFIED

~~SECRET~~ / RD



b(3)

b(3)

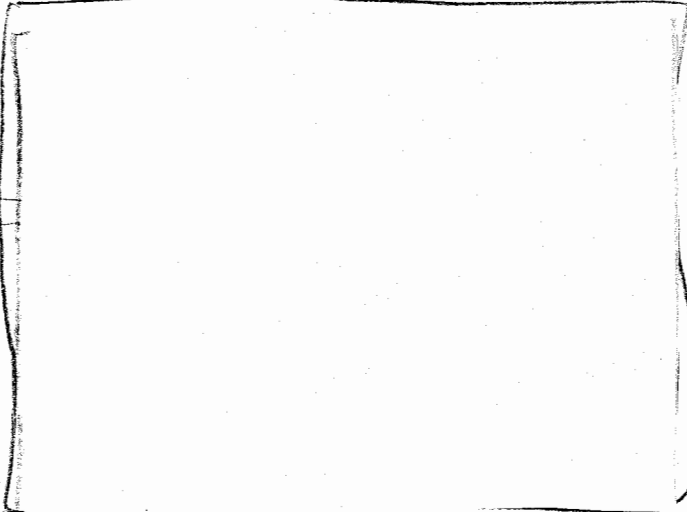
67090564

UNCLASSIFIED

~~SECRET~~ / RD

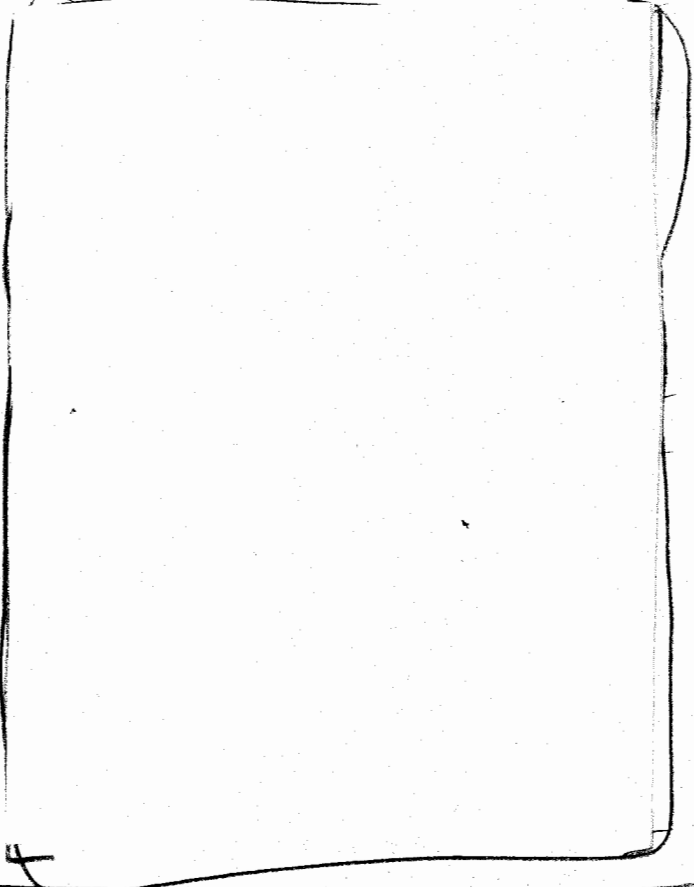
X-Ray Diagnostics

Further costs and complexity reductions were derived from decreasing the size of the LOS pipe to 6-in. diameter and utilizing K-F flanges on the roughing vacuum compatible sections. We also did not use an ultrahigh vacuum backup system.



b(3)

The major differences in this experiment are engineering modifications aimed at reducing the cost of this experiment and simplifying the vacuum system requirements.

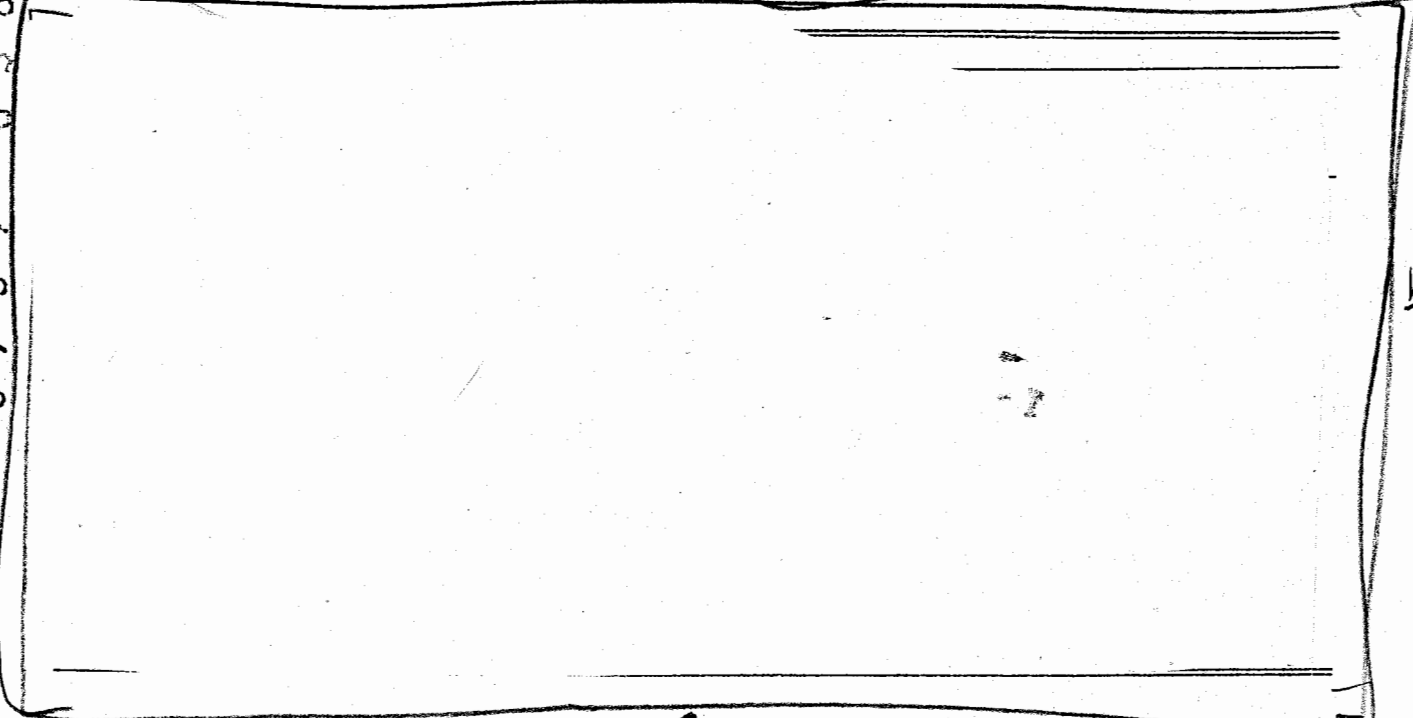


b(3)

b(3)

Ultrahigh vacuum conditions were maintained in the windowless detectors with appendage ion pumps on each x-ray detector. A thin vacuum window was placed in each detector forming the post filter for the channel. We avoided downhole high-voltage cables for each ion pump by implementing a distributed downhole, high-voltage power supply.

b(3)



b(3)

6702036

b(3)

0 5 6 6

6 7 0 7

b(3)

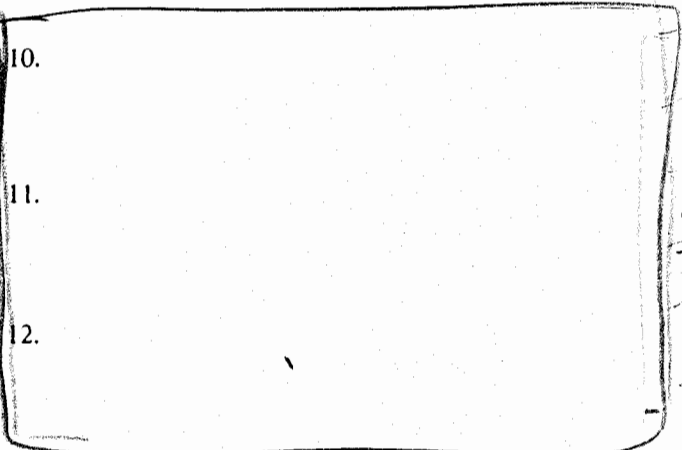
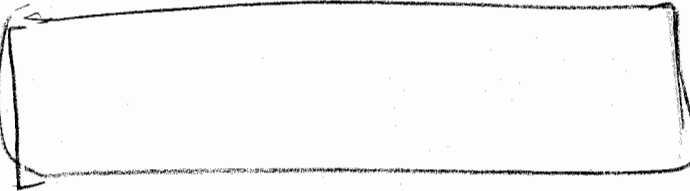
A synthesis of this resolution identified the camera, particularly the microchannel plate intensifier, as the largest contributor.

FUTURE PLANS

The progress made to date in Centurion has created considerable enthusiasm and generated many objectives to pursue.

- 2

(B)



REFERENCES

- 1.
- 2.
- 3.
- 4.
- 5.
- 6.
- 7.
- 8.
- 9.

- 10.
- 11.
- 12.

13. G. J. Berzins and N. S. P. King, "Pinex (Pinhole Neutron Experiment) (U)," in *Weapons Monthly*, Los Alamos Scientific Laboratory report LA-8244-PR (SRD) (December 1979), p. 9.

14. R. J. Young, "Interpreting Pinex Images of Implosion Anomalies (U)," in *Defense Science*, Los Alamos National Laboratory report LA-9430-PR (SRD) (May-June 1982), p. 15.

- 15.
- 16.
- 17.
- 18.
- 19.

(A3)

67070367

UNCLASSIFIED

~~SECRET/AD~~

APPENDIX A

COMPTON DETECTORS

Compton detectors were developed a little more than 20 years ago to meet a need in downhole diagnostic measurements for a detector with characteristics of ruggedness, very low sensitivity, high electrical bandwidth, and large dynamic range.

Two types of Compton detectors are in general use today: a thin vacuum variety with a thin center electrode developed by LLNL and a thick, oil-filled variety with a thick center electrode developed by Los Alamos.

The vacuum Compton diodes go by the generic designation VCD; there are various model numbers, mostly denoting the diameter of the central electrode (emitter). At present, there is only one type of oil-filled Compton detector in use, the HFK (High-Frequency Kenertium), so-called because of the 1-in.-thick Kenertium center electrode. (Kenertium is a machinable alloy of tungsten.)

Early versions of Compton detectors had only one output connector. However, it was discovered that putting two output connectors opposite each other more than doubled the electrical bandwidth at the expense of halving the sensitivity. This loss is no penalty when the observed source is a nuclear explosion.

Both types of detectors depend on the Compton effect for their operation, but the process is somewhat different in each case.

The conceptual design for a VCD is illustrated in Fig. 1A. Incident rays penetrate the thin entrance window (usually stainless steel) and cause Compton electrons to be emitted from the 4.8-mm-thick aluminum center electrode, resulting in a positive pulse propagation down the electrical cable. Neutrons have a similar effect; gamma rays are produced by (n, γ) reactions in the aluminum, again resulting in the emission of Compton electrons and a positive electrical pulse.

In the HFK, incident gamma rays produce Compton electrons in the oil; those within range of the Kenertium surface are collected by the electrode. The transmission through the electrode for gamma rays is ~10% so that

the emission of Compton electrons from the back side of the electrode is down by a factor of 10 from the collection on the front side. Consequently, gamma rays result in a negative electrical pulse. Neutrons produce knock-on protons in the oil, to be collected by the electrode plus (n, γ) reactions in the Kenertium resulting in Compton electron emission. Both of these processes produce a positive electrical pulse. Hence, the HFK produces a negative electrical pulse for gamma rays and a positive pulse for neutrons, providing unambiguous signals. The reader should note that a theoretical treatment of the HFK should include ionization and polarization effects in the oil.

Compton detectors are operated with zero electrical bias. Because the detectors can have energies as high as several MeV, the detectors could, in principle, generate several-million-volt electrical pulses. In practice, the detectors become nonlinear at 5000 V across 50 Ω (100 A) and saturate at about 20,000 V.

An early problem with VCDs was the emission of Compton electrons from the entrance window. This process causes a negative precursor to the detector step-function response and, in an extreme case of a particular gamma-ray spectrum, could result in zero output current. This problem was reduced to an acceptable level by using a thin entrance window, placing a lead electron stopper an appropriate distance in front of the detector, and putting an electron sweeping magnetic field between the lead and the entrance window.

The shaping of the ends of the electrodes shown in Fig. 1A gives an approximate match to the 50- Ω cable used to conduct the signals uphole.

The HFK detector has a collector diameter of 76.2 mm and an electrical bandwidth of about 900 MHz.

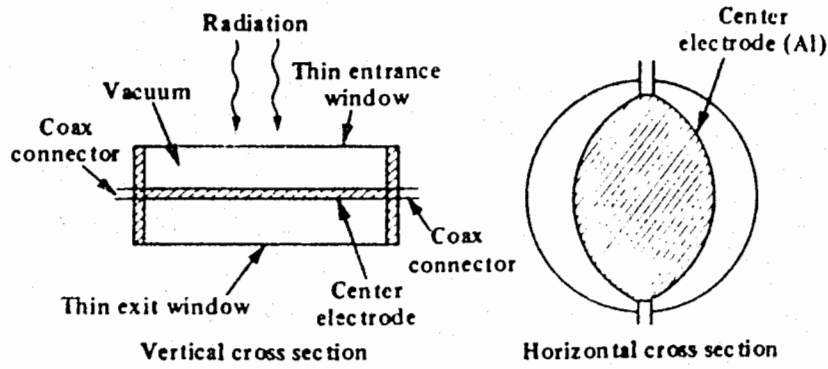
67070560

UNCLASSIFIED

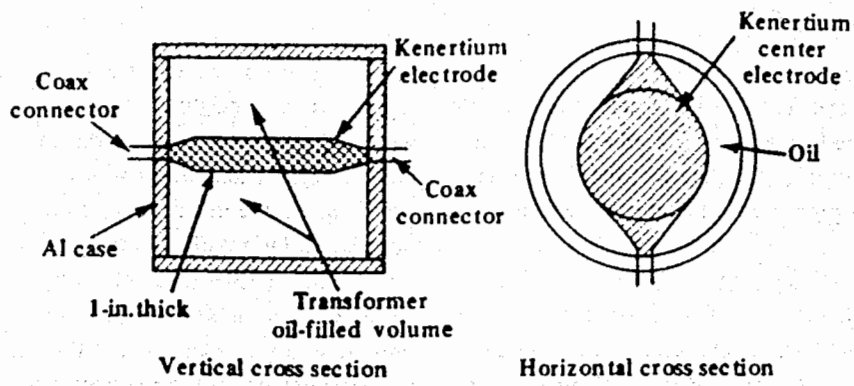
~~SECRET/AD~~

UNCLASSIFIED

~~SECRET/AD~~



Vacuum-Compton Diode (VCD)



High-Frequency Kenertium (HFK)

Fig. 1A. Conceptual drawings (not to scale) of the design principles of the VCD and HFK detectors used for downhole diagnostics.

67070569

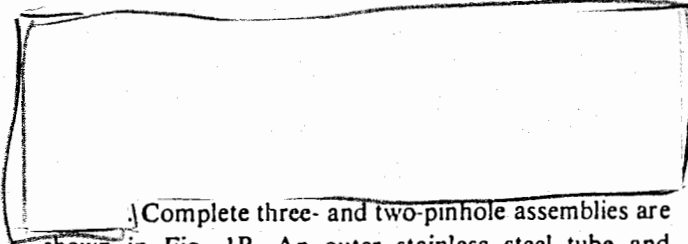
UNCLASSIFIED

~~SECRET/AD~~

APPENDIX B

MANUFACTURING OF PINHOLE ASSEMBLIES

b(3)



Complete three- and two-pinhole assemblies are shown in Fig. 1B. An outer stainless steel tube and flanges are used to support the whole assembly. Inside the stainless steel tube is a solid brass tube split longitudinally and bored to support and align the actual pinhole tubes. Fabrication of the pinhole tubes with their very small pinhole presented the most demanding challenge.

The center sections of each pinhole assembly (insert B) were the most difficult to make. The fabrication started with nickel wire that had a diameter equal to the desired center diameter (0.0508, 0.1016, or 0.1524 mm) of the pinhole. The wire was held in a rotating fixture and coated with copper by physical vapor deposition. A trapezoidal metal wedge was moved slowly between the copper source and the rotating wire to prevent copper from depositing on the center 5.08 cm of the 15.24-cm-long wire. As the wedge was slowly moved inward, it blocked more and more of the wire length. As a result, a cone-shaped copper layer formed on each end of the wire. Beginning at 2.54 cm on either side of the center, the copper tapered smoothly from 0.0508 mm in diameter to 0.3175 mm in diameter at the extreme ends. Mandrels for the 0.1016- and 0.1524-mm-diam pinholes were prepared in a similar manner.

The copper-coated mandrels were then electroplated with gold to a diameter of approximately 3.81 mm. During the gold electroplating operation, the area of the 0.0508-mm-diam cylindrical mandrel increased by a fac-

tor of 75. To maintain a constant current density and therefore a constant plating rate, the current had to be increased continuously and was accomplished by measuring the voltage of the part or its cathode potential relative to a reference electrode potential and using this potential difference to control a power supply through a feedback configuration.

After plating, the exact center and the two transition regions from straight to tapered sections (see insert B) were located and marked on the outside of the gold plating. This designation was done by having reference points at each end of the wire that were masked off and not plated. Originally, it was intended to make the center pinhole in one piece, but the long leaching times needed to remove the nickel-copper mandrels precluded this action.

The other parts of the pinhole assembly (inserts A and C) are tapered sections that "funnel" the neutron and gamma-ray flux into and out of the small-diameter central sections. Tapered sections as depicted by insert A are made of gold, and tapered sections as depicted by insert C are made of copper. Both "A" and "C" sections were made by a combination of electroplating and machining. The gold tapered sections were plated on 0.2794-mm-diam copper wire and the copper sections were plated on 0.7874-mm-diam aluminum wire. After cutting to length, the copper wire was removed with nitric acid and the aluminum wire was dissolved in sodium hydroxide. The taper was machined into the gold "A" and copper "C" tubes by EDM using a computer-programmed revolving tungsten wire.

67090570

~~SECRET/BD~~

UNCLASSIFIED

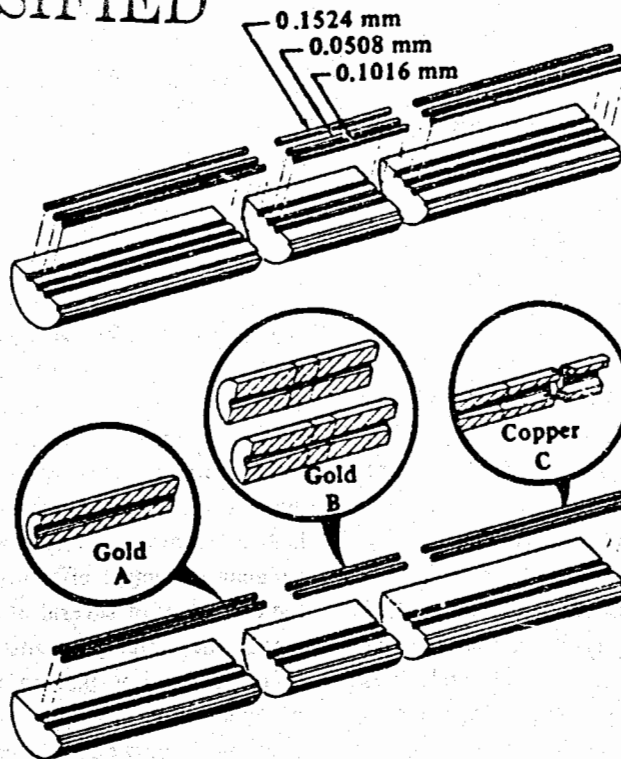


Fig. 1B. Manufacture of pinhole assemblies.

67090571

UNCLASSIFIED

~~SECRET~~

BD

UNCLASSIFIED

CO₂ LASER PLASMA INTERACTIONS

by David W. Forslund and Philip D. Goldstone

INTRODUCTION

The enormous pressures required to compress the inner portion of an Inertial Confinement Fusion (ICF) target to densities greater than the interior of the sun are accomplished by the conversion of the laser energy to x rays and particle energy in the plasma corona and by ablation of the target.

To achieve these compressions efficiently and effectively, we must understand the physics of matter from 10^{-3} - 10^3 g/cm³ over distances of 10^{-5} - 10^0 cm and times of 10^{-5} - 10^{-8} s with particle energies ranging from 0.1 to 10^6 eV and magnetic fields ranging from none at all to 10^3 T. The physics involved is nearly collisionless plasma physics including the effects of spontaneously generated magnetic fields, high-density collisional physics, the atomic physics of weakly to highly ionized materials, and their effects on transport of photons of all energies as well as particles. Frequently, the processes are far from equilibrium and require elaborate rate equations to describe their effects with reasonable accuracy.

Finally, we must understand thermonuclear burn, including the transport of all of the nuclear fragments, such as alpha particles, in the compressed fuel. We must be able to control radiation flow with a precision of a fraction of a per cent, and the hydrodynamic implosion may be complicated by the mixing of materials due to hydrodynamic instabilities and their subsequent effects on the thermonuclear burn process.

In order to be a competitive, economical energy producer, the gain of the target must be as high as possible with the lowest possible energy input.

The biggest problem for inertial fusion in general, and laser fusion in particular, has been the mechanism of

deposition of (laser light) energy into the target and subsequent transport of that energy to the ablation surface. The very properties of lasers that allow them to produce extremely high power and intensity (which is necessary for fusion) can work against a desirable form of energy deposition. In particular, the wave nature of the light, the high coherence, and narrow bandwidth all contribute to peculiar collective effects in the deposition that reduce the efficiency of several of the above processes. In other words, these highly organized properties of the laser tend to drive the hot plasma in the target far from thermodynamic equilibrium with potentially serious consequences. In particular, laser fusion with CO₂ lasers at 10^6 μm is dominated by such effects.

These collective mechanisms initially result in the production of energetic electrons by the absorption of laser radiation in the target corona. The hot-electron energy then cascades into a number of energy flow channels (magnetic fields, acceleration of energetic ions, bremsstrahlung emission, heating of a dense "thermal" plasma, soft x-ray emission, and microwave emission). Shorter wavelength laser-plasma interactions tend to be more collisional, and the collective processes which result in hot electrons, are generally less dominant.

Early in the history of laser fusion, researchers hoped to get quickly into the regime of significant thermonuclear burn. Many papers were published on the thermonuclear burn properties and the required conditions involving small amounts of fuel. Indeed, the energy required to compress and heat the fuel to ignition conditions is very small compared with the energy released. However, to achieve the necessary conditions of compression requires precise control of the input energy as the incident driver energy is decreased. Specifically, the very small fuel masses are susceptible to preheat, which will generate sufficient back pressure to prevent compression. Again, the smaller the fuel mass, the smaller the fraction of preheat allowed because one must compress to increasingly higher densities to accomplish fuel burn. The required precision of the implosion increases

6709 0572

b(3)

dramatically with decreasing target mass; whether or not there are fundamental barriers to this required precision is unknown at present but suggested by some of the existing data. The present-day estimates of ~10 MJ of driver energy to achieve high gain are based on a relatively conservative requirement for burning the deuterium-tritium (DT) fuel.

As a consequence of the difficulty of sufficiently compressing small amounts of fuel in the laboratory, the inertial fusion program has been actively pursuing two important, but separate, approaches to fusion.

In the laboratory, the major effort has gone into understanding and optimizing the drive conditions necessary to implode targets and the initial physics of imploding targets to moderately high density. We have studied the problems of preheat and hydrodynamic stability. After an initial phase of studying the properties of compressions with direct laser drive, the program at Los Alamos underwent an extensive experimental shift that sought to optimize the conversion of CO₂ laser light into soft x rays in hohlraums and to other forms of energy that would be more efficient at imploding targets than direct drive.

Whereas much of our understanding of absorption processes has been theoretical because of the limited number of unambiguous experimental signatures of these processes at 10 μm, our understanding of energy flow into these different energy channels following the absorption has largely been empirical, with theory providing explanation of our observations and a basis for predicting scaling of these phenomena.¹ In many cases, these theoretical explanations have provided new hypotheses to test experimentally as well as new insights into how the energy flow might be altered.

THEORETICAL TOOLS

We will begin by describing the methods we have used to study these processes and by explaining a little about how they have developed and improved over the years. The inertial fusion program has had a well-balanced program with considerable strength in both the

theoretical and experimental areas. Because of the extreme complexity of the physics, it has been at the forefront in developing new theoretical tools as well as experimental techniques. The phenomena of interest change over time scales of picoseconds with the entire experiment occurring in about a nanosecond. Spatial resolution required to study the physics of targets measured in hundreds of micrometers to millimeters typically approaches 10 μm (the wavelength of the CO₂ light). Because much of the truly microscopic (sub-micrometer, subpicosecond) phenomena cannot be readily measured, but strongly influences the macroscopic behavior, computer simulation is relied on heavily to couple the microscopic phenomena to macroscopic observables.

The WAVE code is a 2D particle simulation code that solves Maxwell's equations and the relativistic Newton's laws for the particles in the self-consistent, three-component electric and magnetic fields. It typically advances 10⁶ particles on a grid of 10⁵ cells for 10⁴ time steps to determine the processes that absorb the laser light and transport the energy from the low-density, hot-plasma regions to the denser regions. Only a portion of the physical problem can be modeled because one must limit the time step to a small fraction of the laser period and the grid size to the distance light travels in one time step. Consequently, the time that can be covered is only a few picoseconds, and the distance is only about 10 wavelengths of light. Because of the limited time and space scale, the boundary conditions and initial conditions for fields and particles are unknown and must be estimated. Much of the skill in using the code involves guessing the right boundary and initial conditions that appear to be consistent with themselves, with hydrodynamic calculations, and with the experiment.

An implicit form of the code, called VENUS,² has enabled one to greatly increase the time step and grid size (at the expense of some high-frequency phenomena) to consider realistic spatial scales, which allow the study of the central role of self-generated magnetic fields in electron transport and fast-ion emission. After their development by the ICF program, these new-generation codes rapidly spread to the magnetic fusion and space physics communities. Although quantum mechanical and atomic physics process are not included in these codes, they can accurately describe the fully developed strong turbulence that can occur in laser-plasma interactions, limited only by the computer resources. To better utilize the results of these codes, we test and evaluate

b(2)
67090573

UNCLASSIFIED

~~SECRET~~

various models to obtain scaling laws that can be reliably extrapolated into new regimes. For example, simplified models of the propagation and absorption of light in the plasmas have been verified concerning their accuracy and range of validity with the WAVE code. In the last decade, the improvement in scale of problems accessible has increased by a couple of orders of magnitude because of improvements in computer hardware speed and in numerical algorithms (VENUS). This change has greatly increased our understanding of the physical processes as discussed below.

EXPERIMENTAL TOOLS

In addition to the theoretical tools that have greatly aided our insight into the complex processes in these plasmas, a wide variety of experimental tools and techniques has provided the basic empirical information against which the theoretical models must be compared in an iterative process. Overall energy balance can be obtained by measuring the nonabsorbed light directly or by calorimetrically measuring all of the ion and x-radiation energy emitted from the target. Some hot electrons escape the target and can be detected with electron spectrometers; however, the bulk of the electron energy is observable primarily by measurement of the bremsstrahlung radiation from several kiloelectron volts to large fractions of a megaelectron volt where possible with subnanosecond time resolution.³ A variety of instruments can be used to determine the spectra of accelerated ions.

The heated target material emits soft x rays that are detected by multichannel soft x-ray spectrometers utilizing filtered vacuum x-ray (photo) diodes, along with ultrafast oscilloscopes developed in the nuclear weapons program, to provide time resolution of about 200 ps. Spatially restricting the area viewed by the soft x-ray diodes enables measurements restricted to the diagnostic port of a hohlraum without complication from emission near the laser entrance ports. This is provided by multichannel x-ray collimators. The small diagnostic ports (400 μm) require that these collimators be made of precisely machined pinholes approximately 150 μm in diameter, aligned with respect to each other and the target to an accuracy of 25 μm using optical techniques.

Optical and x-ray emission can be spectrally resolved with spectrographs or multichannel spectrometers or imaged using simple optical cameras or pinhole cameras, and either images or spectra can be time resolved to tens

of picoseconds using image-converter streak cameras. The detailed atomic physics of the plasma corona, often far out of local thermodynamic equilibrium, can be examined using high-resolution x-ray and xuv spectrometers to examine the spectra from the corona. Details of the spectra such as line broadening and line shapes can be used together with detailed atomic physics models as a probe of the plasma conditions surrounding the ions of interest, which can be particularly useful in spectroscopically examining the conditions of the imploded fuel. The pinhole cameras, soft x-ray collimators, and x-ray spectrometers must be close to the target and must survive the intense x-ray and particle debris "blast" from each shot.

Imaging of the target plasma in x-rays characteristic of some transition of interest in the target or corona, for example, a K-line resulting from a hot-electron-caused, inner shell vacancy, enables the experimenter to track the flow of electron energy into the hohlraum wall, for example.

Detailed microfabrication technology is used to produce complex targets with specific materials placed at strategic locations so that their x-ray emission can be used as a "tracer" to determine the amount, or the time, of energy flow to these locations. In addition, such localized tracer techniques allow detailed examination of plasma conditions from a well-defined region without having to average over all densities and temperatures achieved in the plasma.

The availability of such a wide range of measurement technologies, together with the detailed ability to design experiments by microscopic modification of the targets, has allowed us to develop a detailed empirical base against which the theoretical picture of the processes involved can be compared.

RADIATION FLOW AND HYDRODYNAMICS

The insight gained from WAVE/VENUS simulations and verification of various models had led to the improvement in various physics packages in the 2D radiation flow/hydrodynamics code LASNEX and to a better choice of input conditions to the code. LASNEX then is used to model the hydrodynamics, electron transport, and radiation flow and possible thermonuclear burn in the target. Sometimes it can be used to evaluate models by observation of their effect on the macroscopic target behavior.

~~SECRET~~ UNCLASSIFIED

67070074

LASNEX and its postprocessing packages such as TDG allow it to generate outputs directly from various diagnostic instruments, such as pinhole photographs, streak camera images, bremsstrahlung spectra, ion emission, and soft x-ray emission. Because the code also calculates the source spectra, it can be used to assist in the deconvolution of, for example, the electron temperature from the hard x-ray bremsstrahlung spectrum or the compressed-fuel properties from the x-ray pinhole images and x-ray spectra. By simultaneous modeling of a variety of phenomena on a given target shot, the use of the code greatly enhances one's confidence in understanding the target behavior. Frequently, there has to be an iteration in LASNEX input conditions to match the experimental data. In other cases suggestions can be made to modify existing diagnostics or develop new ones to search for specific predicted signatures of physical phenomena.

The virtuosity of the target fabrication effort makes possible radical changes in target configuration. From this iteration process, new target concepts have been developed in an attempt to better utilize the energy flow.

ENERGY ABSORPTION AND TRANSPORT

In large laser systems, the light must travel from the last large optical surface over a long distance through a near vacuum to the target. The intensity at the target is controlled to a large extent by the focal properties of the

final optical element and is usually adjusted to achieve nearly uniform illumination at the target.

Drive symmetry is achieved in a hohlraum by a combination of the light reflecting around inside and the deposition and re-emission of the soft x rays from the case of the hohlraum. The initial illumination uniformity is not maintained, however. As the target heats up, hot plasma is blown off. Because the index of refraction n of a plasma depends on density as $n = 1 - \omega_p^2/\omega^2$, where $\omega_p^2 = 4 \pi n e^2/m$ is the square of the local plasma frequency, ω is the laser frequency, and n is the electron density, the propagation of light in this plasma is altered from what it is in a vacuum. The incident radiation may refract and not strike the target where it was originally directed, or it may break up into filaments because of localized heating of the plasma or to the infinite pressure of the light itself. This situation may cause local regions of the incident radiation to be much more intense than others, which may degrade the symmetry of the implosion or increase the energetic electron generation. In addition, the blow-off plasma may close the hohlraum laser entry holes, preventing useful absorption of laser light.

An important first step in the overall energetics of laser fusion is the determination of how much of the incident radiation is absorbed in the target. Absorption is measured in a variety of ways, including measuring the light scattered (and therefore not absorbed) at the target and measuring the integrated ion blow-off energy from the target. Figure 1 shows the absorption on spheres of various sizes as a function of intensity.⁴ Typically, at the

6 7 0 9 0 5 7 5

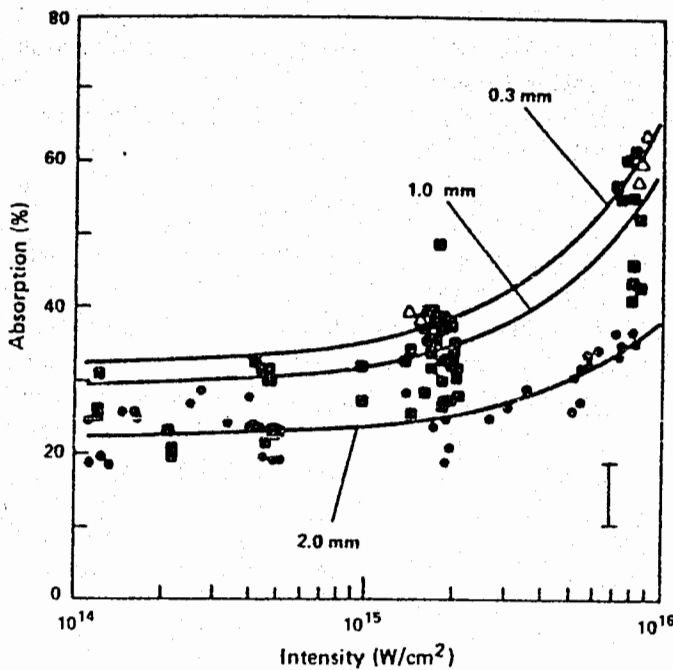


Fig. 1. Absorption, as measured by ion calorimetry, for spheres of varying size.

UNCLASSIFIED

lower intensities shown at the left, the absorption is about 30%, whereas at high intensities it can exceed 60%. In hohlraums, the absorption is typically 50 to 75%, depending on the laser entry hole size relative to the target size. In principle, it is possible to increase this absorption to greater than 90%.

What are the mechanisms of absorption and how can we identify which ones are actually operative in laser target experiments? Although inferences can be made from a variety of experimental data, most of the information on absorption processes has come from computer simulations and analytic theory, which have been iterated to reproduce the experimental data base.

The simplest form of absorption of laser light results from collisions of electrons oscillating in the laser electric field with the background ions. This process, known as inverse bremsstrahlung, works by randomly scattering the oscillating electrons off the ions. Thus, coherent oscillation energy is converted into random energy. By equating the dissipated light energy, $\nu E^2/8\pi$, to the heating rate, $\nu_{ei} nmv^2/2$, where $v = eE/m\omega$, we find that the bremsstrahlung absorption frequency is $\nu = \nu_{ei} n/n_c$, where n_c is the density at which $\omega_p = \omega$. The absorption length for light then is c/ν . Because the electron-ion collision frequency ν_{ei} varies as v^{-3} , inverse bremsstrahlung preferentially heats low-velocity electrons and thus keeps the plasma close to thermodynamic equilibrium. If L is the density scale height, then significant absorption occurs for $\omega L/c \approx 1$. If we balance the absorbed energy with the electron heat flux, we see that significant absorption only occurs for

$$I < 5 \times 10^{14} Z L(\text{cm})/\lambda^4,$$

where Z is the ion charge state, L is the plasma scale length in cm, and λ is the laser wavelength in micrometers.

Thus, for $L \approx 1$ mm and $Z = 79$, inverse bremsstrahlung is negligible for the CO_2 wavelength of $10 \mu\text{m}$ at intensities above 10^{12} W/cm. Therefore, some form of collective absorption that is somewhat less desirable than inverse bremsstrahlung must be relied on. At wavelengths less than $1 \mu\text{m}$ (for example, the $0.25\text{-}\mu\text{m}$ light of KrF lasers), inverse bremsstrahlung is very important and appears experimentally to dominate the absorption process, although some undesirable forms of collective absorption are still present to a modest extent.

An important quantity that affects the collective absorption processes is the pressure of the incident light

wave, the so-called pondermotive force, $F = \omega_p^2/\omega^2 \nabla |E|^2$. It is a low-frequency force proportional to the light intensity and the ratio of the plasma density to the critical density of the incident light. For example, at 10^{16} W/cm², the pressure of the light at its reflection point is about 5 Mbars! This large force is able to distort the flow of expanding plasma at low densities and is responsible for most of the instabilities induced by the incident radiation in the underdense plasma.

Because of this strong pondermotive force, two basic mechanisms of collective absorption have been identified as important in all laser-plasma interactions and particularly important for CO_2 lasers.

The first is called resonant absorption,^{5,6} in which the electric field of an obliquely incident laser beam can linearly couple to a longitudinal plasma wave in the low-density expanding plasma. For a wave with an incident angle θ , the electromagnetic wave is reflected from the region $n = n_c \cos^2 \theta$ but may still tunnel to the resonant matching point as shown in Fig. 2. At the resonant point, the component of the electric vector along the density gradient induces time-dependent density fluctuations at the local plasma frequency, acts as a source of plasma waves, and extracts energy from the incident electromagnetic wave. The conversion efficiency depends sensitively on the incident angle and the scale length between these two points. For angles of incidence of the order of 20° , the scale length must be less than a wavelength of light to obtain an absorption of greater than 20%. In fact, the large pondermotive pressure gradient of the reflecting light wave and the locally generated plasma wave produce a sharp density gradient in that region, which allows resonant absorption to be an effective process.

In Fig. 3, we show the sharp density gradient from a WAVE simulation⁷ that extends to densities far above the critical density. An important experimental identification of resonant absorption at high laser intensities is from the large, second harmonic emission of light produced. The nonlinear coupling of the density fluctuations of the plasma wave to the incident light produces the second harmonic through the current $j(2\omega) \approx v \delta n$. Its intensity is proportional to the incident light wave intensity and the plasma wave intensity. The scaling of the second harmonic emission is a strong function of incident laser intensity. At low intensity the 2ω emission is proportional to I^2 . At high intensity, where δn saturates because of nonlinearities, the 2ω emission is proportional to I .

UNCLASSIFIED

67090576

UNCLASSIFIED

~~SECRET~~ RD

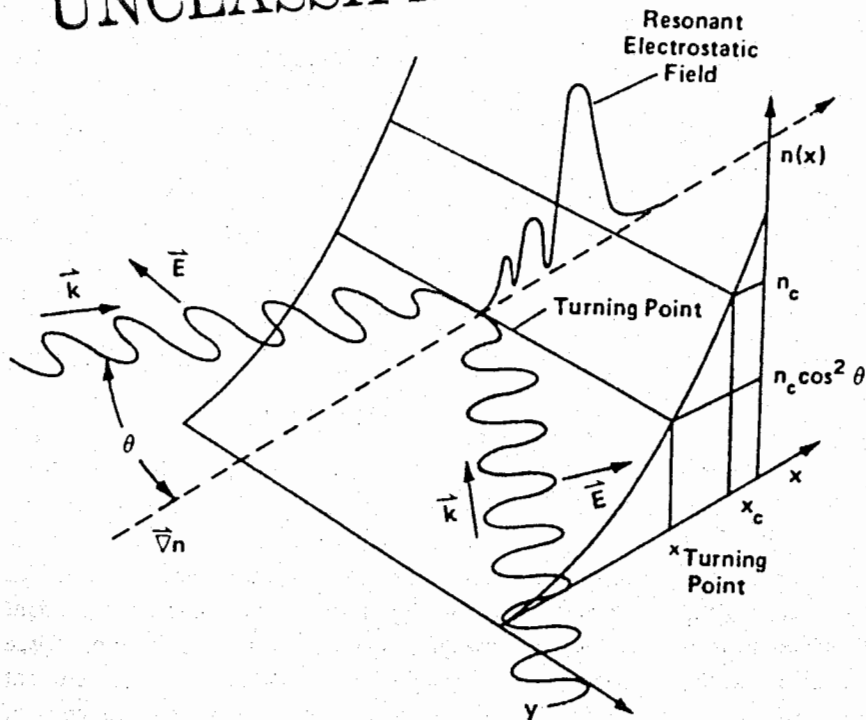


Fig. 2. The resonance absorption process.

6709 0577

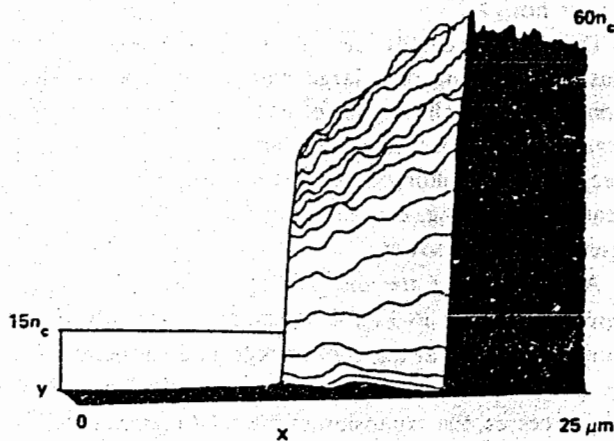
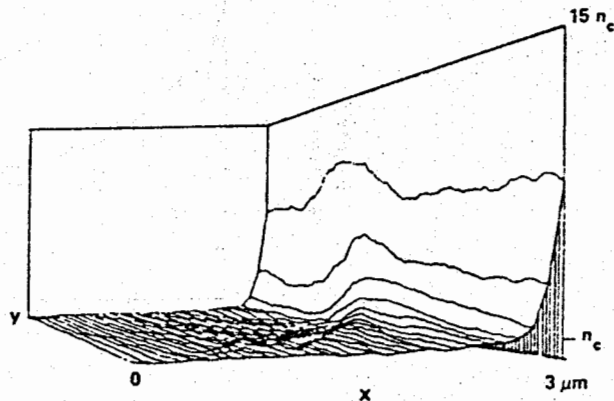


Fig. 3. Density gradients obtained from the WAVE code.

(a)



(b)

UNCLASSIFIED

~~SECRET~~ RD

WAVE BREAKING

Once the energy is placed into the plasma wave, it is quickly dissipated into the plasma by a number of mechanisms. Because of the extremely high intensity of the laser, the primary way in which the energy is absorbed is by a process known as wave breaking. In this process a few electrons can gain energies of hundreds of kiloelectron volts in less than one laser cycle (about 10^{-14} s) over distances of less than a micrometer as they are accelerated by the plasma wave. The energy they gain is proportional to the electric field of the plasma wave and its width. Because the width is narrower due to the steepened profile, the electron energy is reduced over the one that would occur in some gentle profile.⁸ Although the acceleration process is quite coherent, it is observed in computer modeling to have a small random change from cycle to cycle, which injects stochasticity into the distribution, resulting in a near-Maxwellian hot-electron distribution.⁹ Although nearly all of the electrons at the critical density can be heated by this process, only a small fraction of electrons above the critical-density surface is hot.

Thus, we typically see a two-component electron plasma consisting of a large number of "cooler" electrons with a small number of energetic electrons over a broad energy spectrum that carries most of the heat. Because the equilibration time between the two components is quite long, this situation persists as long as the laser is at high power.

An example of the distribution of electrons at high density is shown in Fig. 4. A major uncertainty in the simulations is what the cool background temperature is. Because the temperature depends on the radiative cooling processes, the expansion of the solid material, ioniza-

tion rates, and so forth, it cannot be determined self-consistently with the WAVE code but must be modeled with LASNEX. Nevertheless, this relatively simple theory has resulted in a reasonable match between theory and experiment⁸ concerning the magnitude of the hot-electron temperature and the nearly constant absorption of 20-30% that is observed from 10^{14} - 10^{15} W/cm².

The most spectacular confirmation of this process is the observation in experiment and simulations of high harmonics of the incident laser light.⁷ In fact, experiments as illustrated in Fig. 5 have shown more than 35 harmonics of the incident light in the scattered-light spectrum, confirming the extreme nonlinearity of the interaction in the steepened density gradient. These high harmonics are a signature of the extremely anharmonic character of the acceleration seen by the electrons in the intense coherent resonant absorption plasma wave,¹⁰ as shown in Fig. 6. The plasma wave in the steep gradient "sees" a strongly, spatially varying, restoring force proportional to ω_p^2 . The maximum harmonic content theoretically expected is up to the plasma frequency of the upper density shelf. The experiment then implies that the plasma wave is probing densities up to 1000 times the critical density, or essentially solid density.

In recent years, however, experiments at higher intensity and with more extensive calculations have indicated that this very steep gradient may not last for a long time. When the high harmonics are time resolved using ultrafast optical streak cameras, they are observed to last only during the risetime of the laser pulse, about 200 ps, which is partially due to the expansion of the plasma outward from solid density so that the plasma wave no longer experiences the strong acceleration at those high densities. In addition, the nearly constant absorption

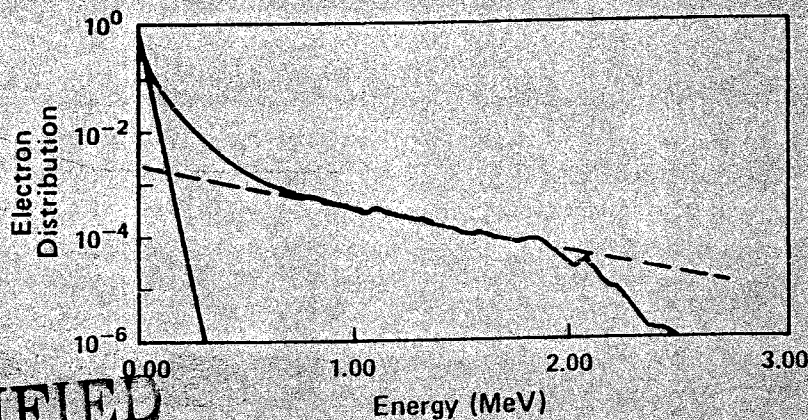


Fig. 4. The heated-electron distribution from WAVE.

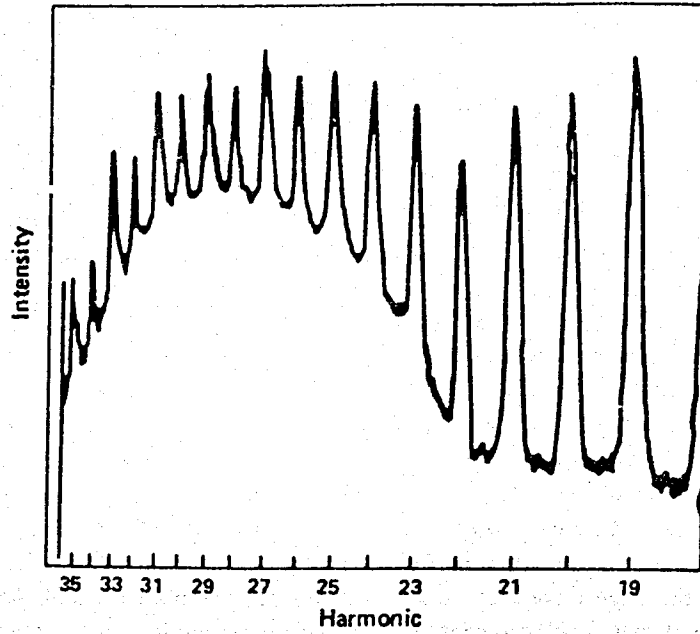
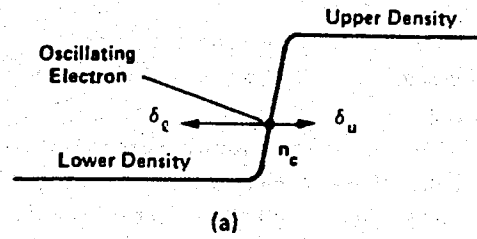
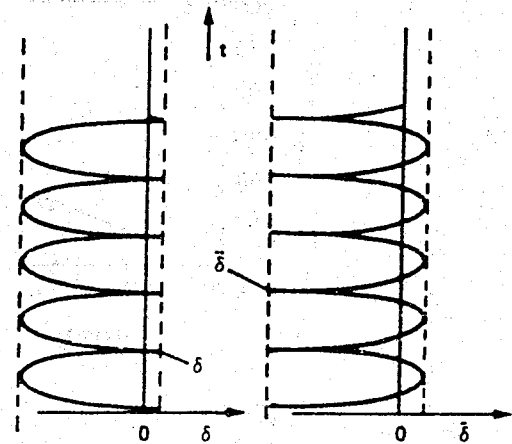


Fig. 5. Harmonics of the incident 10- μ m light produced by nonlinear coupling mechanisms in the steep plasma gradient.



(a)

Fig. 6. The anharmonic restoring force on oscillating electrons near the density jump.



(b)

67090579

coefficient observed at low intensity is observed to increase dramatically above about 10^{15} W/cm², as shown in Fig. 1, suggesting that an additional absorption process occurs at high intensity, which we attribute to a second mechanism discussed next.

PARAMETRIC INSTABILITIES

A second mechanism of collective absorption involves parametric instabilities, which are the nonlinear coupling of the light through the pondermotive force to various plasma models.^{11,12} In these processes the pondermotive force couples the harmonic oscillator equations for plasma waves with those for light waves at a different frequency from the laser. Typically, the conditions for instability are met most readily when the three natural frequencies, ω_1 , ω_0 , and ω , and the three wave vectors, k_1 , k_0 , and k , satisfy conservation of energy and momentum:

$$\omega_1 = \omega_0 - \omega$$

and

$$k_1 = k_0 - k,$$

where the subscript 0 represents the pump laser, 1 represents the scattered (light) wave, and no subscript represents the plasma wave.

The most important modes appear to involve coupling of light waves to electron plasma waves and ion sound waves. The coupling to electron plasma waves, known as stimulated Raman scattering, occurs at low

densities, $\omega_p^2 < \omega^2/4$, and excites a broad spectrum of electron plasma waves that accelerate electrons to high energy over a long (typically 1-mm) distance. (The production of extremely energetic particles is being harnessed in the beat wave acceleration process. In this process, two lasers with a frequency difference equal to the plasma frequency are used to enhance the plasma wave amplitude over that generated by Raman scattering itself.) This acceleration over relatively large distances contrasts to the resonant absorption process described above.

In addition, right at the quarter-critical density, the incident light can directly decay into two plasmons. The nonlinear state of these instabilities depends strongly on the density scale length and temperature of the underdense plasma. Unfortunately, plasma simulations are not able to self-consistently calculate the large-scale underdense plasma blowoff, and the experiments at 10 μ m have been unable to accurately measure it. Therefore, only representative calculations can be made in which one estimates the plasma initial conditions. These calculations suggest that, as the plasma scale lengths approach a millimeter, this process may begin to dominate. This process is believed to be the most important in hohlraum targets where long, underdense plasma can quickly fill the large initial vacuum region. The hot-electron temperature and absorption scaling from simulations are shown in Fig. 7. The hot-electron temperature is much higher at moderate intensities than it is from resonant absorption.

An additional coupling path of light to ion sound waves in underdense plasma (known as stimulated Brillouin scattering)¹³ results in less plasma heating

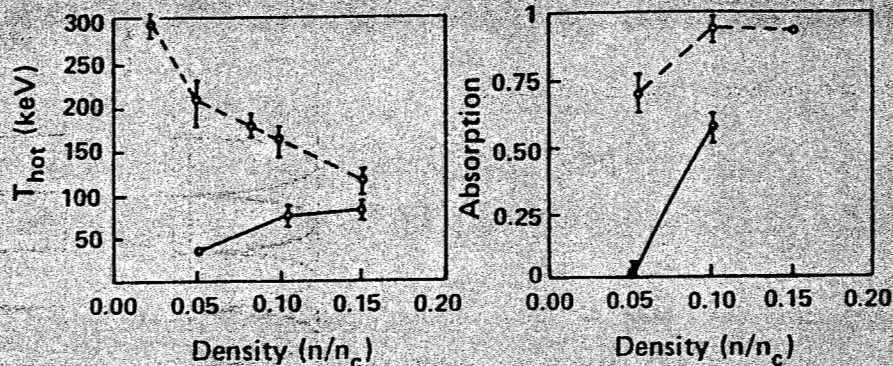


Fig. 7. Hot-electron temperatures and absorption in a long-scale-length plasma from WAVE. The solid curves correspond to a single pass of the laser light through the plasma. The dashed curves correspond to a reflection of the laser light at the plasma boundary and two passes through the plasma.

67090530

because of the greater mass of the ions, although it has the potential of reducing the absorbed laser intensity. Calculations suggest that the ion waves become nonlinear so rapidly that the light is not scattered away but merely adds to the plasma heating rate. This heating rate, however, is lower than that from electron plasma waves. This process may be much more important at short laser wavelengths, where the ion sound waves do not become as nonlinear.

In addition to backscattering, there are also self-focusing and filamentation instabilities of the incident light.¹⁴ Pondermotive, force-driven filamentation has a similar gain length to Brillouin scattering when the ions are very warm, $T_i = T_e$. At low intensities there is a thermal, self-focusing instability resulting from bremsstrahlung heating that can reduce the density in a channel, refracting the light within the channel, which raises the intensity and further heats the plasma. This latter process may be particularly troublesome at short wavelengths. This instability can be viewed as arising from the strong anisotropy in the pressure of the incident light wave.

A number of parametric instabilities at the critical surface have been identified theoretically.¹⁵ However, in general, the steep density gradients induced by the pondermotive force severely reduce these instabilities.

If fusion with CO₂ lasers is to work, one must stay at intensities and plasma conditions that do not allow parametric instabilities to develop and rely on resonant

absorption in a steepened density gradient to maintain the lowest hot-electron temperature. These conditions appear difficult to achieve at best. As mentioned earlier, some additional absorption process appears to be occurring above 10^{15} W/cm². Recent simulations at an intensity of 2.5×10^{15} W/cm² run for tens of picoseconds instead of only a few picoseconds⁴ (made possible by the substantial increase in size of the Los Alamos computer facility) show a similar phenomenon.

Figure 8 shows a contour plot of the density surface late in time. Note that the originally smooth, sharp density gradient has begun to break up and become rough. Associated with this roughness is a substantial increase in the absorption coefficient from about 25 to 60%. At the same time, the hot-electron temperature increases by a factor of 2 or 3 over that calculated for resonance absorption on the initially smooth surface. At 10^{16} W/cm², the surface is observed to become even more turbulent. Basically, the parametric instabilities at the critical density that were suppressed by the sharp gradient appear to become dominant at high intensity. This process may explain the increased hot-electron temperatures (hundreds of kiloelectron volts) observed on Helios at high intensities.^{1,3}

We see then that the large amplitude of the laser radiation results in a highly nonequilibrium state of the plasma. It is so far from equilibrium that, for example, classical shock waves are altered. The region where resonant absorption occurs corresponds to a phase transition

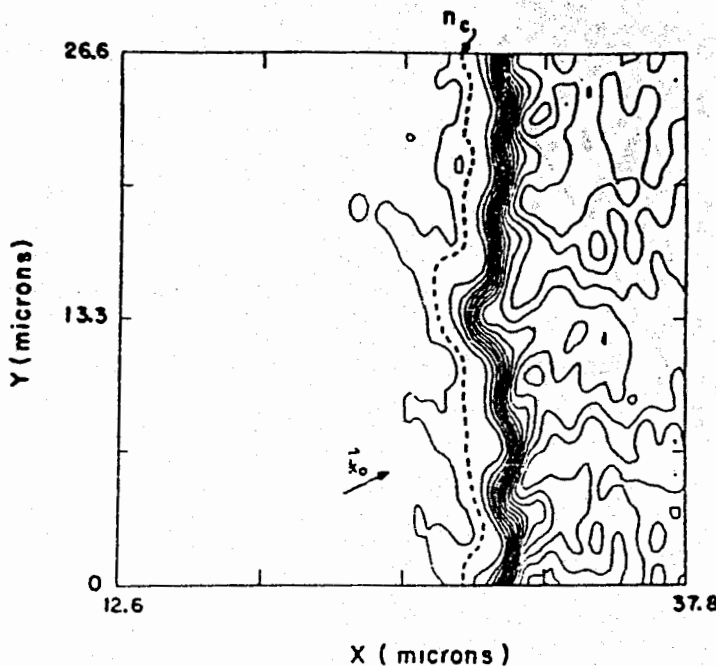


Fig. 8. Contour plot of the density late in time.

UNCLASSIFIED

~~SECRET/RD~~

UNCLASSIFIED

between a hot plasma in the presence of the laser light to a colder plasma without the laser light present. In this region, rarefaction shocks¹⁶⁻¹⁸ are generated, which have very different properties from conventional shock waves. Matter is put into an extremely unusual state that is probably only reproduced in exotic astrophysical situations. The fact that most of the absorbed laser energy is placed into a few energetic particles significantly reduces the implosion efficiency of fusion targets and makes the task very difficult.

ENERGY FLOW

Hierarchy of Energy Flow Channels

Once hot electrons are produced by the absorption process, they proceed to convert their energy in one of two ways. Hot-electron pressure in the corona can collectively accelerate the coronal ions to extremely high energies by collisionless processes. In the simplest model, some electrons leave the target (they are initially ejected outward from the critical surface by the resonance-absorption mechanism), but the nonzero impedance and inductance of the target support stalk allow electrostatic potentials of hundreds of kilovolts to develop at the

target, confining the remainder. The confined electrons accelerate ions by working against the coronal plasma as they try to escape.

Experimental measurement of the fast-ion energy shows that a substantial fraction of the absorbed laser light goes into fast ions, particularly at high intensity (Fig. 9). Alternatively, the electrons can lose their energy by collisional stopping in the bulk of the target. Because the range of hundred-kiloelectron-volt electrons in matter is quite long compared with the amount of material that can expand into vacuum under the influence of hot-electron heating during the laser pulse, the target material is to a first approximation isochorically heated. This collisionally deposited electron energy is partitioned into internal energy of the material, kinetic energy (thermal or "slow" hydrodynamic in contrast to the collisionless fast-ion expansion of the corona), and thermal, soft x-ray radiation.

If the target is thick compared with the hot-electron range, the motion of the target will be quasi-ablative. If the target is thin to electrons, it will explode. The collisional stopping of the hot electrons also produces hard x-ray bremsstrahlung^{1,3} and characteristic x-ray emission,^{19,20,21} which are not in themselves energetically important. However, they provide unique observables

67090382

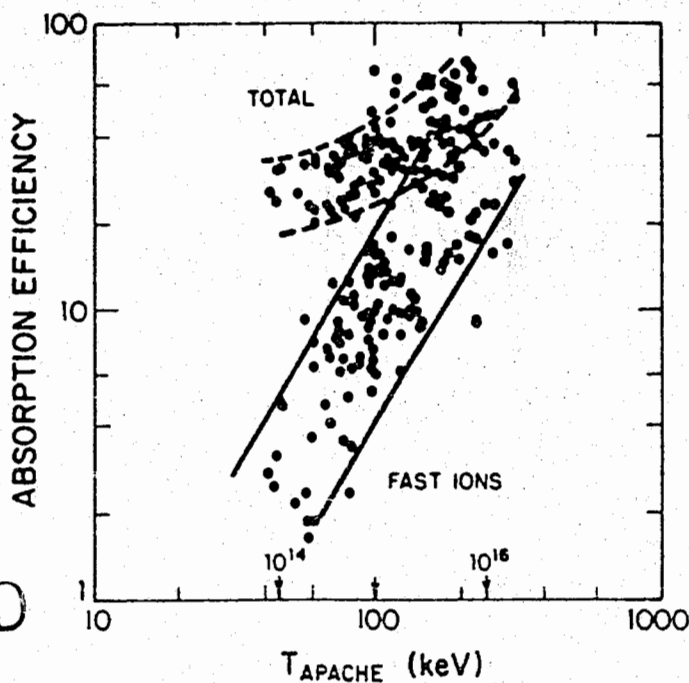


Fig. 9. Fast-ion production efficiency as a function of the hot-electron temperature (from the APACHE hard x-ray spectrometer) and intensity.

UNCLASSIFIED

~~SECRET/RD~~

that we have used to determine the hot-electron temperature, the amount of deposited electron energy, and the location where the hot electrons are depositing their energy.

Our experimental measurements, together with computer modeling, allow us to piece together a generally consistent picture of the energy budget and energy flow. The absorption, as noted above, can be as high as 60% at 10^{16} W/cm², although generally closer to 30% below 10^{15} W/cm². The energy partition to fast ions depends on a number of factors described below. However, because the energy partition to fast ions also increases with intensity (Fig. 9), the amount of energy that is collisionally deposited in, for example, a spherical target, is only about 20% of the incident radiation, independent of intensity. Ultimately, we wish to use one or more of these energy channels to provide energy to the ablator of a target capsule, either directly or indirectly, leading to the symmetric implosion of the capsule and thermonuclear burn. These basic energy channels also provide a "natural" set of observables we can use to trace the physical processes taking place: soft and hard x-ray emission; the fast-ion energy, spectrum, and angular distribution; and the slow- (thermal) ion distribution.

Fast Ions and the Energy Budget

Because fast ions can carry such a large part of the energy budget, we have studied these ions extensively with a wide variety of diagnostics. Many of the ion calorimeters that we have used to infer the absorption of laser light have been filtered with thin foils (typically 0.5- μ m nickel) to detect only these fast ions and reject thermal ions and x rays. Such a filter will pass ions of 100 keV/amu (about 4×10^8 cm/s) with a weak dependence on the ion atomic number. In the simplest model of ion expansion, the ion distribution is an isothermal

$$N(v) = e^{-v/c_s}$$

with the sound speed driven by the hot-electron temperature

$$c_s = \sqrt{\frac{Z}{A} T_H}$$

For a hot electron temperature of 250 keV (obtained at 10^{16} W/cm²) and for a $Z/A = 1/2$ appropriate for highly stripped ions such as carbon (for example, from a plastic target), the sound speed is approximately equal to

the velocity of an ion that just passes through the filter. Because most of the ion kinetic energy is in ions above the sound speed, the ion energy transmitted through such a filter is a good estimate of the total fast-ion energy at high intensities, but at lower intensities where $c_s \ll 4 \times 10^8$ cm/s, this measurement is a lower bound.

The data in Fig. 9, in which the fraction of absorbed energy in the fast ions increases with intensity to as much as two-thirds of the absorbed energy, were obtained using filtered ion calorimeters as just described. The increase of fast ion fraction with intensity persists even after filter-thickness effects at lower intensities are estimated and corrections to the raw data in Fig. 9 are applied. Thus, the fast ions are a major energy channel and a major energy loss unless exploited for driving targets. The absorption (A) and the fraction of absorbed energy in fast ions (F) can be used to provide an indication of the energy remaining for collisional deposition, $E_c = A(1-F) \leq 0.25 E_{inc}$, for spherical targets. Measurements of the ion velocity distributions with magnetic analyzer spectrometers [so-called Thomson parabolas, which are ion spectrometers with parallel E and B fields and which produce velocity spectra $N(v)$ along parabolic tracks in the detector plane with different parabolas for each Z/A] indicate that much of the ion energy is carried by hydrocarbons independent of the target material. These hydrocarbons are surface contaminants on the target that are accelerated to the highest velocities because the lowest Z ions are accelerated most rapidly in the complex multispecies ion expansion. Although the ion spectrum from such a multispecies expansion is remarkably complex²² and difficult to calculate theoretically, its gross properties are deceptively simple.

As the ion mean energy is not far above that required to penetrate a 0.5- μ m nickel filter, we can determine the ion "spectrum" by a set of transmission measurements in an array of differently filtered calorimeters. Figure 10 shows examples of such ion spectra for high- and low-intensity cases. Not only are these transmission curves well behaved, they can readily be fit to an isothermal expansion model taking the hot-electron temperature T directly from the bremsstrahlung measurement if we assume $Z/A \approx 1/2$. Transmission data as in Fig. 1 are useful in evaluating target design concepts. For example, the mass required to stop one half of the ion energy is an important parameter that can be used to determine whether this ion energy is exploitable in target design.

Whereas ion stopping powers are a weak function of Z, very heavy ions (such as tantalum and gold) have an appreciably shorter range than protons or carbon. Based

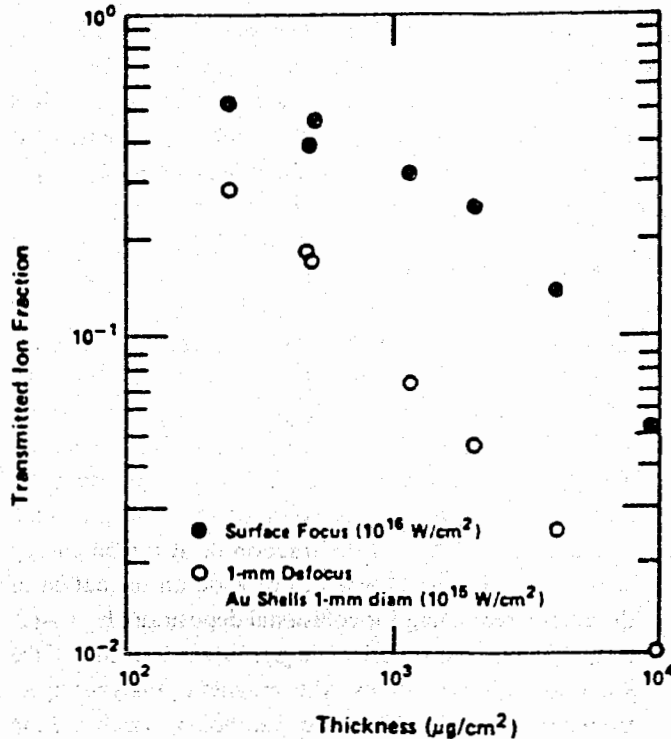


Fig. 10. Ion transmission spectra.

on an analysis of the multispecies ion expansion, we conjectured that if low-Z surface contaminants could be removed, atoms of high-Z target material could be accelerated to similar velocities (the fastest proton in a typical expansion, measured with time-of-flight scintillator detectors, typically has a velocity of about 2×10^9 cm/s). In an experiment in which tantalum targets were heated with electron bombardment to white heat to drive off hydrocarbon, we observed energetic tantalum ions. The fastest ion observed corresponded to an energy of 500 MeV for tantalum, and Thomson spectrometer data confirmed the absence of protons in the expansion while indicating that the tantalum ions were as much as 60 times ionized.

For targets with a thickness less than the hot-electron range, electrons can pass through the target many times, reflecting off the expanding plasma sheath each time. This situation can greatly increase the absorbed energy placed into fast ions.

For targets that are thick to hot electrons, causing an electron to have only a single chance to bounce off the electrostatic sheath surrounding the target and to work against the coronal ions, theoretical calculations (ignoring albedo effects) indicate that the fraction of energy in fast ions cannot exceed 5-10%, which is the fraction of electron energy lost in reflecting from the expanding plasma.

Thus, we infer from these data that a mechanism exists to trap the electrons in the corona, allowing them to lose more of their energy to fast ions. This process is generically known as flux-limited transport. That is, there is some process that reduces the mean penetration velocity to less than it would be from a simple diffusion model. One process that can cause this phenomenon involves the generation of intense magnetic fields by the high-energy electrons themselves.

For a laser spot of finite size on a target surface or for not completely uniform illumination of a target, there are a temperature gradient along the surface over the laser spot, a strong density gradient along the surface over the laser spot, and a strong density gradient normal to the surface under the spot. These density and temperature gradients, which are perpendicular to each other, cause a magnetic field to be generated by the curl of the ambipolar electric field:

$$\partial B / \partial t = - \nabla \times E = \nabla n \times \nabla T / n .$$

The generation rate is extraordinarily high with a field of 1 MG reached in 1 ps with a density gradient of 10 μm, a spot size of 100 μm, and a temperature T of 50 keV. In the time it takes an electron to cross the laser spot, the field is strong enough to reduce the gyroradius of an electron to less than the density scale height. The electrons

can no longer free-stream into the target but are confined by the magnetic field. In VENUS simulations,²³ the electrons $E \times B$ drift along the target surface to great distances from the initial laser spot.²⁴ This reduces the transport inward under the laser spot and enhances the electron energy carried far from the laser spot. One of the consequences of the self-generated fields is that many of the ions are accelerated in an intense ion jet or plume normal to the target surface.

Figure 11 shows the angular distribution of ions leaving a disk target as measured by calorimeters with three different thresholds provided by filtering. The plume has half-width at half maximum of about 10° , in excellent agreement with particle simulations using VENUS. For targets smaller than about 1 mm, including small spheres, the effect is washed out and the ion angular distribution becomes more isotropic. The effect is also washed out in thin targets, where electrons can travel from the laser spot by reflexing through the shell and disrupting the current flow that creates the magnetic fields. For large, thick-walled spheres, however, the jets persist.

Because in a spherical target experiment these jets will be directed back toward the focusing optics where they are not measurable, we believe that the apparent reduction in absorption in larger spheres as measured by calorimetry (Fig. 1) is due to this extremely forward-peaked, angular distribution. However, the appearance of a strongly directed ion jet, along with a large component of the energy budget in fast ions, raises the possibility that the ion energy might be directed from the laser target to the capsule and the ions used to drive the capsule either directly or indirectly.

TARGET DESIGNS TO EXPLOIT THE ENERGY FLOW

Because the details of the energy budget are in some measure affected by the target characteristics, we can design target concepts to use various energy channels and optimize them through design based on both empirical data and theoretical extrapolation.

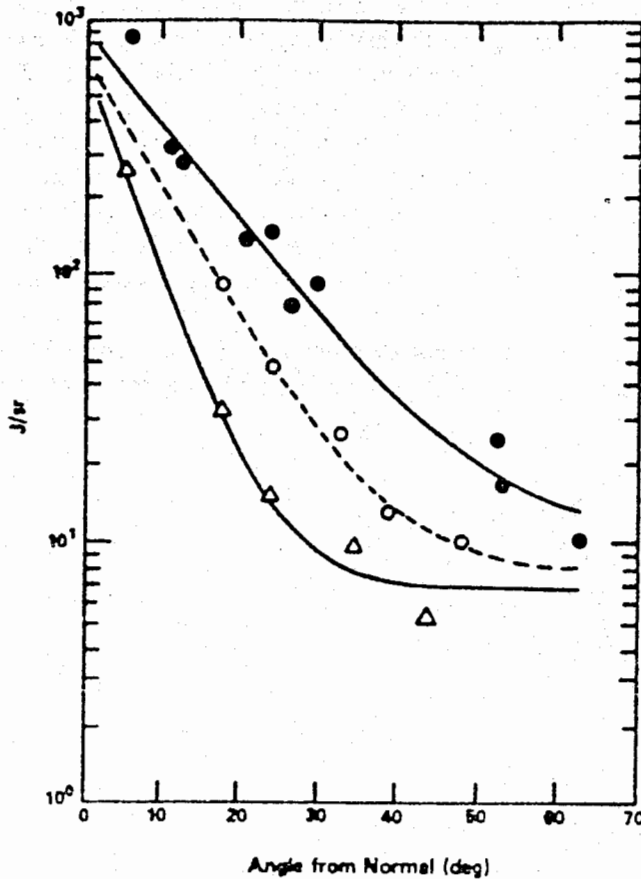


Fig. 11. Fast-ion angular distribution: ● all ion energies, ○ $E \geq 100$ keV/amu, $\Delta E \geq 500$ keV/amu.

67090485

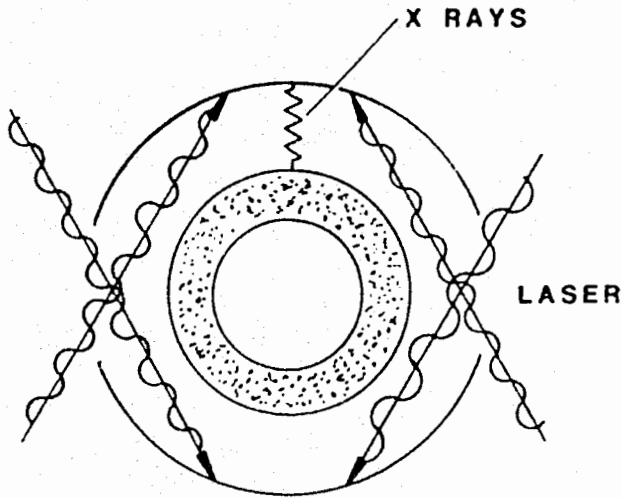


Fig. 13. Schematic of hohlraum target (Chamisa). Laser light is trapped inside case and absorbed, heating walls. Resulting x rays drive implosion. Issues are volume absorption of light by processes producing high, hot-electron temperatures, deep deposition of energy in walls, low efficiency of producing x-rays, and plasma closure of entrance holes.

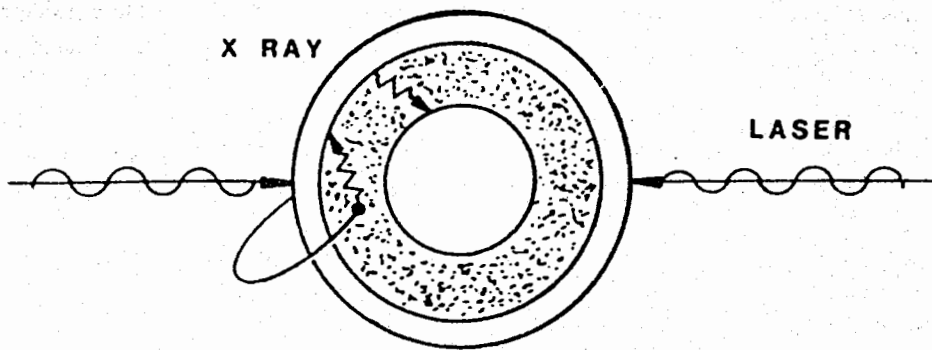
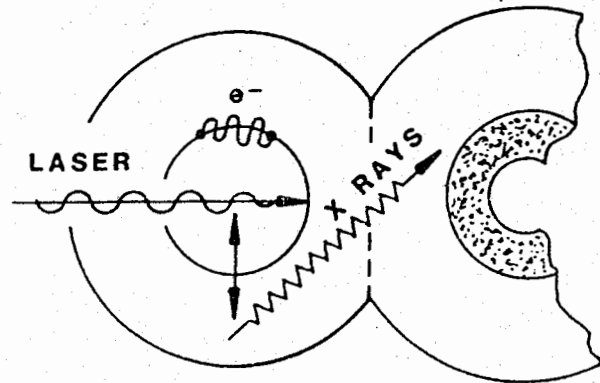


Fig. 14. Electron greenhouse target (Arcturus). Laser incident on high-Z case; hot electrons penetrate case and deposit in low-Z radiation generator/ablator. Radiation trapped inside case. Issues are low effective absorption, long range of hot electrons in ablator, resulting in low energy per unit mass, and coronal decoupling at long pulse suitable for high gain capsules.

67090586

Fig. 15. X-ray driven target using stagnation-produced x rays (Canopus). Hot electrons explode inner shell, which stagnates against wall of pod, converting kinetic energy to x rays, which enter main hohlraum containing capsule. Issues are high hot-electron temperature and loss of vacuum insulation, fast-ion production, and inefficient radiation flow from pod primary to secondary.



Chamisa target, requiring the concept of "vacuum insulation." Hot electrons cannot move much beyond the leading edge of the ion expansion because of electrostatic effects (the same effects that, in fact, drive the ion expansion). Thus, if the space between the inner shell and outer pod wall is too small, the ions will cross the gap during the laser pulse; and the hot electrons, rather than exploding the inner shell, will be deposited in the pod wall. This situation will put a lower limit on the target size.

A major advantage that Canopus targets offer is that a short laser pulse (about 1 ns) can produce a long radiation pulse (about 10 ns) because of the change in characteristic times from that of the laser to that of the slow-ion stagnation. As target capsules generally desire long shaped pulses for optimum implosion efficiency and high compression, this concept provides an advantage by pulse shaping in the target rather than in the laser.

The Chamisa and Arcturus targets use the collisional deposition channel to produce x-ray drive. The direct-drive target uses this same channel to go directly to hydrodynamics (slow hydro). Canopus attempts to use both the collisional channel (to produce the slow hydro of the inner shell explosion) and the fast-ion channel. We can attempt to use both the high energy and beam-like nature of the fast ions to drive the final target type discussed here. In the Procyon target concept, the laser is incident at high intensity to maximize the fast-ion channel on an ion converter and acts as an ion diode, producing a beam of fast ions that can be directed toward an ion-driven target (Fig. 16). Because the fast-ion range is long, we utilize an ion-driven version of the greenhouse Arcturus target concept to turn the ion "beams" into x-ray drive.

There are a few other target concepts (we have studied nine in detail), but they are largely variants of these basic

attempts to exploit the various energy flow channels available. Below, we summarize the ultimate performance of these targets based on an evaluation of Helios data. We then describe some of the experiments and the results we have used to reach our conclusions, thus briefly illustrating both the physics and the techniques used to unravel the problems.

ANALYSES OF TARGET DESIGN CONCEPTS

To evaluate the potential of these target design concepts, we chose to factor the problem into the capsule implosion physics and the drive mechanisms. In essence, we asked, "What is the efficiency with which one can provide the drive energy to the ablator?" We assumed that any drive concept could be made to produce the requisite drive symmetry. We also ignored—temporarily for this analysis—the effect of hot-electron or bremsstrahlung preheat on the capsule performance except as a constraint in target design (that is, in some cases we designed the target to limit the hot-electron penetration through the ablator, to the pusher, and to the fuel). We find that the resulting analysis does not crucially rest on these rather simple assumptions.

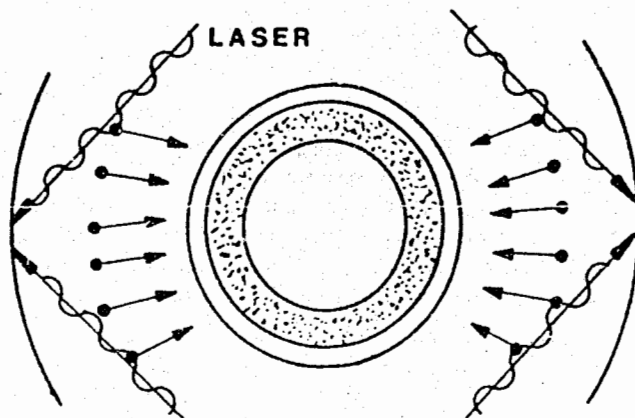
As most of our targets are x-ray coupled, we used a figure of merit called the x-factor to define the target coupling efficiency:

$$X = (\text{x-ray energy absorbed by ablator}) / (\text{driver energy on target}).$$

For direct drive, we converted to the effective x-factor by

$$X = (E_{abl}/E_{inc})(n_e/n_x),$$

Fig. 16. Ion-beam coupled target (Procyon). High intensity CO₂ laser generates collimated jet of fast ions, which drive ion-driven, greenhouse target. Issues are efficiency of conversion to ion energy in the narrow jet.



UNCLASSIFIED

UNCLASSIFIED

~~SECRET~~ AD

where $n_{e,x}$ are the "rocket" efficiencies for direct drive and x-ray drive for an equivalent amount of ablator energy. We estimated from systems studies and capsule gain calculations that $X > 0.25$ is necessary for fusion power production.

We note that for short-wavelength lasers (say, $\lambda = 0.25 \mu\text{m}$) in a Chamisa hohlraum target, the absorption is expected to be nearly 100% (absorption on open targets such as disks or spheres is almost that high) and as much as 80% of this energy may be converted to soft x rays.

About 10% of the x-ray energy is lost out the laser entrance holes; and of the remaining energy, about 60% is used to drive the heat front into the low-Z capsule ablator, and 40% is lost to the heat front in the high-Z radiation case. Therefore, for a short wavelength laser that is nearly ideal,

$$X \cong (1) (0.8) (0.9) (0.6) \cong 0.43 .$$

Experiments at short wavelengths continue to be promising. Recent calculations indicate that the soft x-ray conversion expected may be somewhat less than the desired 80% when extrapolated to megajoule long-pulse experiments, indicating the need for continued experimentation and optimization.

In the Chamisa target, the absorption can be high and fast-ion loss can be small because energy must escape back out the laser entrance holes to be lost. At least 50% of the incident energy can be kept in the collisional channel. However, the hot-electron temperature in these hohlraums is extremely high (about 300 keV), much higher than expected for resonance absorption at the intensity of the laser beams as they first intercept the hohlraum wall. These hot electrons penetrate the hohlraum wall very deeply, and only a very small amount of the deposited energy resides within a radiation diffusion depth of the surface and is available for conversion to soft x rays. When the hohlraum is sized so that it does not fill with plasma above the CO_2 critical density during the long drive time required by the capsule (which would keep the light out of the target), scaling laws derived from Helios experiments indicate the low value of $X = 0.06$. Because the laser entrance ports must also be kept open and unfilled with plasma during the pulse, there is significant, additional loss of radiation out the holes. Thus, the x-factor for a Chamisa hohlraum, scaled to reactor size, is only about 0.02. In fact, more energy reaches the capsule in the form of preheating hot electrons than in the form of x rays.

In the Arcturus target, the basic limitation is the collisional deposition fraction, which for spheres is about 20 to 25% independent of intensity. Once we include the electron energy that does not penetrate the radiation case at the typical hot-electron temperature of 100 keV, only 18% of incident energy is deposited in the converter. To prevent hot-electron preheat of the pusher, much ablator mass is needed, lowering the temperature to which this mass can be raised to uninteresting value (tens of electron volts). Even using variations on the basic target design to work around the problem—the partition of the energy in the converter into internal energy and radiation and the efficiency of absorbing the radiation in the ablator rather than in heating the case—limits the x-factor for such a target to only $X \cong 0.10$. Direct-drive targets are limited by the collisional-deposition fraction of 20 to 25% and the hydrodynamic efficiency of hot electron drive ablator relative to x-ray drive (a factor of 3 poorer), which gives $X = 0.08$.

In Canopus targets, all of the absorbed energy (which can be as high as about 80% in the inner hohlraum) can be converted to thermal and suprathreshold hydro. However, the conversion to x-rays at the pod wall is inefficient, fast ions mostly go deeper in the pod wall than desirable, and extrapolation based on empirical scaling laws shows that only about 45% of incident energy reappears as thermal x rays. Of this relatively large fraction of the energy, about 22% is lost to heating the pod wall; 22% enters the main hohlraum where only about one-half, for an x-factor of 0.12, is finally deposited in the ablator. Whereas this is a higher x-factor than the concepts above, the scaling data that predict this eventual x-factor also predict that acceptable drive temperature in the main hohlraum requires significantly greater than 10 MJ in the laser pulse.

Procyon targets use the fast-ion channel, which at 10^{19} W/cm^2 takes <40% of incident energy. However, experiments have shown that only about 10% of incident energy is contained in the highly collimated ion jet, which can be transported to the capsule. The remainder of the ion energy is found at large angles in the wings of the peaked angular distribution. With the typical loss of efficiency in converting the ion energy to energy in the capsule ablator (similar to Arcturus), we have found the x-factor to be only 0.03 to 0.07.

This description summarizes the performance of the target concepts we investigated to exploit the various energy flow channels. Although there are a number of uncertainties in extrapolating our empirical data at <10 kJ

67070538

UNCLASSIFIED

~~SECRET~~ AD

to the megajoule range, none of these concepts shows promising scaling. Antares experiments, now under way, play a key role in determining the energy flow in regions where Helios data are ambiguous concerning conclusions about the x-factor (for example, hot-electron temperature scaling in hohlraums). In addition, Antares experiments have tested some concepts, such as the use of externally imposed magnetic fields to limit hot-electron penetration of the hohlraum wall and increase the energetic efficiency. In the remainder of this discussion, we explain some of the experiments, techniques, and results that have led to our analysis of target performance for Chamisa hohlraums.

HOHLRAUM TARGET PHYSICS

In determining the drive efficiency of hohlraums, we must examine the ability of the laser to successfully pass through the entrance hole, the efficiency of conversion of incident energy to soft x rays, and the potential problem of preheat in the presence of energetic electrons and bremsstrahlung. All of these processes have been charac-

terized experimentally with respect to their magnitude and their scaling with drive intensity.

Hole Closure

If a small amount of the laser beam or thermal energy from the inside strikes the hole, blown-off plasma can intercept the laser beam and refract it, causing it to be absorbed at or outside the hole. This effect has been studied both by measuring the transmission through holes at low intensity and by measuring the absorption and hot-electron temperature of hohlraums with varying size entrance holes. Figure 17 shows the scaling of the hot-electron temperature (inferred from the slope of the bremsstrahlung spectrum) as a function of hole size. Note that the temperature is independent of hole size for sufficiently large holes. Below a certain size, the hot temperature rises to a value close to that with no laser entry hole, which apparently indicates the point at which hole closure dominates the absorption process.

Additional evidence for hole closure and its effect on hohlraum energetics can be obtained from examining absorption and ion loss in these targets. Figure 18 shows

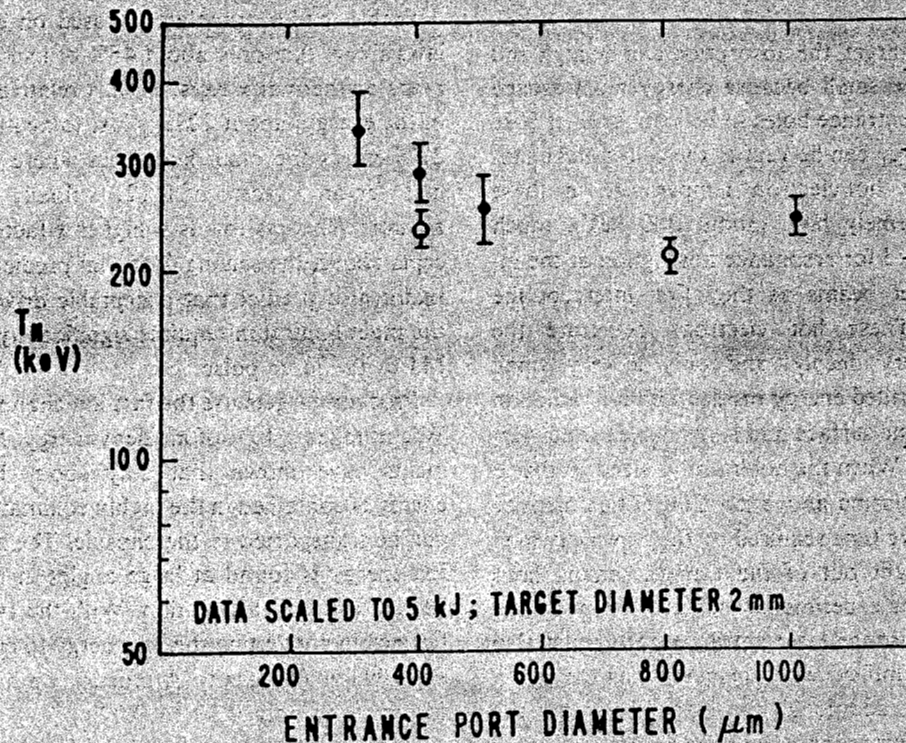


Fig. 17. Hot-electron temperatures from hard x-ray bremsstrahlung vs laser entrance port diameter. Higher temperatures result for ports $< 500 \mu\text{m}$.

67090589

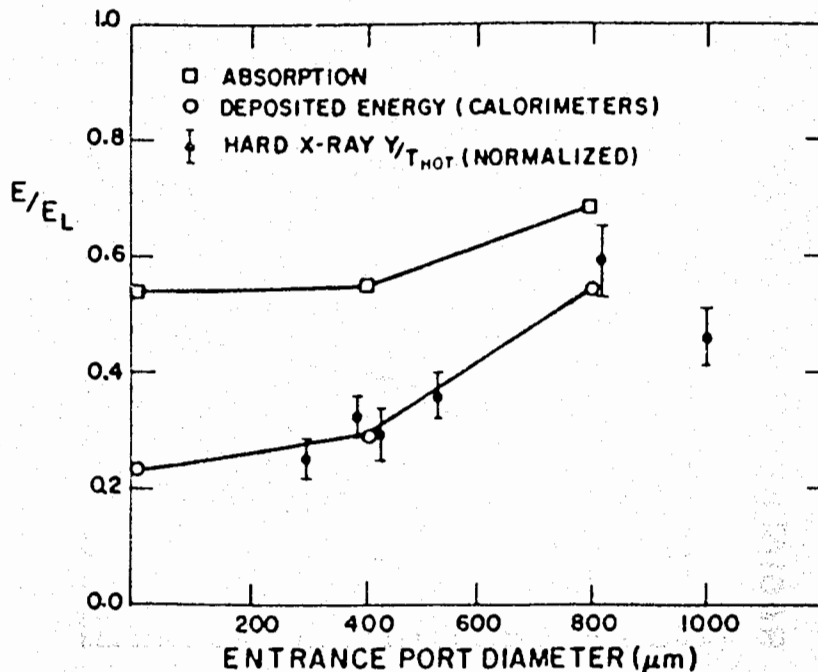


Fig. 18. Energy balance as a function of port diameter from calorimetry and analysis of bremsstrahlung (normalized to calorimeters for one particular diameter port) shows port closure for $< 800 \mu\text{m}$ in diameter.

the absorption and the net deposited energy after fast ion losses are subtracted, as a function of entrance port diameter. The solid points with error bars are the ratio of the hard x-ray yield to the hot-electron temperature; it is simple to show from thick-target bremsstrahlung cross sections that this ratio is proportional to the net collisionally deposited electron energy. The yield/ T_H data are normalized to the calorimeter data from 400- μm -diam ports. Clearly, only half as much energy is usefully deposited in a hohlraum with a 400- μm port as in a target with an 800- μm port; from the point of view of energy balance, targets with entrance ports $\leq 400 \mu\text{m}$ behave roughly like targets with no hole at all. These data are consistent with a plasma expansion velocity of about $2 \times 10^7 \text{ cm/s}$ with only a very weak dependence on laser intensity.

Radiation Temperature Scaling

Figure 17 shows that the hot-electron temperature is greater than 100 keV (for a given energy on target) for targets with holes that do not close. As indicated earlier,

at this temperature the electron range in gold is quite large; and, as a consequence, the efficiency of conversion to soft x rays is quite low. We measured the interior radiation temperature of small, spherical hohlraums by looking through a small (400- μm) hole in the wall with a collimated 7-channel soft x-ray detector array with 200-ps time resolution. X-ray imaging and tests with varying diameters of this diagnostic hole indicate that closure of the diagnostic hole to soft x rays is unimportant in this parameter regime. The measured temperature as a function of energy per unit wall area is shown in Fig. 19. If the process were at its maximum efficiency, the temperature would follow the upper curve in Fig. 19. Although the temperature follows this scaling fairly well, the magnitude of the temperature indicates that only a small percentage of the incident energy is converted into soft x-ray flux.

Hot-Electron Temperature Scaling

Measurements of the hot-electron temperature and its scaling with drive parameters show us the reason for this

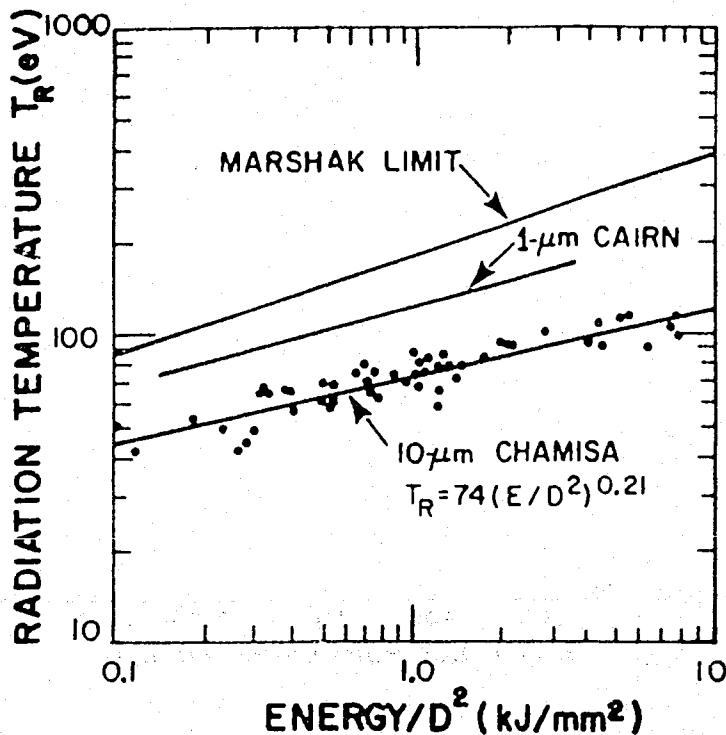


Fig. 19. Hohlraum temperatures at 10 μm compared with 1- μm Cairn experiments and the theoretical limit for Marshak thermal diffusion wave penetrating the wall.

low x-ray conversion efficiency. Figure 20 shows the hot-electron temperature for Chamisa targets as a function of energy divided by diameter squared; the larger (lower E/D^2) targets with 800- μm entrance ports, unaffected by hole closure, show a roughly $(E/D^2)^{1/2}$ dependence of hot-electron temperature; for 400- μm ports, the temperature converges asymptotically to that obtained for targets with no entrance port.

The high-temperature hot electrons in Chamisa penetrate the wall deeply, heating the large wall mass to a rather low temperature. Neglecting radiation loss from the holes and assuming that the electrons penetrate to a depth r_0 , the surface temperature of the wall will be given by

$$T_R^{1.5} \sim \text{Energy/Mass} \sim E/(Ar_0) \sim (E/A)T_H^{-1.6}$$

or

$$T_R \sim (E/A)^{2/3} T_H^{-1.1}$$

UNCLASSIFIED

More detailed LASNEX calculations in which E/A and T_H are considered independent parameters show a similar scaling

$$T_R \sim (E/D^2)^{0.55} T_H^{-0.7},$$

where from the empirical scaling of $T_H \sim (E/D^2)^{0.5}$ we find that

$$T_R \sim (E/D^2)^{0.2},$$

which is very close to the observed $(E/D^2)^{0.23}$ scaling of T_R . However, for hot-electron spectra characterized by a single Maxwellian, the quantitative LASNEX scaling predicts a somewhat lower radiation temperature than is measured, indicating that some additional heating of the wall surface may be present compared with that assumed in the LASNEX simulations. Because so little of the energy is deposited by the hot electrons near the surface, this additional heating can be caused by a modest fraction of the energy budget.

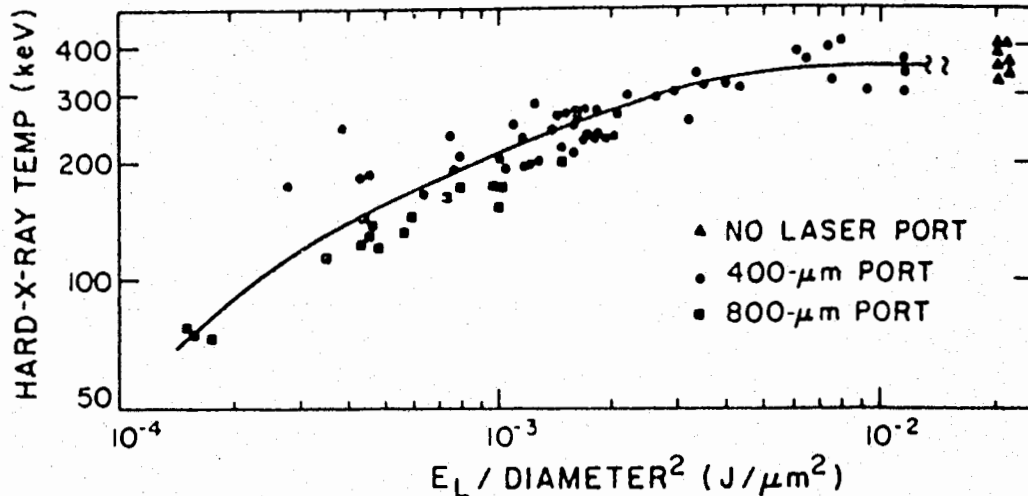


Fig. 20. Hot-electron temperatures for Chamisa hohlraums. Targets with 400- μm ports show saturation at high E/D^2 , which may be due to hole closure.

Hot-Electron Range

To confirm this picture of the hot-electron transport in hohlraums, direct measurements of hot-electron transport in the hohlraum wall were made using hohlraums of copper and nickel layers (the copper on the inside, nickel on the outside). The copper was used as a variable-thickness electron attenuator. Characteristic inner-shell (K_α) x rays from the nickel are emitted at a rate roughly proportional to the energy deposition in the nickel. Thus, by observing the nickel K_α emission as a function of copper thickness, we can trace the specific deposition of electron energy as a function of depth in the wall. The targets were overcoated with 200 μm of CH to prevent false signals from being produced in the nickel by electrons migrating out of the hole to the target exterior.

The resulting electron range data (Fig. 21) can be well modeled using analytic electron transport calculations or LASNEX with a Maxwellian temperature close to the temperature measured by bremsstrahlung. In addition, quantitative fits of LASNEX calculations to the data are in general agreement with the measured energy balance for these experiments.

However, there is evidence for a small, additional component of electron energy with a lower temperature. This evidence comes from both K_α transport measurements and detailed x-ray spectra in the < 25 -keV region on spheres and disks. From these measurements we infer

a small enhancement of electron number at low-electron energies roughly sufficient to raise the near-surface energy deposition and, therefore, the wall radiation temperature from the LASNEX calculations to measured values.

Thus, the basic issues for CO_2 -hohlraum scaling are hole closure and hot-electron temperature scaling. Our ability to understand the physics of these hohlraums is excellent with the exception of having few definitive measurements from which the mechanisms of hot-electron production can be determined. However, simulations indicate that Raman scattering is likely to be exceptionally virulent in the long-scale-length plasmas in these hohlraums. On one hand, very little scattered light indicative of Raman scatter is observed in our experiments. On the other hand, the simulations show that little scattered light is expected in these circumstances even when a large amount of laser light is absorbed through Raman processes.

Experiments with disk-and-washer hohlraum "mockups" showed increasing hot-electron temperature with increasing degrees of plasma confinement; that is, few hot electrons were produced with a washer (entrance port) alone, and few with a laser beam focused in front of a disk. However, when both disk and washer are present, providing some confinement of the disk plasma and allowing long scale lengths to develop, the hot-electron production rapidly increased. Experiments have also shown little change in the hot-electron temperature in

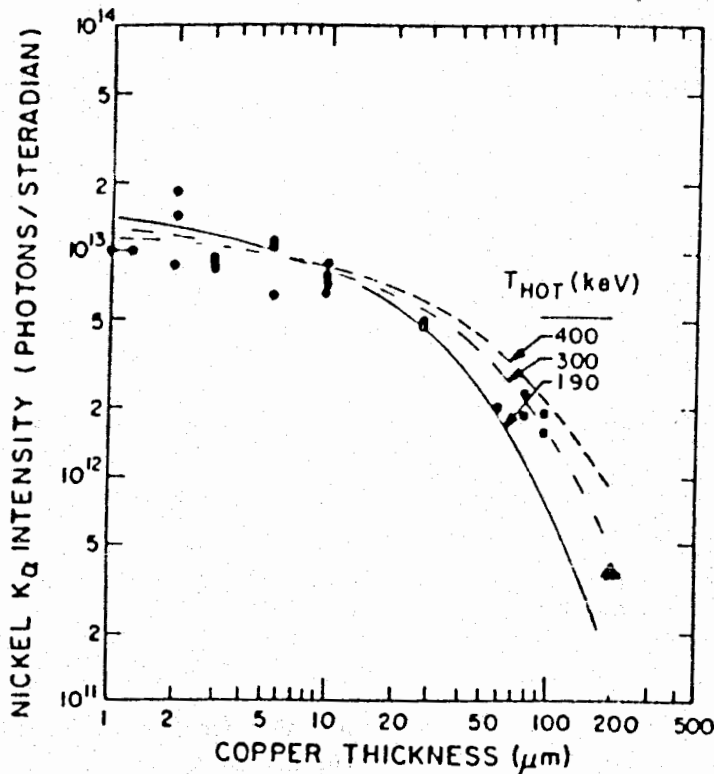


Fig. 21. Nickel K_{α} yield vs thickness of copper attenuator shows deep penetration of hot electrons. Agreement with LASNEX simulation is excellent.

67090593

hohlraums for beams focused at the hole, at the center of the hohlraum (converging at the hole), or at one radius outside the hole (diverging at the hole) as long as the average energy density E/D^2 remained the same. Thus, there is strong evidence from simulation and experiment that the hot electrons in hohlraums are produced by parametric instabilities in the underdense plasma in the hohlraums, most probably Raman scattering.

SUMMARY

Los Alamos has developed a fairly comprehensive understanding of CO_2 laser/matter interactions with some remaining uncertainties and has identified the remaining uncertainties of most importance as hot-electron-generation mechanisms and hot-electron temperature scaling to fusion environments, the plume fast ions (the spectra and the control of production efficiency and angular distribution of the plume fast ions), and long-pulse coupling. The efficiencies for a number of drive concepts with variants that constitute a near continuum

of attempts to use the major energy channels have been estimated. A very detailed analysis of these targets and a number of variations on their designs have been reported elsewhere²⁵ and only a summary of those findings will be given here.

We believe we have a fairly good understanding of hot-electron generation based upon empirical scalings and numerical calculations, although our detailed understanding of the generation processes is not as thorough as we would like. We have found that the hot-electron temperature for both open and hohlraum targets is considerably higher than we once thought. Our best empirical fits to Helios data give scaling laws as follows for hot-electron temperature:

$$\text{open targets: } T_{\text{hot}} \text{ (keV)} = 826 \left[\frac{E}{A} \right]^{0.55}$$

$$\text{hohlraum targets: } T_{\text{hot}} \text{ (keV)} = 6660 \left[\frac{E}{A} \right]^{0.51},$$

where E is in joules and A is the wall area in square microns.

These experimental data are all produced at a nominal laser pulse length of 0.7 ns. Although our best fit to our own data suggests that the hot-electron temperature scales approximately as the square root of the energy per unit hohlraum area, it can be plotted with short-wavelength data that include pulse-length variations, and the whole body of data is found to be consistent with a fit

$$T_{\text{hot}} \sim \left[\frac{E \lambda^2}{A \tau} \right]^{0.4}$$

The basic problem with CO₂ is that the long-wavelength light is absorbed at low density leading to high electron temperatures with resulting deep penetration, vacuum insulation failure, and fast-ion loss. It also leads to low absorption on open targets at low intensity (or low hot-electron temperature) and to port-closure and decoupling problems. The latter problems force either short-pulse operation (with resulting multishell penalties and uncertainties) or very large targets. These closure and decoupling problems also force limitations on intensity reduction and, hence, on hot-electron temperature reduction achievable in a practical fashion. The hot-electron-generation problems will probably be aggravated at fusion conditions because of the long-scale-length plasmas and large f-number beams of reactor systems that give a longer interaction distance than did Helios (the f/2.4 beams of Helios provided a depth of focus of only about 200 μm, which is probably smaller than the scale length of plasmas in Helios experiments).

We have tried various ways to finesse the hot-electron problem:

- low-intensity targets,
- the incorporation of vacuum insulation (as in Canopus),
- the use of ion drive (as in Canopus and Procyon), and
- the use of foam (in Chamisa) with the hope of anomalous stopping of the high-energy electrons.

Foam has not been found to produce obvious improvements. The other attempts have generally led to greater complexity in target design and to new energy channels that introduce additional inefficiencies in the process.

It is worthwhile to ask what issues have enough leverage to significantly alter this picture. Because absorption on open targets at low intensity or low T_{hot} is

low, there is a potential leverage of a factor of 3 or more in target absorption if we could find a way to improve the absorption without increasing the hot-electron temperature. Absorption increases at high intensity, and it increases in hohlraums but with an accompanying increase in hot-electron temperature. Similarly, we have seen hot-electron temperature increases in experiments with laser beams incident on low-density materials with rough surfaces.

Another possibility is to find a favorable, large change in the hot-electron temperature-scaling conditions closer to fusion. We have no basis for suggesting any particular change (except for the worse), but a factor-of-2 reduction in hot-electron temperature could gain a factor-of-1.2 efficiency in Canopus or a factor-of-2 efficiency in Chamisa. We have looked for such a favorable change in T_{hot} scaling by continuing scaling studies at Antares. We have a larger f-number beam and can go to longer pulses and larger energy per unit area in hohlraums on Antares. However, initial Antares scaling results indicate increased hot-electron temperatures over the Helios scaling as one moves to larger, longer-scale-length hohlraums. Other target concepts to ameliorate hot-electron effects are now being tested with Antares, and a final decision on the feasibility of CO₂ for fusion will await their completion.

REFERENCES

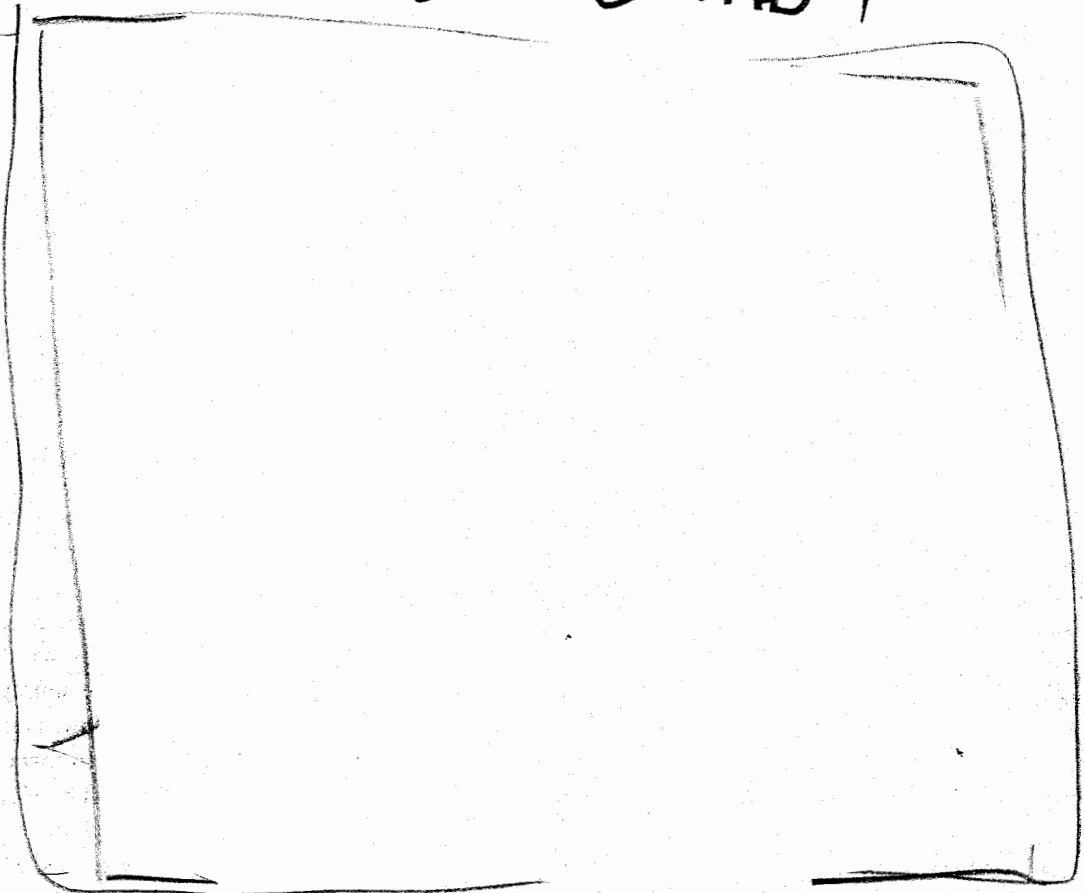
1. A. Hauer, R. S. Goldman, R. Kristal, M. A. Yates, M. M. Mueller, F. Begay, et al., "Suprathermal Electron Generation, Transport, and Deposition in CO₂ Laser Irradiated Targets," in *Laser Interaction and Related Plasma Phenomena, V. 6*, H. Hora and G. H. Miley, Eds. (Plenum Publishing Corp., New York, 1984), p. 479.
2. J. U. Brackbill and D. W. Forslund, "An Implicit Method for Electromagnetic Plasma Simulation in Two Dimensions," *J. Comp. Phys.* **46**, 271 (1982).
3. W. Priedhorsky, D. Lier, R. Day, and D. Gerke, "Hard-X-Ray Measurements of 10.6-μm Laser-Irradiated Targets," *Phys. Rev. Lett.* **47**, 1661 (1981).
4. D. R. Bach, D. E. Casperson, D. W. Forslund, S. J. Gitomer, P. D. Goldstone, A. Hauer, et al.,

67090594

- 67090595
- "Intensity-Dependent Absorption in 10.6- μ m Laser-Illuminated Spheres," *Phys. Rev. Lett.* 50, 2082 (1983).
5. D. W. Forslund, J. M. Kindel, K. Lee, E. L. Lindman, and R. L. Morse, "Theory and Simulation of Resonant Absorption in a Hot Plasma," *Phys. Rev. A* 11, 679 (1975).
 6. D. W. Forslund, J. M. Kindel, K. Lee, and E. L. Lindman, "Two-Dimensional Stability of an Electromagnetic Wave Obliquely Incident on a Non-uniform Plasma," *Phys. Rev. Lett.* 34, 193 (1975).
 7. R. L. Carman, D. W. Forslund, and J. M. Kindel, "Visible Harmonic Emission as a Way of Measuring Profile Steepening," *Phys. Rev. Lett.* 46, 29 (1981).
 8. D. W. Forslund, J. M. Kindel, and K. Lee, "Theory of Hot-Electron Spectra of High Laser Intensity," *Phys. Rev. Lett.* 39, 284 (1977).
 9. B. Bezzerides, S. J. Gitomer, and D. W. Forslund, "Randomness, Maxwellian Distributions, and Resonance Absorption," *Phys. Rev. Lett.* 44, 462 (1980).
 10. B. Bezzerides, R. D. Jones, and D. W. Forslund, "Plasma Mechanism for Ultraviolet Harmonic Radiation Due to Intense CO₂ Light," *Phys. Rev. Lett.* 49, 202 (1982).
 11. D. W. Forslund, J. M. Kindel, and E. L. Lindman, "Plasma Simulation Studies of Stimulated Scattering Processes in Laser-Irradiated Plasmas," *Phys. Fluids* 18, 1002 (1975).
 12. D. W. Forslund, J. M. Kindel, and E. L. Lindman, "Theory of Stimulated Scattering Processes in Laser-Irradiated Plasmas," *Phys. Fluids* 18, 1017 (1975).
 13. D. W. Forslund, J. M. Kindel and E. L. Lindman, "Nonlinear Behavior of Stimulated Brillouin and Raman Scattering in Laser-Irradiated Plasmas," *Phys. Rev. Lett.* 30, 739 (1973).
 14. D. W. Forslund et al., "Two-Dimensional Simulations of Single-Frequency and Beat-Wave Laser-Plasma Heating," *Phys. Rev. Lett.* 54, 558 (1985).
 15. D. W. Forslund, J. M. Kindel, K. Lee, and E. L. Lindman, "Two-Dimensional Stability of an Electromagnetic Wave Obliquely Incident on a Non-uniform Plasma," *Phys. Rev. Lett.* 34, 193 (1975).
 16. D. W. Forslund, J. M. Kindel, K. Lee, and E. L. Lindman, "Absorption of Laser Light on Self-Consistent Plasma Density Profiles," *Phys. Rev. Lett.* 36, 35 (1976).
 17. K. Lee, W. W. Forslund, J. M. Kindel, and E. L. Lindman, "Theoretical Derivation of Laser-Induced Plasma Profiles," *Phys. Fluids* 20, 51 (1977).
 18. B. Bezzerides, D. W. Forslund, and E. L. Lindman, "Existence of Rarefaction Shocks in a Laser-Plasma Corona," *Phys. Fluids* 21, 2179 (1978).
 19. B. Yaakobi, I. Pelah, and J. Hoose, "Preheat by Fast Electrons in Laser-Fusion Experiments," *Phys. Rev. Lett.* 37, 836 (1976).
 20. J. D. Hares, J. D. Kilkenny, M. H. Key, and J. G. Lunney, "Measurement of Fast-Electron Energy Spectra and Preheating in Laser-Irradiated Targets," *Phys. Rev. Lett.* 42, 1216 (1979).
 21. A. Hauer, W. Priedhorsky, and D. VanHulsteyn, "Inner Shell Satellite Lines in CO₂ Laser-Produced Plasmas," *Appl. Optics* 20, 3477 (1981).
 22. F. Begay and D. W. Forslund, "Acceleration of Multi-Species Ions in CO₂ Laser-Produced Plasmas: Experiments and Theory," *Phys. Fluids* 25, 1675 (1984).
 23. D. W. Forslund and J. U. Brackbill, "Magnetic-Field-Induced Surface Transport on Laser-Irradiated Foils," *Phys. Rev. Lett.* 48, 1614 (1982).
 24. M. A. Yates, D. B. VanHulsteyn, H. Rutkowski, G. A. Kyrala, J. Brackbill, et al., "Experimental Evidence for Self-Generated Magnetic Fields and Remote Energy Deposition in Laser-Irradiated Targets," *Phys. Rev. Lett.* 49, 1702 (1982).
 25. G. R. Spillman, R. O. Bengert, C. Barnes, S. D. Gitomer, "The Los Alamos Evaluation of CO₂ Laser Fusion Target Drive Concepts (U)," Los Alamos National Laboratory report LA-9919-MS (SRD) (March 1984).

UNCLASSIFIED

~~SECRET~~ RD



b(3)

Fig. 1. Schematic of a typical fusion target. As described in the text, each component plays a specific role in conversion of radiation from the driver to the implosive energy necessary for fusion of the fuel.

67090597

process produces tampers of very uniform thickness and great smoothness (Fig. 4). Electroless plating of substrates smaller than 500 microns in diameter is performed in an apparatus in which the spheres are kept in constant, random motion in a reaction chamber by alternating the flow direction of the metastable solution.^{1,2}

Some recent target designs call for tampers of metals, such as beryllium and aluminum, that cannot be deposited from aqueous solution. We are therefore investigating deposition from organic solvents and possibly molten salts. The major obstacle in this research is the hazardous nature of such deposition media.

After the electroforming process, the substrate is removed from the tamper by leaching with an appropriate chemical through a hole drilled in the plating. The hole is then fitted with a separately fabricated plug containing small radial channels for entrance of the gaseous fuel. After the tamper is filled, the plug is sealed and joined to the tamper by laser welding, a process described in Ref. 3.

Antimix Layer

The antimix layer smooths the hydrodynamic instabilities generated in the outer shells of the target and thus helps achieve symmetric implosion. This layer consists of a full-density polymer, which may be cast and machined separately in the form of two mating hemishells or deposited directly on the tamper. Because we have discussed the former method in Ref. 3, we discuss here two methods for direct deposition of polymers from the gas phase: the low-pressure plasma (LPP) process and the vapor-phase pyrolysis (VPP) process. When fully developed, these processes will probably be the methods of choice for depositing antimix layers of the required thickness uniformity and surface smoothness.

In the LPP process a radio-frequency voltage between two electrodes produces a low-pressure plasma of the monomeric material, which then polymerizes on the tamper surface. Small tampers (less than 500 microns in

100 UNCLASSIFIED

~~SECRET~~ RD

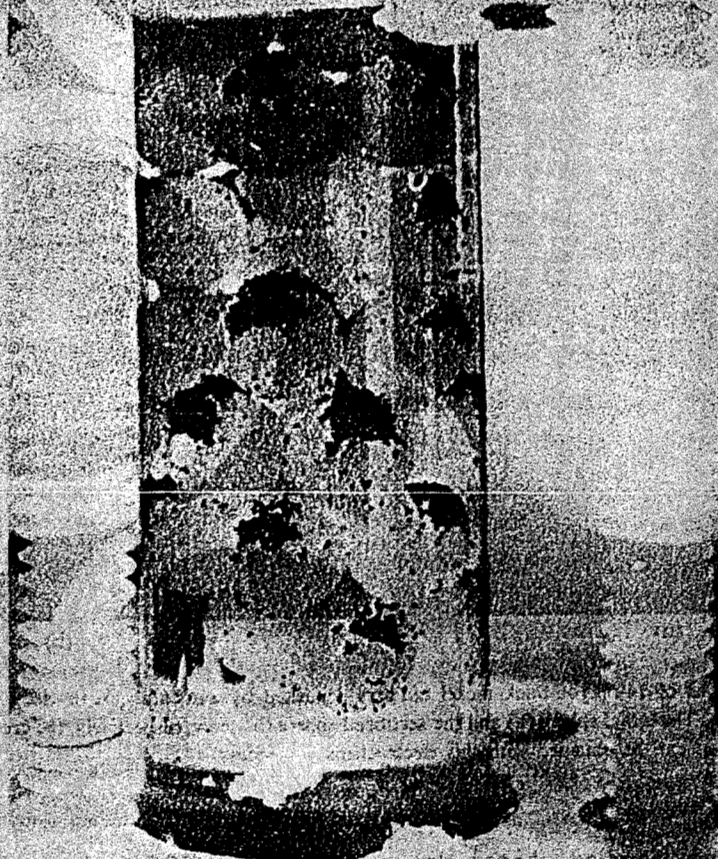


Fig. 2. An apparatus for electroplating small (less than about 500 microns in diameter) conducting spheres. The spheres are forced against first one and then the other of two cathodes of fine-mesh screen by alternating the flow direction of the electroplating solution. The constant, random motion of the spheres assures uniform deposition of the plated material. The large polyethylene balls prevent agglomeration of the small spheres.

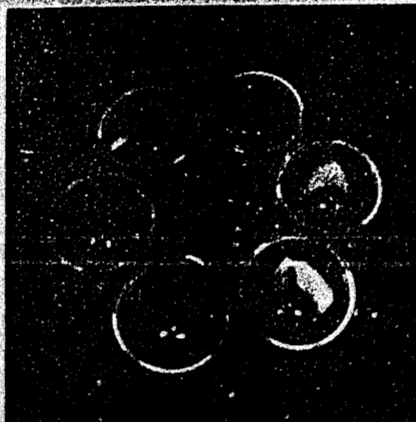


Fig. 3. A track-plating apparatus for electroplating conducting spheres greater than about 500 microns in diameter. The spheres are separately confined within cylindrical sleeves atop a washer-shaped cathode (the track). As the cathode rotates, the spheres, bathed in filtered electroplating solution, roll randomly over its surface. The randomness of the spheres' motion, and thus the uniformity of the plating, is increased by alternating the direction of rotation of the cathode and varying its angle of tilt. The spheres are burnished by contact with the track. This burnishing produces strong, fine-grained deposits.

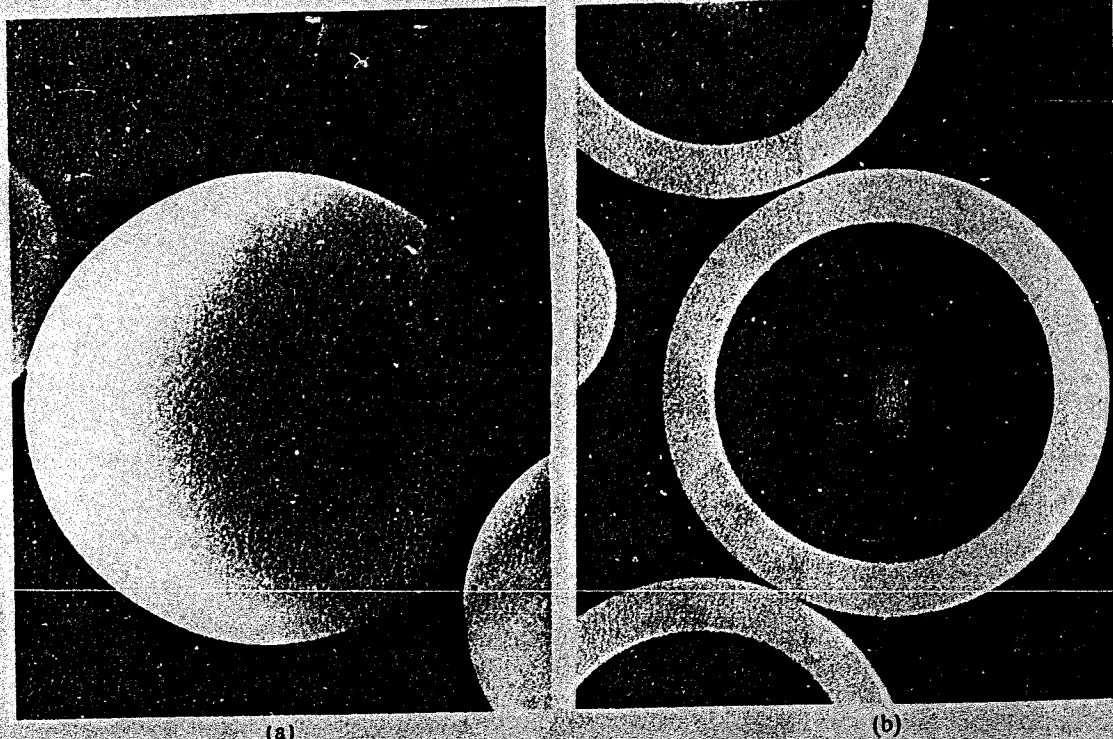


Fig. 4. Photomicrographs of 14-micron-thick nickel tampers deposited by autocatalysis, or electroless plating, on a spherical glass substrate. The intact sphere (a) and the sectioned sphere (b) show, respectively, the great smoothness and thickness uniformity that can be obtained with this electrochemical process.

diameter) are levitated above vibrating, shaped electrodes during the coating process. By pulsing in the monomeric vapor and maintaining the temperature of the electrodes below -10°C , we have formed very smooth antimix layers with thicknesses between 1 and approximately 60 microns from such monomers as p-xylene and cyclooctatetraene (Fig. 5).⁴

In the VPP process, p-xylene is pyrolytically degraded to the reactive diradical species, which then polymerizes on the surface of the object to be coated. We have adapted this well-known process to deposit uniformly thick, smooth, antimix layers on stalk-mounted or levitated tampers. The uniformity of a 600-micron-thick antimix layer prepared by the VPP process varies by less than 3%, and its smoothness is marred only by a few micron-size "bumps." Greater surface smoothness of thinner antimix layers can easily be obtained by increasing the turbulence of the reactive gas. We have, for example, prepared defect-free coatings up to 70 microns thick with surface variations of less than 0.1 micron from peak to valley.²

Both the surface smoothness and thickness uniformity of these deposited antimix layers can be greatly enhanced by lapping techniques originally developed for metals

and since refined for polymers. These techniques will be discussed below in connection with the fabrication of ablators.

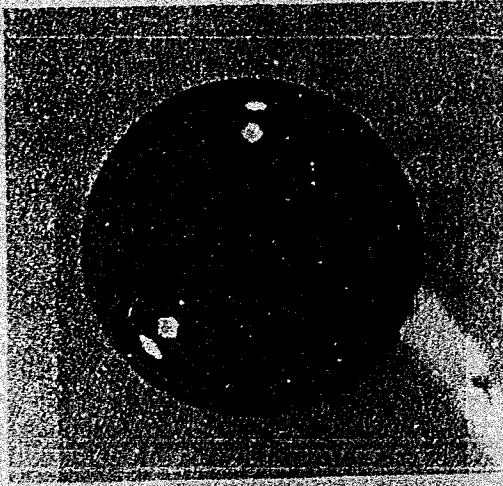


Fig. 5. Scanning electron micrograph of a 300-micron-diam hollow glass sphere laser fusion target coated by the low-pressure plasma process with a 5-micron-thick layer of p-xylene. Note the surface smoothness of the coating.

67090599

Cushion

The cushion provides a stand-off distance between the tamper and the ablator.

For good implosion hydrodynamics the foam must have a very low density (0.05 g/cm³ or less) and small cell size (less than 2.0 microns in diameter), and must be free of impurities and amenable to fabrication to precise tolerances. Such foams were unknown before their development at Los Alamos.

We make the foam by cooling a homogeneous polymer solution to induce an inverse phase separation at the temperature at which the polymer and solvent become immiscible (the spinodal point). The polymer forms a foam matrix, and the solvent forms discrete, uniform droplets in this matrix. Removal of the solvent droplets from the matrix generally results in a porous, open-cell, rigid plastic foam in which the voids are replicas of the solvent droplets. The density of the foam is determined by the concentration of the polymer solution.

We have prepared small-cell, low-density, rigid foams from such polymers as polystyrene, poly(4-methyl-1-pentene), and substituted celluloses and starches. Figure

6 is a scanning electron micrograph of a carboxymethylcellulose foam. Hemishells of this foam are made by performing the inverse phase separation process in an appropriate mold. Foams made from poly(4-methyl-1-pentene) have a very uniform structure, but the low compression strength of such foams (about 10 lb/in.²) makes them difficult to machine to exact tolerances by normal techniques. To eliminate this difficulty, we have developed a polymer-solvent system in which the solvent droplets are solid at room temperature. The solid solvent reinforces the delicate cell walls and thus protects them from damage during machining. The solvent is then extracted with alcohol.

Ablator

The energy of the radiation from the driver is deposited in the shell known as the ablator (see Fig. 1). The absorbed energy causes material to be ejected outward from the ablator, producing a "rocket" effect that transfers inward momentum to the ablator, which results in compression of the fuel.

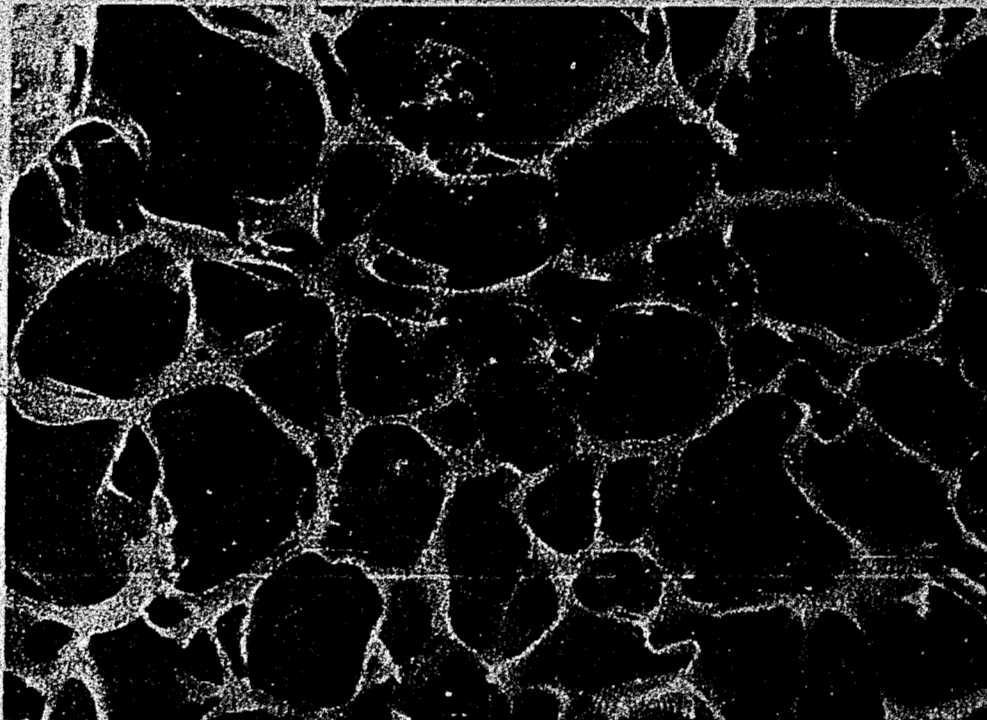


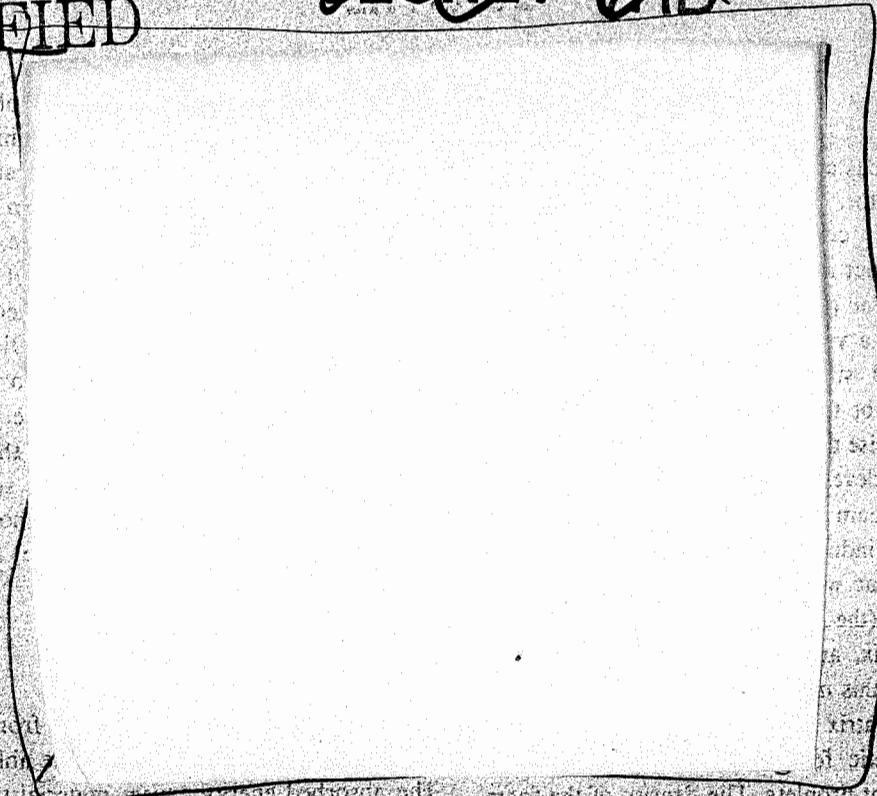
Fig. 6. Scanning electron micrograph of a carboxymethylcellulose foam. The density of the foam is 0.05 g/cm³ and the average cell size is between 1 and 2 microns.

6709 0600

b(3)

b(3)

b(3)



b(3)

The small sizes and close dimensional tolerances typical of fusion targets dictate that ablators be machined with ultraprecision tools. With such tools and single-crystal diamond tool bits we can, for example, produce surfaces with a peak-to-valley roughness of 0.05 micron.

An important aspect of precision turning is the constancy of rotational speed and rotational axis provided by air-bearing spindles. We have available two smaller lathes with air-bearing spindles and vibration-isolating, magnetically coupled, drive motors. We also have a larger ultraprecision lathe (Fig. 8), built to Los Alamos specifications by Pneumo Precision, Inc., that combines the features of air-bearing spindles and slideways with those of computer control. Figure 9 shows an example of what the Pneumo lathe can produce.

To increase our machining capability, we are now preparing specifications for another lathe with a programmable rotary axis and the same accuracy as that of the Pneumo lathe.

Although the surface finishes produced by ultraprecision turning are excellent, they can be further improved (except on many face-centered cubic materials) by lapping or polishing with fine abrasive particles. By using submicron-size grit and air balancing to check the progress of the lapping, we can obtain surfaces that are smoothed to about 0.003 micron. These are the

smoothest surfaces attainable with a mechanical technique. Shapes other than spheres or hemispheres can be lapped with special equipment.⁶

Pulse-Shaping Layer

Some recent target designs have called for a pulse-shaping layer, a very thin (less than 50 microns), uniform, seamless layer of metal that modifies the intensity and duration of the radiation pulse from the driver before it interacts with the ablator. Because at this stage of fabrication the target contains both temperature-sensitive materials and high-pressure DT fuel, the pulse-shaping layer must be deposited on the ablator without increasing its temperature above about 100°C. The techniques available are therefore limited to either electrochemistry or physical vapor deposition. We have discussed the former in connection with tamper fabrication and will discuss here only the latter.

The term "physical vapor deposition" includes electron-beam evaporation, sputtering, and ion plating. To achieve uniform deposits on spherical targets with these line-of-sight processes, we have designed parallax-compensated rotators (Fig. 10) that orient all areas of the sphere equally (on the average) toward the vapor source.⁷ We are also investigating the possibility of

67090601

UNCLASSIFIED

SECRET RD

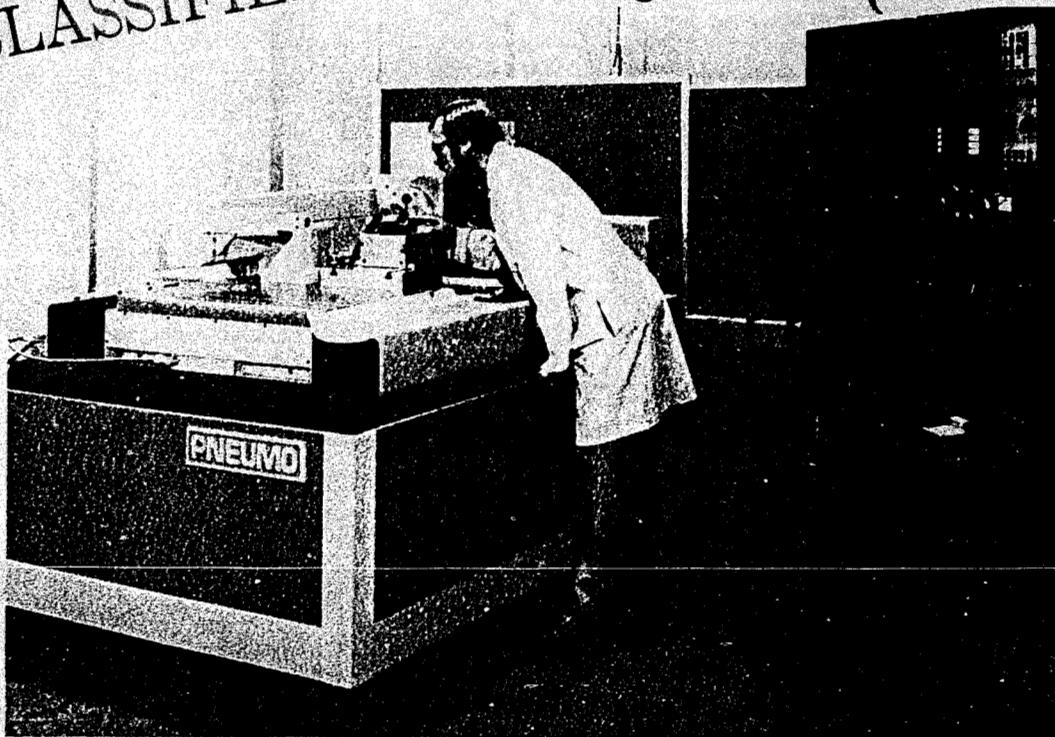


Fig. 8. Ultraprecision lathe built to Los Alamos specifications by Pneumo Precisions, Inc. The position feedback system of this machine, which is based on laser interferometry, has a resolution of 0.025 micron. Its low-friction, air-bearing slideways allow precise contouring, and any surface of revolution can be generated by simple programming. The slideways are mounted on a massive granite block, which in turn is supported on three air-bag vibration isolators. With this lathe we use single-crystal diamond tool bits for machining most plastics and some nonferrous metals and cubic boron nitride and conventional carbide tool bits for machining materials (such as beryllium) that are incompatible with diamond tool bits.

levitating smaller targets during coating by vibration or with a molecular beam (Fig. 11).⁸

Hohlraums

The hohlraum (hollow room) provides a very symmetric radiation environment for the target by reflecting the radiation from the driver multiple times.

(By a fluidized bed, we mean the churning mass of particles that can be formed by directing a flow of gas upward through a volume of particles with appropriate size and density.) The continuous, random motion of the fluidized substrates ensures that all surfaces are exposed (on an average) to the same temperature and

UNCLASSIFIED

SECRET RD

0602
670

b(3)

UNCLASSIFIED

~~SECRET~~ RD

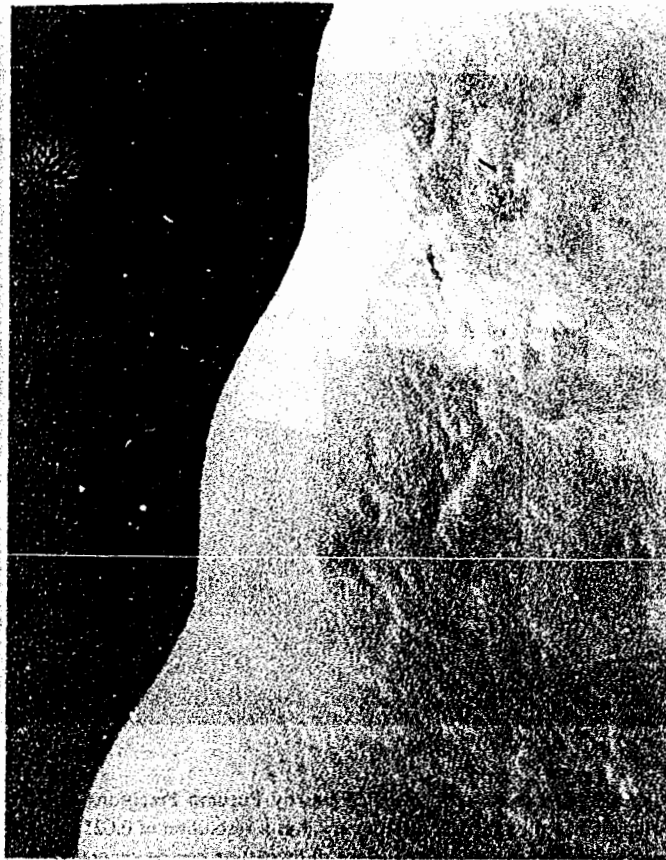


Fig. 9. Scanning electron micrograph of a sinusoidal surface, magnified 2000 times, machined with the Pneumo lathe on a cylindrical aluminum mandrel. The amplitude of the sinusoidal surface is 1 micron and its wavelength is 25 microns. The lathe was equipped with a 25-micron-radius diamond tool bit and was controlled by a tape generated on an external computer.

gas flux, and very uniform coatings are deposited even on substrates with complex geometries. In addition, the collisions among the substrates provide a peening action that helps to break up growth patterns that produce large, columnar grains. As a result, the coatings usually consist of fine, equiaxed grains and are thus strong and smooth.

technologies of interest and benefit to other research and development programs. We mention briefly a few of these other applications to indicate the variety of problems in which materials science plays a fundamental role.

The polymeric foams developed for the cushion layer may benefit biomedical research. Recent experiments have shown that artificial veins fabricated from microporous polymeric foams may result in less scar tissue than do those fabricated from fibrillated Dacron and Teflon, which are currently in use. This advantage is believed to be due to the greater control of porosity, which can be achieved with the polymer foams. Another application of the polymeric foams is in the x-ray laser program. When doped with high-Z metals, the foams show excellent promise as lasing media.

OTHER APPLICATIONS

It is not surprising that our efforts on the multifaceted task of target fabrication have led to materials and

UNCLASSIFIED

~~SECRET~~ RD

6704 0603

b(3)

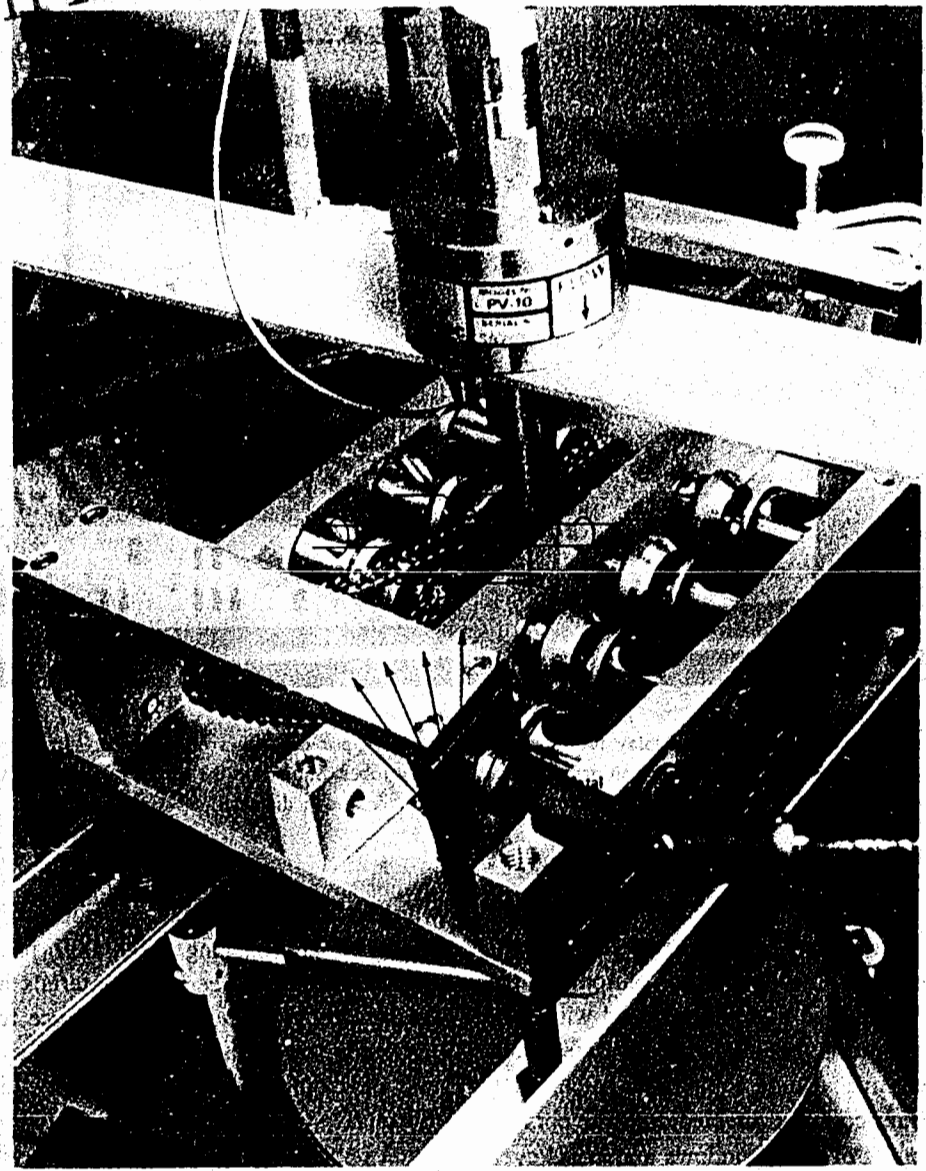
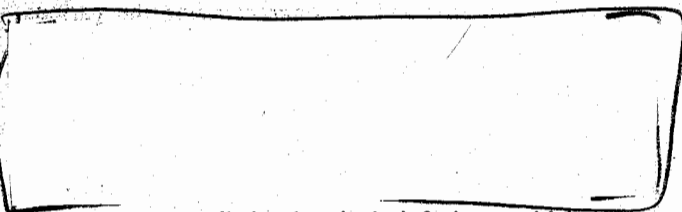


Fig. 10. (a) Photograph of a parallax-compensated rotator for obtaining uniformly thick pulse-shaping layers by physical vapor deposition. As shown in the accompanying schematic diagram (b), the target is in contact with two rotators, each of which rotates at a different speed. This unequal rotation, when coupled with periodic halts of one of the rotators, results in completely random orientation of the target toward the vapor source. The mask limits the angles of incidence to those near 90°, which yield the best surface smoothness.

When the target is in contact with two rotators, each of which rotates at a different speed. This unequal rotation, when coupled with periodic halts of one of the rotators, results in completely random orientation of the target toward the vapor source. The mask limits the angles of incidence to those near 90°, which yield the best surface smoothness.

6704
0504
4
6704



A process called chemical infusion, which was developed for smoothing polymeric surfaces, may also benefit biomedical research. Experiments on laboratory animals have shown that silicone rubber veins infused by

this process with stearate ions are rejected less often than are untreated artificial veins.¹⁰

Miniature coaxial cables fabricated in support of inertial confinement fusion may simplify surgical removal of brain tumors. High-frequency electrical signals transmitted through such a cable, which is less than 0.1 mm in diameter, may enable the destruction of cancerous cells without damage to surrounding tissue.^{11,12}

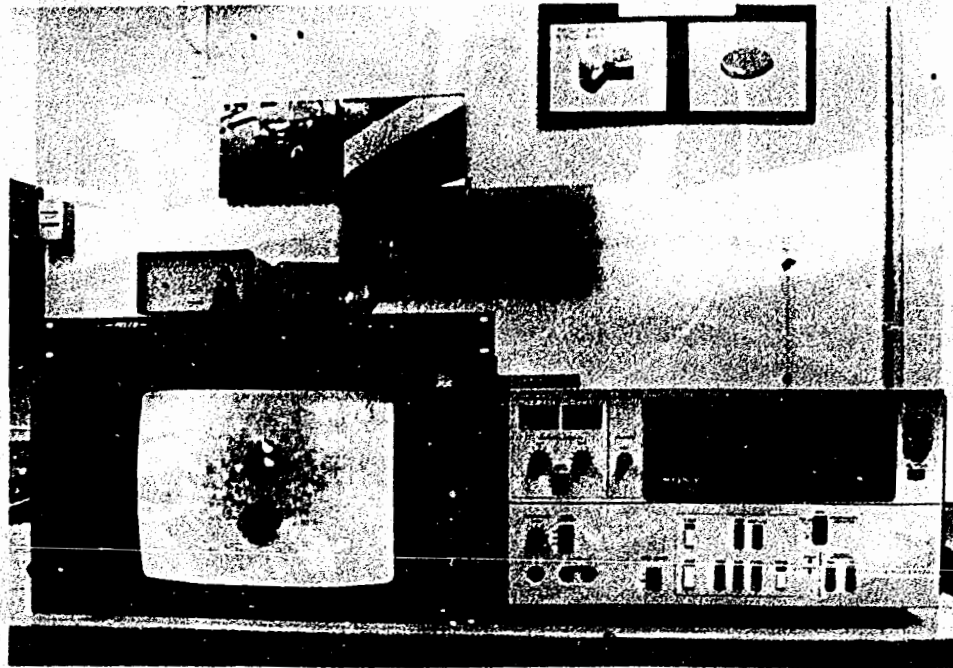


Fig. 11. Magnifying video display for monitoring physical vapor deposition on spherical substrates levitated by flow of gas through an array of fine capillary tubes. Shown on the screen (along with its shadow) is a levitated hollow glass sphere, which is 300 microns in diameter.

Laser welding, the method used to seal tampers, may greatly simplify fabrication of components for conventional nuclear weapons. Components of plutonium, for example, must be welded in a glove box, and with conventional techniques this condition necessitates contamination of expensive welding equipment. In contrast, a laser welding beam could be directed onto the component through special glove-box windows and could even be transported throughout a facility along optical fibers.

whiskers of silicon carbide or silicon nitride have tensile strengths approaching 4,000,000 psi. Composites of such whiskers and ceramic materials have even greater tensile strengths and high resistance to fracture.

Clearly, target fabrication and the associated research and development encompass many diverse endeavors. Formerly, these projects were pursued at several scattered Laboratory sites. But since the fall of 1983, most of our activities have been gathered in a single, specially designed building, the Target Fabrication Facility. This facility includes clean rooms for target assembly, a laboratory in which the targets are filled with the DT fuel, a machine shop, and laboratories for electroplating and physical and chemical vapor deposition, for developing and producing polymer foams, for laser welding and solid-state bonding, and for characterizing the various target components. Beyond the obvious advantages of space and equipment, the facility allows greater ease of communication among those individuals involved in materials science, fabrication technology, and materials characterization. This important factor will permit us to further an established tradition of excellence.

Tools like those developed for uniformly coating target components by physical vapor deposition are now routinely used for coating rare-earth radiochemical tracers on experimental nuclear weapon components.

High-strength, single-crystal whiskers, which were fabricated and studied for possible use as support structures in laser fusion targets, are now the key component in the Laboratory's structural ceramics program. These

6709 0605 b(3)

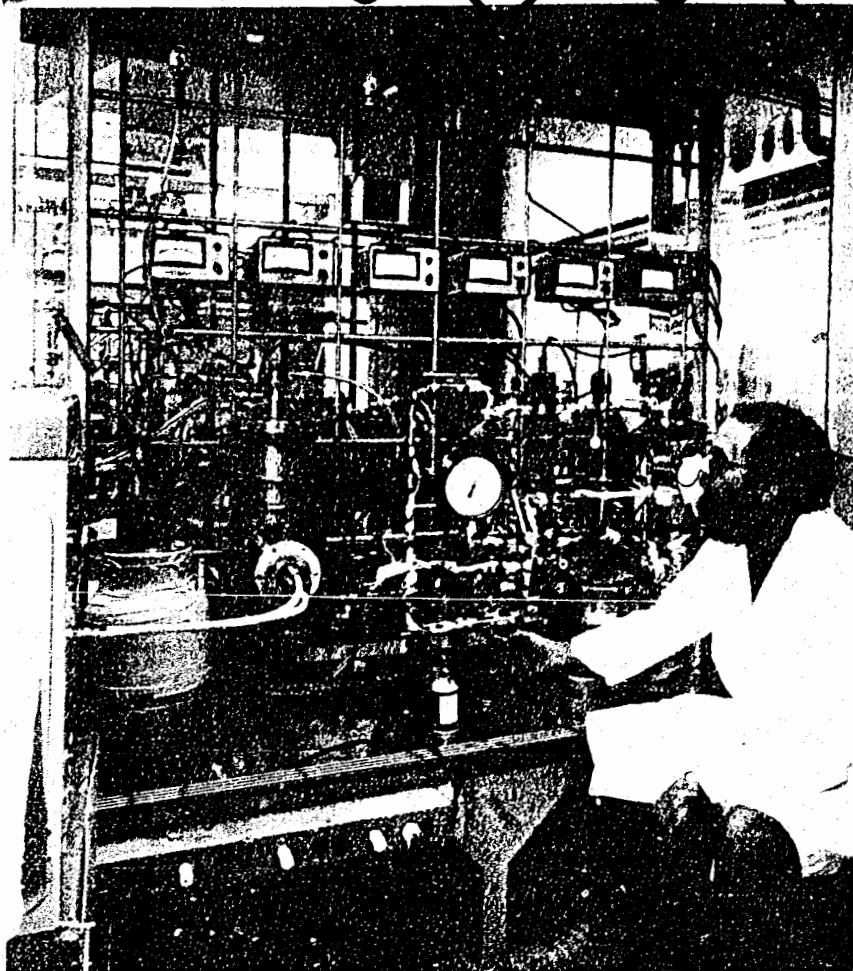


Fig. 12. Photograph of an apparatus for coating a fluidized bed of substrates by chemical vapor deposition. The fluidized bed is created in the cylindrical vessel heated by an external induction coil as the reactive gas flows upward through an orifice at the bottom of the vessel. The array of meters monitors process conditions such as gas flow and temperature.

0 6 0 6
0 7 0 3
6 7 0 3
REFERENCES

1. A. Mayer and W. Doty, "Advances in Plating and Forming Inertial Fusion Targets," in *Technical Digest-Conference on Inertial Fusion* (Opt. Soc. America, San Diego, California, 1980) p. 96.
2. A. Mayer and D. S. Catlett, "Plating Discrete Microparticles for Laser Fusion Targets," *Plating and Surface Finishing* (March 1978) p. 42.
3. H. Casey, W. R. Doty, R. Mah, A. T. Young, Jr., R. L. Rhorer, M. E. Kenyon, and G. A. Simonsic, "Capsule Fabrication (U)," in *Defense Science*, Los Alamos National Laboratory report LA-9140-PR (SRD) (May-August 1981) p. 53.
4. R. Liepins, M. Campbell, J. S. Clements, J. Hammond, and R. J. Fries, "Plastic Coating of Microsphere Substrates," *J. Vac. Sci. Technol.* 18(3), 1218 (1981).
5. A. T. Young, D. K. Moreno, and R. G. Marsters, "Preparation of Multishell ICF Target Plastic Foam Cushion Materials by Thermally Induced Phase Inversion Processes," *J. Vac. Sci. Technol.* 20(4), 1094 (1982).
6. R. L. Rhorer, "Update on Precision Machining at Los Alamos," in *Proceedings of the Society of Photo-Optical Instrumentation Engineers Annual Meeting*, San Diego, California, Vol. 433 (1983) p. 107.

UNCLASSIFIED

UNCLASSIFIED

~~SECRET/AD~~

7. G. A. Reeves, "Physical Vapor Deposition onto Small Spheres," in *Technical Digest-Conference on Inertial Fusion* (Opt. Soc. America, San Diego, California, 1980) p. 60.
8. S. F. Mayer, "Metallic Coating of Microspheres," *J. Vac. Sci. Technol.* 18(3), 1198 (1981).
9. D. W. Carroll and W. J. McCreary, "Fabrication of Thin-Wall Free-Standing Inertial Confinement Fusion Targets by Chemical Vapor Deposition," *J. Vac. Sci. Technol.* 20(4), 1087 (1982).
10. D. V. Duchane, "Polymeric Mandrels—Supersmooth Finish by an Infusion Process," *J. Vac. Sci. Technol.* 18(3), 1183 (1981).
11. W. L. Bongianni, "Fabrication and Performance of Strip-Centered Microminiature Coaxial Cable," in *Proceedings of the Institute of Electrical and Electronic Engineers*, Vol. 22 (September 1984).
12. M. Kachmer, Ed., "Brain Tumors Succumb to New Microwave Probes," in *Microwave and RF* (November 1983) p. 30.

67090607

UNCLASSIFIED

~~SECRET/AD~~